CHARACTERIZATION OF THE RENAL AND THE BONE PHENOTYPES OF THE Npt2 KNOCK OUT MOUSE

By

Hannah M. Hoag

Department of Biology

McGill University, Montreal

August, 1999

A Thesis submitted to the Faculty of Graduate Studies and Research in partial fulfillment of the requirements for the degree Master of Science

1 ABSTRACT

This study shows that mice homozygous for the disrupted renal sodium-phosphate (Na^+-Pi) cotransporter, *Npt2*, (Npt2 KO) failed to show an age-dependent decrease in renal Na^+-Pi cotransport or an adaptive increase in renal Na^+-Pi cotransport in response to dietary Pi restriction. None of the other known renal Na^+-Pi cotransporters could compensate for the loss of *Npt2*. Additionally, *Npt2* gene ablation resulted in a marked decrease in osteoclast number that persisted with age. Although mineral apposition rate was normal at 25- and 115-days of age in Npt2 KO mice, bone formation rate was increased at 115-days of age. These data demonstrate that *Npt2* gene expression is necessary for an age-dependent decrease in renal Na^+-Pi cotransport and for the renal adaptive response to dietary Pi deprivation, and that *Npt2* expression is essential for normal osteoclast function and influences bone formation.

2 RÉSUMÉ

Cette étude démontre que les souris qui manquent le gène pour un cotransporteur de rein de sodium et de phosphate (Na^+-Pi), *Npt2*, (Npt2 KO) n'ont pas montré une diminuation de cotransport Na^+-Pi avec l'âge, ni une augmentation adaptive du cotransport Na^+Pi dans des régimes pauvres en Pi. Aucun des autres cotransporteurs Na^+-Pi n'ont pu compenser pour la perte. En .plus, l'élimination de *Npt2* a réduit le nombre d'osteoclastes à plusieurs âges et a affecté la formation d'os. Bien que l'apposition de mineraux était normale dans les souris Npt2 KO, la formation d'os était augmenté chez ces souris à 115 jours. Les resultats indiquent que l'expression de *Npt2* est nécessaire pour que le cotransport du Na^+-Pi du rein diminue avec l'âge et pour augmenter le cotransport Na^+-Pi pendent l'administration d'une diète à faible teneur en phosphate, et que l'expression de *Npt2* est essentielle pour la fonction normale de l'osteoclaste et pour la formation d'os.

3 ACKNOWLEDGEMENTS

It goes without saying that any project of two years in duration involves the support of many people. Although I am only mentioning a few by name, the contributions of those not mentioned have not gone unnoticed. I appreciate everything.

To Dr. Susie Tenenhouse, my thesis supervisor, who tracked me down in equatorial East Africa to offer me the position. Her enthusiasm, encouragement, and guidance were greatly appreciated through out the course of this project.

To my colleagues Claude Gauthier, Josée Martel, Youssouf Soumounou, and Laurent Beck. All of who were instrumental in the completion of various aspects of this project. You provided me with the encouragement that was needed to continue with confidence when not everything worked as it was intended, acted as a sounding board for new ideas, and provided me with well thought-out suggestions. I appreciated your patience while I struggled with the spoken French word. Most importantly, you all added light-heartedness to the lab environment with stimulating conversation about politics, education, sports, and economy, both here at home and in distant lands.

To Danielle Boulais the best animal care technician with whom anyone could ever hope to work. Your attention to detail and attentiveness did not go unappreciated. It would have been impossible to complete what I did without your help, and your meticulous control of the mouse colony.

To all of the other students and coworkers in the DeBelle laboratory, and the departments of Biology and of Human Genetics. How could any graduate student be successful without clean glassware, borrowed gel combs, and reminders to register for

school? I thank you for listening and providing advice when it was needed, and for the friendships that developed over time.

To all of my other friends, both new and old, both in Montreal and elsewhere. I thank you for helping me adapt to life in Montreal, and I enjoyed all of the conversations about the highs and lows of the life of a graduate student.

Finally, I must thank my Mom, Dad, Matt, and Ian for their interest in my endeavors and their constant understanding. I enjoyed trying to explain the details my project to you all, even if you didn't understand them. Your support and enthusiasm in all of my interests have always provided me with the fuel to continue.

This research was supported by a grant from the Medical Research Council of Canada (Medical Research Council Group Grant in Medical Genetics to H.S. Tenenhouse), and a Medical Research Council Studentship award.

Contribution of Authors

Although this is not a manuscript-based thesis, it should be noted that most of the data contained within this thesis have been included in two manuscripts, and several others have contributed to the work.

> Hoag, H.M., Martel, J., Gauthier, C., and Tenenhouse, H.S. Effects of *Npt2* gene ablation and low-phosphate diet on renal Na^+/phosphate cotransport and cotransporter gene expression. ***Journal of Clinical Investigation***. Accepted, and expected date of publication September, 1999.
>
> Gupta, A., Hoag, H.M., Wang, D., Alvarez, U.M., Tenenhouse, H.S., and Hruska, K.A. Identification of the type II Na^+-Pi cotransporter (Npt2) in the osteoclast and its implications in *Npt2* $^{-/-}$ mice. ***To be published.***

Josée Martel contributed the Western analysis of Npt1 protein in WT and Npt2 KO mice fed control and low Pi diets; Claude Gauthier performed the ribonuclease protection assays. Both Josée Martel and Claude Gauthier are research assistants under the supervision of Dr. H.S. Tenenhouse.

Drs. Anandarup Gupta and Keith Hruska and their technicians performed the histochemical and histomorphological analysis of the bone sections upon their receipt. Each conducts their research from the Barnes-Jewish Hospital of St. Louis, in collaboration with the Washington University School of Medicine, St. Louis, MO.

4 ABBREVIATIONS

$1,25(OH)_2D_3$	1,25-dihydroxyvitamin D_3
1α-hydroxylase	25-hydroxyD-1α-hydroxylase
$24,25(OH)_2D_3$	24,25-dihydroxyvitamin D_3
24-hydroxylase	25-hydroxyD-24-hydroxylase
25-hydroxylase	25-hydroxyD-25-hydroxylase
25(OH)D	25-hydroxyvitamin D
[α-^{32}P]UTP	[alpha-phosphate-35] uracil triphosphate
%L	% labeled surface
ARF	activation-resorption-formation
ATP	adenine triphosphate
BBM	brush border membrane
BFR	bone formation rate
bp	base pairs
BS	bone surface
Ca	calcium
cAMP	cyclic adenosine monophosphate
cDNA	complementary deoxyribonucleic acid
Cl^-	chloride
Cr	creatinine
cRNA	complementary ribonucleic acid
C-terminal	carboxy-terminal
dLS	double labels
DNA	deoxyribonucleic acid
dNTP	deoxy-N-triphosphate
DTT	dithiothreitol
ECaC	epithelial calcium influx channel
EDTA	ethylene diamine tetra acetic acid
EGF	epidermal growth factor
E.Pm	eroded perimeter
EtBr	ethidium bromide
EtOH	ethanol
FEI	fractional excretion index
GI	gastrointestinal
Glvr-1	gibbon ape leukemia virus
Gy	Gyro

HHRH	hereditary hypophosphatemic rickets with hypercalciuria
Hyp	Hypophosphatemic
IGF-1	insulin-like growth factor-1
Ir.L.Th	interlabel thickness
Ir.L.time	interlabel time
kb	kilobases
kDa	kilodalton
LiCl	lithium chloride
MAR	mineral apposition rate
MDCT	murine distal convoluted tubule
Mg	magnesium
mRNA	messenger ribonucleic acid
MS	mineralizing surface
Na^+-Pi	sodium dependent
NaPi-I or Npt1	sodium dependent phosphate transporter type I
NaPi-2 or Npt2	sodium dependent phosphate transporter type II
neo^r	neomycin resistance gene
nOC/TA	osteoclast index
Npt2 KO	Npt2 gene knockout mouse
N-terminal	amino terminal
og1	osteocalcin gene 1
og2	osteocalcin gene 2
OK	opossum kidney
org	osteocalcin related gene
osc^{ml}/*osc*^{ml}	osteocalcin deficient mice
PCR	polymerase chain reaction
PCT	proximal convoluted tubule
Phex	phosphate-regulating gene with homology to endopeptidases
Pi	inorganic phosphate
poly(A) RNA	polyadenylated ribonucleic acid
PT	proximal tubule
PTH	parathyroid hormone
Ram-1	rat amphotropic virus
RPA	ribonuclease protection assay
rpm	revolutions per minute
RT-PCR	reverse transcriptase-polymerase chain reaction
SDS	sodium dodecylsulfate

SDS-PAGE	sodium dodecylsulfate polyacrylamide gel electrophoresis
SEM	standard error of the means
sLS	single labels
SSCP	single stranded conformation polymorphism
TAE	tris-acid EDTA
TALH	thick ascending limb of the loop of Henle
Tb.Ar	trabecular area
Tb.N	trabecular number
Tb.Pm	trabecular perimeter
TRAPase	tartrate-resistant acid phosphatase
UVB	ultraviolet B
UI	international units
VDR	vitamin D receptor
V_{max}	maximum velocity
WT	wild-type
XLH	X-linked hypophosphatemia

5 TABLE OF CONTENTS

6 LIST OF FIGURES

7 LIST OF TABLES

8 INTRODUCTION

8.1 MAMMALIAN Pi HOMEOSTASIS

Phosphate (Pi) is essential for a variety of cellular and metabolic processes; it is a component of genetic material, proteins, and membranes. Eighty-six percent of Pi is located within the bone and 14% of Pi found in the intracellular fluid. Less than 1% of Pi is found in the extracellular fluid.

Dietary Pi intake, intestinal absorption of dietary Pi, and renal Pi excretion all function coordinately to maintain serum Pi levels. The extent of bone formation and bone resorption is determined indirectly by the concentration of serum Pi. In the normal adult mammal, renal Pi excretion is balanced by Pi absorption by the gastrointestinal (GI) tract. During periods of growth, GI Pi absorption exceeds that of urinary excretion allowing Pi to accumulate in the bones and tissues. While the kidney is usually capable of maximal reabsorption of Pi, certain pathological conditions are characterized by a net loss of Pi through urinary excretion.

In the event that dietary Pi intake is insufficient, intestinal Pi absorption and bone resorption may be increased to maintain serum Pi concentrations. However, it is the tight regulation of renal Pi excretion that determines mammalian Pi homeostasis. A number of hormonal and metabolic factors function coordinately to alter renal Pi excretion in order to maintain Pi homeostasis. Many of these actions affect the activity of renal Na^+-dependent Pi (Na^+-Pi) cotransporters. To date, there are 3 families of Na^+-Pi cotransporters: type-I, -II, and -III, each with distinct properties, and characteristic tissue localization. Although all 3 types of Na^+-Pi cotransporters are expressed in the kidney, none of them are exclusive to the kidney. The identification and characterization of these

Na^+-Pi cotransporters has led to a better understanding of the characteristics of renal, intestinal, and skeletal Pi transport.

8.2 RENAL Na^+-DEPENDENT Pi TRANSPORT

The renal proximal tubule (PT) is the major site of Pi resorption in the kidney. Following glomerular filtration, approximately 60% of the filtered Pi load is reabsorbed in the proximal convoluted tubule (PCT) in a sodium-dependent manner by Na^+-Pi cotransporters situated in the brush border membrane (BBM) of these cells. A further 15-20% is reclaimed in the proximal straight tubule, and <10% in the distal tubule, leaving ~10% to be excreted in the urine. The proportion of excreted Pi can be adjusted to accommodate modifications in the physiological Pi requirement or in dietary Pi intake, through the tightly regulated actions of hormones or other modulators on renal BBM Na^+-Pi cotransporters.

PCT transepithelial Pi transport involves the rate-limiting step of Pi uptake at the apical membrane by Na^+-Pi cotransporters, translocation across the cell, and efflux at the basolateral membrane (Figure 1). Na^+ K^+-ATPase pumps located on the basolateral membrane maintain the Na^+-gradient that drives the Pi transport process. While little is known about the transcellular and basolateral routes of Pi travel (although basolateral efflux is thought to occur via a passive mechanism), the BBM Pi transport process has been thoroughly investigated.

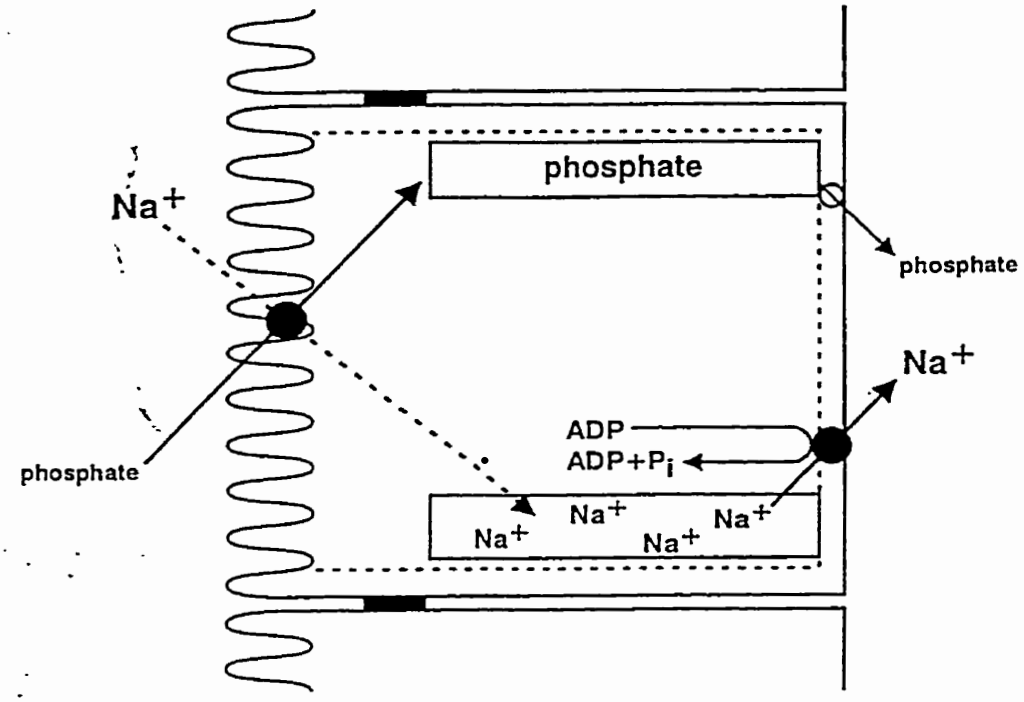

Figure 1: Phosphate transport in renal proximal tubular cells.

Phosphate transport across the apical membrane of the renal proximal tubular cell is driven by a sodium-gradient. Entry into the cell is the rate limiting step of Pi resorption, and is the target of regulation. Phosphate efflux occurs at the basolateral membrane, but is poorly defined.

From: Murer, H., 1992. *J. Am. Soc. Nephrol.* 2:1649-1665.

8.3 PHYSIOLOGICAL REGULATION OF BBM PROXIMAL TUBULAR Na^+-Pi COTRANSPORT

There are both extrinsic and intrinsic factors that have major regulatory effects on PT Na^+-Pi cotransport. Parathyroid hormone (PTH), dietary Pi intake, and vitamin D ($1,25(OH)_2D_3$) alter renal BBM Na^+-Pi reabsorption by affecting the activity of BBM Na^+-Pi cotransporter protein. Fasting, on the other hand, causes a decrease in renal Pi resorption, but through the physiological response to metabolic acidosis.

An increase in circulating PTH elicits an increase in renal Pi excretion. PTH affects Na^+-Pi cotransport by directly reducing the V_{max} of BBM Pi transport by removing Na^+-Pi protein from the PT BBM (reviewed in (1-3)).

A diet low in Pi causes an increase in PT Na^+-Pi cotransport through an increase in the V_{max} of Pi transport, with no change in the affinity for either Na^+ or Pi (4). Studies performed in cultured opossum kidney (OK) cells grown in culture media deficient in Pi, indicate that the adjustment to extracellular Pi can occur independently of circulating factors or hormones (5). The mammalian response to a high Pi diet following adaptation to a diet low in Pi elicits the opposing response. Altering dietary Pi content from low to high causes a significant decrease in BBM Na^+-Pi cotransport activity in both intact and parathyroidectomized rats, demonstrating that PTH is not regulating Na^+-Pi cotransport under these conditions (6). The exact mechanism by which the PT cell is capable of 'sensing' and responding to dietary Pi independent of hormones or other circulating factors is poorly understood.

Alterations in the serum concentration of $1,25(OH)_2D_3$ stimulate renal BBM Na^+-Pi cotransport. However, it is not clear whether or not these effects are the direct effects

of $1,25(OH)_2D_3$ on PT cells, or are dependent on vitamin D-mediated changes to serum Ca and PTH concentrations (reviewed in (1)).

8.4 TYPE I Na^+-Pi COTRANSPORTERS (Npt1)

The first renal Na^+-Pi cotransporter cDNA identified, and capable of inducing Na^+-Pi cotransport in *Xenopus laevis* oocytes was termed *NaPi-1* (7). However, it soon became apparent that the type I Na^+-Pi cotransporter lacked the functional characteristics of renal Pi transport (8). The original *Npt1* cDNA was obtained from a rabbit kidney cortex library (7). Subsequently, other members of the NaPi-I family were cloned from human (9-11), rat (12,13), and mouse (14).

Immunoreactive Npt1 protein expression has been localized to the apical membrane of the brush border membrane (BBM) of the renal proximal tubule (14-18) (Figure 2) and to a lesser extent to the distal tubule. Npt1 accounts for approximately 13% of total mouse renal Na^+-Pi cotransporter mRNA (19). Npt1 has also been identified in the basolateral (sinusoidal) membrane of the liver (18,20,21), and in the brain (10,13). The physiological role(s) of Npt1 in these tissues is in need of further study.

Recently, electrophysiological studies have imposed bifunctional properties on Npt1. Busch *et al.* (22) showed that rabbit Npt1 mediated the transport of both Cl^- and other organic anions in an oocyte expression system, and Yabucchi *et al.* (21) have identified mouse Npt1-mediated hepatic transport of β-lactam antibiotics. While Cl^- conductance in the *Xenopus* oocyte system was time and dose-dependent, maximal Na^+-dependent Pi uptake was observed with low doses of injected Npt1 cRNA and within a short period of time (23). These observations suggest that the Npt1 product may

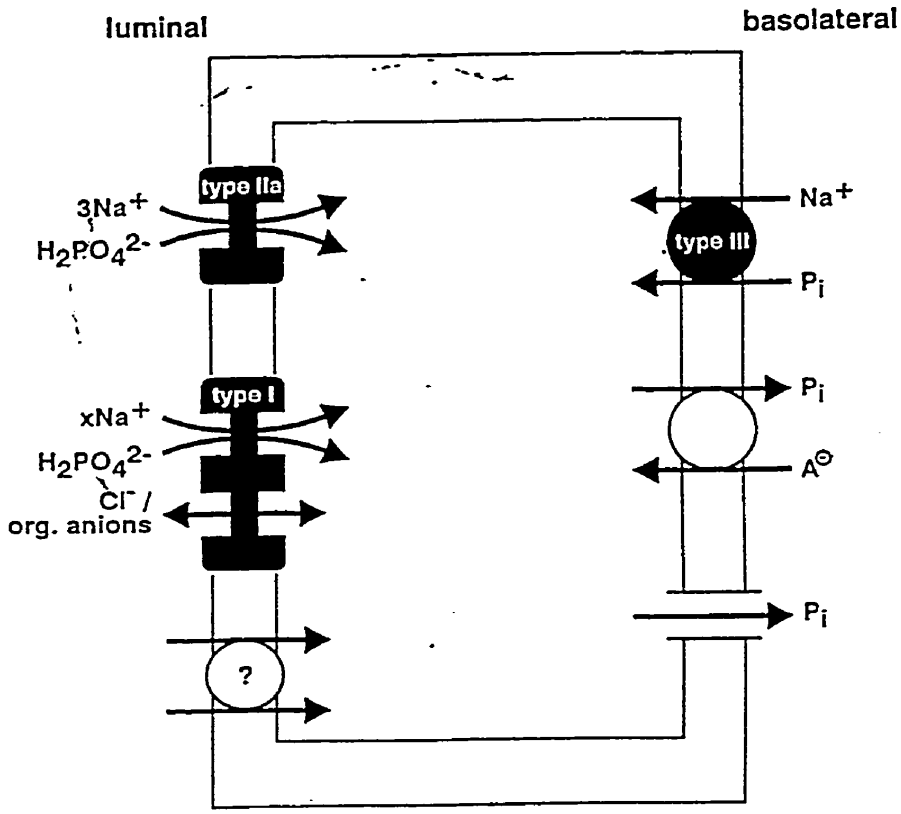

Figure 2: Schematic of the Na^+-Pi cotransporters present in the renal proximal tubular epithelial cell.

Three different Na^+-Pi cotransporters have been identified, however other, unidentified transporters may exist. The type I transporter transports Cl^- and organic anions in addition to Pi; the stoichiometry of Na^+:Pi is not clear. The type IIa transporter preferentially transports divalent Pi, in a Na^+:Pi ratio of 3:1. Both the type I and the type II transporters have been localized to the BBM of PT cells. The type III transporter is thought to be localized to the basolateral membrane and function as a housekeeping Pi transporter.

From: Murer, H., *et al.* 1999. *Am. J. Physiol.* Submitted.

modulate a Na^+-Pi transport that is intrinsic to the oocyte, and not function primarily as a Pi transporter.

Neither Npt1 expression, nor activity is regulated by dietary Pi intake (19,24), nor has Npt1 regulation by PTH been documented. Dietary Pi and PTH are two of the major modulators of renal Pi resorption, it is worth questioning the significance of Npt1 in managing Pi homeostasis. In the rat, liver and kidney Npt1 expression is regulated by fasting and streptozotocin-induced diabetes (20). In addition, primary cultures of rat hepatocytes show an increase in Npt1 mRNA abundance by glucose and insulin, and down-regulation by glucagon and cAMP (20). Li *et al.* suggest that as the extent of Pi resorption appears to correlate to the metabolic state of the cells, thus the role of Npt1 may be more crucial to glucose metabolism, than to Pi homeostasis (20).

8.5 TYPE II Na^+-Pi COTRANSPORTERS (Npt2)

8.5.1 Characteristics of Npt2

Following the identification of the type I Na^+-Pi cotransporter, a type II Na^+-Pi cotransporter cDNA was cloned from kidney cortex cDNA libraries of rat and of human. Expression in the *Xenopus* oocyte system produced Na^+-Pi cotransport characteristic of renal proximal tubular BBM Pi transport (25). Not only do type II Na^+-Pi cotransporters have a higher affinity for Pi than the type I, but they are pH-sensitive, are regulated by extracellular Pi concentrations, and have a strong dependence on extracellular Na^+ content (26), with the stoichiometry of Na^+:Pi binding at 3:1 (27).

Renal Npt2 cotransporters have been cloned from the human, rat (25), rabbit (24), mouse (28), bovine (29), opossum (30), carp, flounder (31), and zebrafish (Nalbant *et al.*

manuscript submitted). The Npt2 transcript is the predominantly expressed renal transcript, accounting for approximately 85% of all rat renal Na^+-Pi cotransporter transcripts (19), with only BBM PT localization in the murine kidney (32) (Figure 2). Apart from its localization to the BBM of the PT, Npt2 has been identified in the apical membrane of the small intestine of the flounder (33) and of the mouse (34), and recently, in the basolateral membrane of the activated osteoclast (35).

A recently identified intestinal Npt2 isoform led to the reclassification of the type II family of Na^+-Pi cotransporters into types IIa (Npt2a) and -IIb (Npt2b), based on similarities in transport characteristics, high homology in putative transmembrane coding regions, and differences in the C-terminus of the translated products (34). Additionally, the pH-dependence of the intestinal Npt2 isoform was opposite to that of the renal Npt2 isoform, i.e. as pH decreased, Na^+-Pi cotransport increased (34), consistent with their physiological environments. The type IIa family now consists of the renal isoforms of mouse, rat, rabbit, opossum kidney cells, and human, while the type IIb family consists of the bovine renal, the flounder renal and intestinal, *Xenopus laevis*, and mammalian intestinal type II isoforms (34). RT-PCR analysis has revealed the presence of *Npt2b* expression in the colon, liver, lung, kidney, and testis, in addition to the upper small intestine, where its expression is greatest (34).

Three alternatively spliced *Npt2a* cDNAs have been identified in a rat renal cDNA library, and designated *NaP-2α*, *-2β*, and *-2γ*. *In vitro* translated NaPi-2α and NaPi-2β cRNAs produce 36 kDa amino acid polypeptides, and *in vitro* NaPi-2γ translated cRNA produces a 29 kDa polypeptide (36). NaPi-2α (337 amino acids) shows little difference from the N-terminal portion of Npt2a; NaPi-2β contains 327 amino acids that

are identical to the N-terminal part of Npt2a, with a novel 146 amino acid C-terminus; and NaPi-2γ encodes the 268 amino acid C-terminal portion of Npt2a (36). C- and N-terminal antibodies, detected the expression of these isoforms in BBM vesicles derived from rat renal proximal tubular cells (36). Using a *Xenopus* oocyte system, the *in vitro* transcribed products of *NaPi-2α* and *NaPi-2γ* were shown to significantly inhibit the activity of coinjected *NaPi-2* (36). Furthermore, an antisense type II Na^+-Pi cDNA was isolated from the flounder, and localized to the kidney, intestine, and male and female gonads. However, direct protein-protein interaction could not be determined (37).

To date, there have been no *in vivo* functions identified for any of the 3 type IIa isoforms or the antisense NaPi-II transcript, and the physiological role of the intestinal type IIb isoform remains to be determined.

Although Npt2 was previously undetected in the bone, Gupta *et al.* localized a type IIa Na^+-Pi cotransporter to the basolateral membrane of active osteoclasts (35). In this orientation it is hypothesized that the transporter may supply Pi for the metabolic needs of the resorbing osteoclast (35).

The type IIa isoform is the most characterized of Npt2 isoforms, and the focus of this study. Unless otherwise indicated, use of the acronym Npt2, will refer to the type IIa isoform of Na^+-Pi cotransporters.

8.5.2 Physiological Regulation of Npt2

The major factors regulating Npt2 are PTH, dietary/extracellular Pi, and vitamin D. A variety of other hormonal and non-hormonal factors have been found either to directly regulate Npt2, or suggest the regulation of Npt2 due to the observed effects on renal proximal tubular Na^+-Pi cotransport.

Npt2 is the major target for regulation by dietary Pi. Pi deprivation causes an increase in BBM Na^+-Pi cotransport through an increase in Npt2 protein at the BBM. Both acute and chronic Pi deprivation are associated with a rapid increase in Npt2 protein at the apical membrane of the proximal tubule, but this increase is independent of increases in Npt2 mRNA (38-40). Studies characterizing the 5' end and promoter region of the *Npt2* gene confirm that there is no stimulation of the *Npt2* promoter under conditions of Pi deprivation (41). In addition, neither actinomycin D, an inhibitor of transcription, nor cycloheximide, an inhibitor of translation, prevent the adaptive response to low Pi diet (40). Nonetheless, an increase in Npt2 mRNA has been observed in numerous studies (39,42). Conversely, the existence of an intact microtubule network within the PT cell is necessary for increased BBM Npt2 expression in response to dietary Pi restriction. Cholchicine treatment of rats destroys this microtubule network in PT cells, and abolishes the rapid upregulation of Npt2 at the BBM (40). To summarize, the adaptive response to low Pi diet has been shown to be independent of *de novo* protein synthesis and dependent on the trafficking of existing Npt2 protein from vesicular storage to the BBM (40).

A diet high in Pi causes a decrease in Npt2 protein at the BBM, followed by a decrease in Npt2 mRNA abundance (39). However, the internalization and retrieval of Npt2 protein does not require an intact microtubule network *in vivo* (40,43), or in OK cells (44).

PTH is a potent inhibitor of BBM Na^+-Pi cotransport. PTH has direct actions on Na^+-Pi cotransport in the proximal tubule by inhibiting BBM expression of the Npt2 protein, thus decreasing the V_{max} of BBM Na^+-Pi cotransport (1-3). The decrease in V_{max}

can be attributed to the PTH-mediated endocytic retrieval (45-47) and subsequent lysosomal degradation (45,48,49) of Npt2. Recovery of BBM Na^+-Pi cotransport from the actions of PTH requires *de novo* protein synthesis (50).

In addition to PTH, a variety of other hormones appear to regulate the activity of Npt2. Thyroid hormone likely causes an increase in BBM Na^+-Pi cotransport through transcriptional mechanisms (51). Insulin-like Growth Factor-1 (IGF-1) also causes an increase in BBM Na^+-Pi cotransport, but likely through post-transcriptional mechanisms (41,52). Dexamethasone and Epidermal Growth Factor (EGF) elicit decreases in BBM Na^+-Pi cotransport through transcriptional (53) and post-transcriptional mechanisms (54,55), respectively.

1,25 dihydroxyvitamin D_3 ($1,25(OH)_2D_3$, or vitamin D) may also regulate Npt2, as observed by the increase in Npt2 mRNA, protein, and BBM Na^+-Pi cotransport in vitamin D deficient rats treated with $1,25(OH)_2D_3$ (56,57). Although the finding that $1,25(OH)_2D_3$ caused an increase in transcription of a construct consisting of the human *Npt2* promoter fused to a luciferase reporter gene (58) supports the notion of direct Npt2-vitamin D interactions, there is still the possibility that the actions of $1,25(OH)_2D_3$ on renal BBM Na^+-Pi cotransport are indirect.

8.5.3 The Ontogeny of Renal BBM Na^+-Pi Cotransport and Npt2

There is an age-related decline in tubular Pi reabsorption that is associated with an age-related decrease in Na^+-Pi cotransport at the BBM of PT cells. Following the cloning of the *Npt2* gene, and with the availability of Npt2 antibodies, it became apparent that decreased expression of BBM Npt2 was linked to the reduction in Pi reabsorption evident in older animals. When compared to 3-4 month old rats, 12-16 month old rats

experienced a 2-fold decrease in BBM Na^+-Pi cotransport in conjunction with a similar decrease in BBM Npt2 protein and mRNA abundance (59). Immunohistochemical staining of rat kidney sections for Npt2 indicate that the age-related decrease in Npt2 protein occurs both at the BBM and intracellularly (59). Studies in 3 week and 12 week old rats showed similar results. Npt2 protein was significantly greater in the younger rats than that of the elder ones, however, in this study the decrease in Npt2 mRNA was not observed (60). BBM Pi transport in the pre-weaned (i.e. prior to 21 days of age) rat is less clear. One early study demonstrated that BBM vesicles derived from 14-day-old rats were shown to have higher Na^+-Pi cotransport activity than those of 21-day-old rats (61). However, more recently it was suggested that suckling rats (12 days old) had 1.8-fold less BBM Na^+-Pi cotransport activity than weaned rats (24 days old), that was paralleled by decreased BBM Npt2 protein and Npt2 mRNA abundance (55).

There has been much suggestion for the existence of a growth-related Na^+-Pi cotransporter (46,60). Subtractive hybridization of Npt2 mRNA, or pretreatment of poly(A) RNA obtained from 3 week old rats with Npt2 antisense oligonucleotides failed to reduce the Na^+-Pi cotransport in *Xenopus* oocytes (46). Although an Npt2-related cDNA distinct from *Npt2* was identified in the kidney cortex of 3 week old rats (46,60), there are no follow-up reports regarding this cDNA clone.

8.6 TYPE III Na^+-Pi COTRANSPORTERS (Glvr-1, Ram-1)

The members of this family of Na^+-Pi cotransporters were originally identified as retroviral receptors for gibbon ape leukemia virus (*Glvr-1*) and for rat amphotropic virus (*Ram-1*). Both of them were found to induce Na^+-Pi cotransport in a *Xenopus* oocyte transport system (62). They are ubiquitously expressed in rat tissues, with the exception

of the spleen (63). In contrast to the specificity and abundance of expression observed for Npt1 and Npt2, and Glvr-1 is expressed throughout the murine kidney, in small quantities. Less than 1% of total renal Na^+-Pi cotransporter mRNA represents each of Glvr-1 or Ram-1 transcripts (19). Glvr-1 immunoreactive protein has been identified in crude kidney homogenates (64) however the cellular localization has not yet been established.

Glvr-1 and Ram-1 are regulated by the concentration of extracellular Pi in some systems, but not in others. Glvr-1 and Ram-1 expression is increased in Pi-deprived 208F fibroblasts (62), but not in Pi-deprived normal or hypophosphatemic (*Hyp*) mice (19). Chien *et al.* (65) attributed an increase in the mRNA abundance of Ram-1 in Pi-deprived human cell cultures to an increase in mRNA stability. However, there is no increase in Glvr-1 protein abundance observed in Pi-deprived OK cells (64). In all, there is still much to be learned about this family of Pi transporters. Their currently known features strongly suggest that they may be located basolaterally, and function primarily as housekeeping Pi transporters to maintain intracellular Pi concentrations (Figure 2).

8.7 VITAMIN D METABOLISM

8.7.1 Biochemistry of Vitamin D

The vitamin D precursor is synthesized in the skin by the action of ultraviolet B (UVB) radiation. Two essential hydroxylation steps are required to convert the inactive vitamin D precursor to a hormonally active metabolite. First, in the liver, the carbon-25 position is hydroxylated by 25-hydroxylase to form 25(OH)D. Subsequently, in the kidney, the enzyme 25-hydroxyD-1α-hydroxylase (1α-hydroxylase) contributes an additional hydroxyl group to form the active $1,25(OH)_2D_3$. Both 25(OH)D and

$1,25(OH)_2D_3$ can be hydroxylated to $24,25(OH)_2D_3$ by the enzyme 24-hydroxylase, and represent the first step towards degradation (Figure 3).

The main physiologic effect of $1,25(OH)_2D_3$ is to maintain serum Ca levels by modulating intestinal Ca absorption, Ca mobilization from the bone, and renal Ca reabsorption, mediating its actions through high affinity binding to the Vitamin D Receptor (VDR). In order to preserve extracellular Ca concentration within a normal range, the production and degradation of $1,25(OH)_2D_3$ are tightly regulated via the expression of 1α-hydroxylase and 24-hydroxylase. Hypophosphatemia stimulates the renal conversion of 25(OH)D to $1,25(OH)_2D_3$ by 1α-hydroxylase. $1,25(OH)_2D_3$ is self-regulating in that it increases the expression 24-hydroxylase. 24-hydroxylase expression is also modulated by PTH (66), and by insulin (67).

8.7.2 Actions of 1,25-dihydroxyvitamin D in the Intestine

As one of the major sites of Ca influx, the intestine is the primary target of $1,25(OH)_2D_3$ to increase Ca absorption in order to maintain blood Ca levels. Normally, approximately 30% of the daily dietary Ca intake is absorbed in the intestinal tract through a three step transepithelial process: apical Ca entry, cellular translocation by $1,25(OH)_2D_3$-dependent calbindins, and extrusion at the basolateral membrane into the circulation by high affinity Ca^+-ATPase and Na^+-Ca^+-exchangers (68). The efficiency of the jejunum and ileum to absorb Pi is also increased in response to $1,25(OH)_2D_3$ (69,70).

Recently an apical Ca influx channel (ECaC) was identified and its tissue distribution, immunolocalization, and functional characterization determined (71). The major site of expression occurs in $1,25(OH)_2D_3$-responsive epithelia, including the upper small intestine where it colocalizes with the expression of calbindin-D_{9k}, and the distal

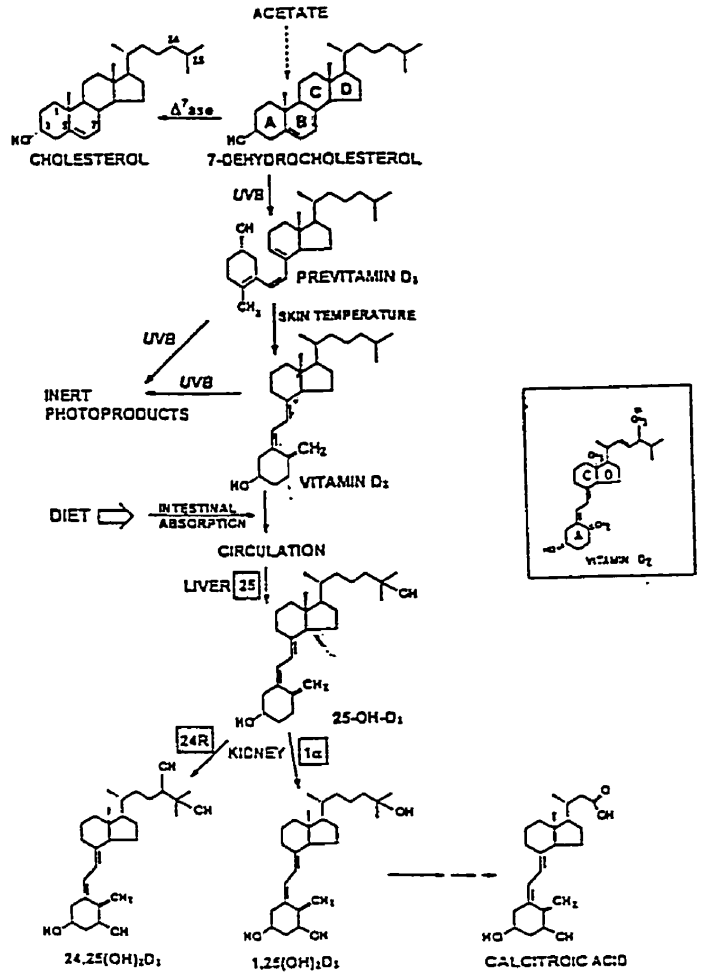

Figure 3: The biochemistry of vitamin D. *Boxed letters and numbers denote specific enzymes.*

UVB transforms 7-dehydrocholesterol to previtamin D_3. Vitamin D-25-hydroxylase [25] hydroxylates vitamin D_3 to produce 25-hydroxyvitamin D [25(OH)D]. In the kidney 25-hydroxyD-1α-hydroxylase [1α] converts 25(OH)D to $1,25(OH)_2D$, the biologically active form of vitamin D. Both 25(OH)D and $1,25(OH)_2D_3$ can be 24-hydroxylated by 24-hydroxylase [24R] as the initial step towards degradation.

From: Holick, MF., 1996. Vitamin D: Photobiology, Metabolism, Mechanism of Action, and Clinical Applications. In: Favus, MJ. (ed) *Primer on the Metabolic Bone Diseases and Disroders of Mineral Metabolism.* Lippencott-Raven, Philadelphia, pp 74-81.

convoluted tubule, connecting tubule, and cortical collecting duct in the nephron where it colocalizes with calbindin-D_{28k} (71).

8.8 SKELETAL DEVELOPMENT

8.8.1 Intramembranous and Endochondral Bone Formation

Classically, there are 2 modes of bone development: intramembranous (flat bones, including the calvaria and clavicle), and endochondral ossification (long bones and vertebrae). The primary difference between the two is the absence or presence of the cartilage scaffold that is observed in endochondral bone formation, but not in intramembranous. The focus of this introduction will be on endochondral bone formation.

Skeletal development is dependent on the appropriate differentiation, activity and interaction of 3 bone cell types: chondrocytes, osteoblasts, and osteoclasts. Chondrocytes and osteoblasts are derived from common mesenchymal precursors and possess the physiological function of forming cartilage, or bone, respectively. Osteoclasts are derived from macrophage precursors, and are involved in the process of bone resorption.

A long bone is composed of 3 distinct regions (Figure 4). The extremities (epiphyses) are divided from the midshaft (diaphysis) by a developmental zone (metaphysis). In the growing bone, the epiphysis and the metaphysis represent independent regions of ossification that are delimited by the epiphyseal cartilage (growth plate). Bones lengthen as a result of a series of coordinated events starting with chondroblast proliferation and matrix synthesis, followed by matrix calcification. Subsequently, osteoclasts are activated, and partially resorb the cartilage matrix, the remnants of which are covered by osteoblast-mediated, collagen deposition that will

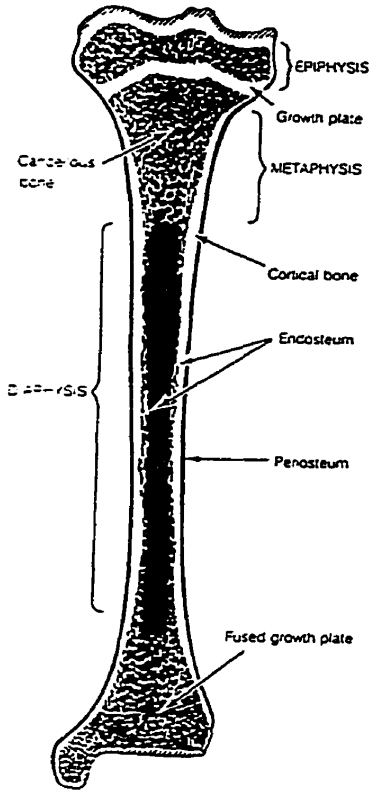

Figure 4: Schematic of a longitudinal section of a growing long bone.

A growing long bone shows widening at either end (the epiphyses), with a narrow tube in the mid-shaft (the diaphysis), and a developmental section between them (the metaphysis). In the growing bone, the epiphysis and the metaphysis are separated by the growth plate and is responsible for the longitudinal growth of a bone.

From: Jee WSS., 1983. The skeletal tissues. In: Weiss, L. (ed) *Histology, Cell, and Tissue Biology*. Elsevier Biomedical, New York, pp 200-255.

eventually mature into woven bone. The trabeculae formed with the completion of the first Activation-Resorption-Formation (ARF) cycle are called primary spongiosum. Deeper within the growth plate, a 2nd ARF cycle occurs, where woven bone is resorbed by osteoclasts and replaced by lamellar bone, generating mature trabeculae (secondary spongiosum). The distinction between woven and lamellar bone lies in the rate of bone formation. Woven bone consists of the random orientation of collagen fibres that result from rapid bone formation, whereas lamellar bone contains organized collagen fibres to maximize the density of collagen.

During the rapid deposition of collagen, osteoid seam width increases, remains constant during collagen maturation and mineralization, and disappears once collagen synthesis ceases and mineralization continues. The mineralization process involves the precipitation of Ca and Pi in the form of hydroxyapatite crystals onto collagen fibres. Defects of bone remodeling can be determined histologically by measuring osteoid seam width, mineral apposition rate, and mineralizing surface, among other parameters.

8.8.2 Regulation of Bone Remodeling

Circulating and local growth factors and hormones influence bone metabolism, acting directly or indirectly on bone cells to alter bone formation and resorption. Vitamin D stimulates bone resorption, although the mature osteoclast does not possess a VDR. The action of $1,25(OH)_2D_3$ on osteoclasts is thought to be mediated via the osteoblast VDR and osteoblast-osteoclast interactions. For example, studies in VDR knockout mice indicate that the absence of a VDR in osteoblasts prevents the stimulation of osteoclast formation (72). Abnormalities in bone development can be observed in states of inadequate or excessive circulating $1,25(OH)_2D_3$, although the effects may be secondary

to the action of $1,25(OH)_2D_3$ on other tissues, and the alteration of extracellular Ca and Pi concentrations.

States of hypovitaminosis D due to inadequate vitamin D, or mutations in the VDR result in rickets and osteomalacia that are characterized by inadequate bone mineralization due to the lack of Ca deposition, or bone resorption, and widening of the osteoid seams (reviewed in (73)). Conversely, the administration of high doses of vitamin D to mice results in an increase in mineral apposition rates and a reduction in the amount of osteoid, associated with an increase in the number of osteoclasts and osteoclastic resorption (74).

8.8.3 Expression of Glvr-1, Osteocalcin, and Phex in Murine Bone

The pH-dependence of Na^+-Pi cotransport in osteoblasts resembles the pH profile of the Glvr-1 Na^+-Pi cotransporter (75). Our laboratory recently identified the presence of Glvr-1 mRNA in bone (19). More recently, Glvr-1 has been localized to early hypertrophic chondrocytes and slightly more mature cells, but was not identified in either fully differentiated hypertrophic chondrocytes, or in osteoblasts (76). Its physiological contribution as a Pi transporter in bone is not fully characterized, however there is evidence to suggest its involvement in matrix calcification (76).

Osteocalcin is the most abundant non-collagenous protein produced by mature osteoblasts (77). Osteocalcin expression coincides with matrix deposition, and mineralization in murine endochondral bone formation (78-80), suggesting that it is involved in regulating matrix mineralization (81,82).

The murine *osteocalcin* gene cluster contains 3 genes, 2 of which (*og1* and *og2*) are expressed only in the bone. The third gene of the cluster, *org* (osteocalcin related

gene) is expressed in the kidney, but not in the bone (79). Mice lacking both the *og1* and *og2* genes show greater bone mass and bones of improved functional quality at 6 months of age, although the altered bone phenotype is absent prior to this age (83). By studying these osteocalcin-deficient mice (osc^{ml}/osc^{ml}), Ducy and colleagues revealed that osteocalcin limits the rate of bone formation (83). Although 6 month old, osc^{ml}/osc^{ml} mice had increased rates of bone formation, there was no increase in osteoblast number implying that each osc^{ml}/osc^{ml} osteoblast was secreting more matrix that those in the normal mice (83). In contrast to the human osteocalcin gene, murine osteocalcin gene expression does not appear to be increased by $1,25(OH)_2D_3$ (84-86).

Mutations in *Phex* have been identified as the cause of X-linked hypophosphatemic rickets in humans and in the hypophosphatemic mouse homologues, *Hyp* and *Gy* (see (87) for review). Delayed growth, rickets and osteomalacia, hypophosphatemia, and defective renal Pi resorption and vitamin D metabolism characterize the disease. The exact physiological function of Phex remains elusive. The name Phex signifies a Phosphate-regulating gene with homology to endopeptidases on the X chromosome. The gene product is thought to be involved in the activation/degradation of a phosphate regulating peptide hormone that also plays a role in skeletal development.

Phex mRNA has been identified in mouse bones (88-90); bones and teeth were determined to be the major sites of Phex mRNA expression in the developing mouse by *in situ* hybridization (78). Phex protein has recently been identified in osteoblasts, osteocytes, and odontoblasts but not in osteoblast precursors (91). Its expression has

been shown to correlate with the beginning of matrix deposition in bones (78), and to be down-regulated by $1,25(OH)_2D_3$ in murine osteoblast cells (92).

8.9 THE Npt2 KNOCKOUT MOUSE

In order to determine the importance of *Npt2* to Pi homeostasis, our laboratory recently generated an *Npt2* gene knockout (Npt2 KO) mouse by ablating exons VI to IX of the *Npt2* gene through homologous recombination (Figure 5a)(93). *Npt2* gene ablation results in a 75% reduction in renal Na^+-Pi cotransport at the BBM of the PT, as indicated by BBM Pi uptake studies (93). Mice homozygous for the disruption are phosphaturic and hypophosphatemic and exhibit the appropriate increase in serum $1,25(OH)_2D_3$, which in turn leads to hypercalcemia and hypercalciuria, and depressed serum PTH levels (Figure 5b) (93).

Aside from the obvious biochemical abnormalities, the mice show a distinct and complex bone phenotype that varies with aging. At weaning, Npt2 KO mice have poorly developed trabecular structure and delayed secondary ossification in the epiphysis in comparison to wild-type (WT) mice. Conversely, by 115 days of age, Npt2 KO mice display a significant increase in trabecular number that is not observed in WT mice (93).

The *Hyp* mouse represents another model of renal Pi wasting disease (reviewed in (87)). While these mice have a large 3' deletion of the *Phex* gene, they also show a defect in renal BBM Na^+-Pi cotransport manifest by a $\geq$50% decrease in BBM Npt2 protein and mRNA abundance in comparison to normal mice (19,94-96). In spite of the alterations to BBM Npt2 expression observed in *Hyp* mice, these mice show an increase in the V_{max} of renal Pi transport when they are Pi-deprived. Although the BBM adaptive increase is blunted in comparison to Pi-deprived normal mice, there is a parallel increase

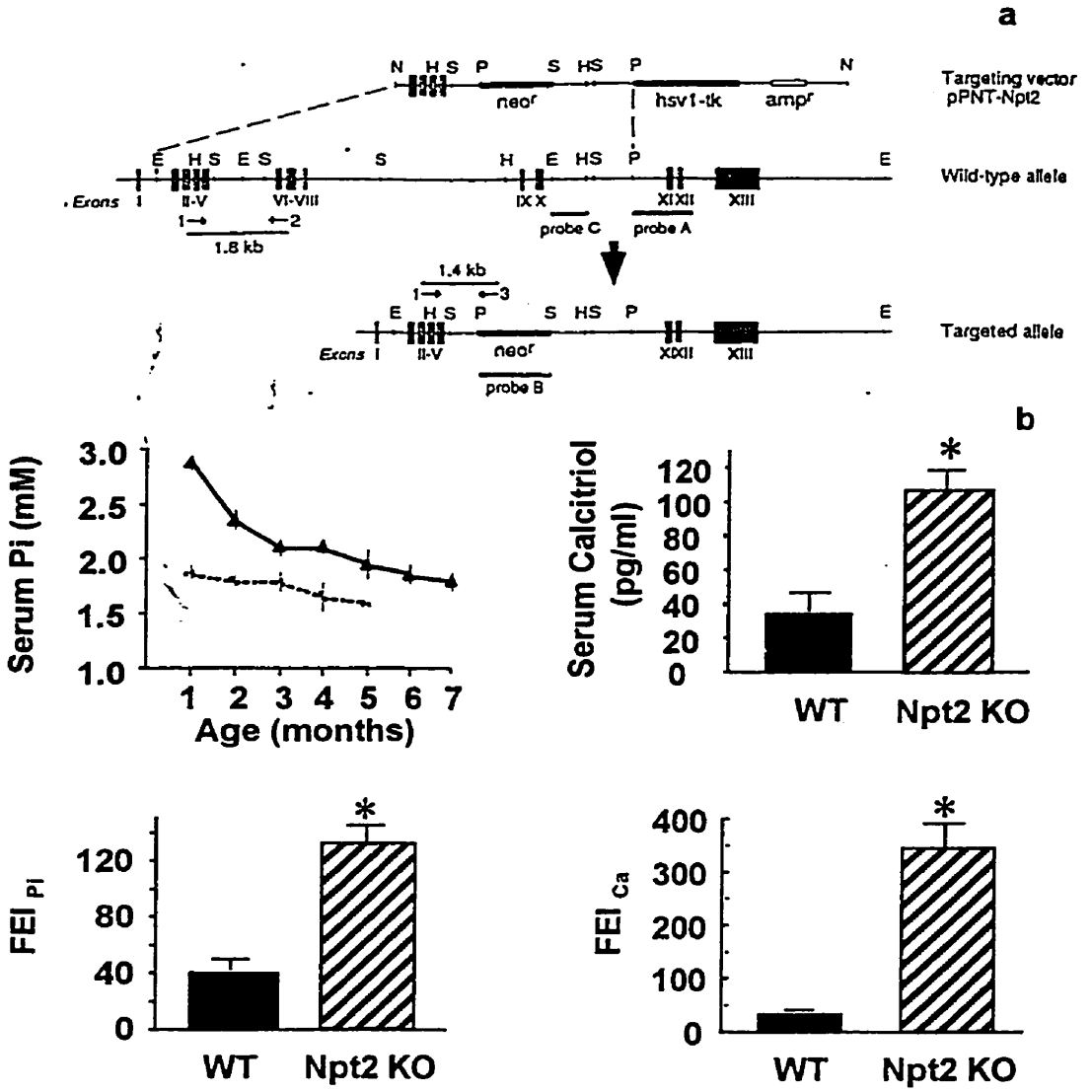

Figure 5: (a) Strategy for *Npt2* gene ablation. The top line represents the pPNT-Npt2 targeting vector, the middle line the wild-type allele, and the bottom line the targeted allele. Exons are numbered and represented by grey boxes. The pPNT-Npt2 targeting vector and the targeted allele contain the *neo*^{r} gene. Numbers (with arrows) 1, 2, and 3 represent the primers 3F, 4R, and PGKR, respectively, used in the PCR genotyping. Expected sizes of the amplified fragments are indicated. (b) Summary of the biochemical features of WT (solid line or filled bars) and Npt2 KO (dashed line or hatched bars) mice. Results are means ± SEM. *, $p<0.05$ for *t* test comparing Npt2 KO with WT mice. FEI indicates the ratio between urine Pi or Ca (mM)/[urine Cr (mM) x serum Pi or Ca (mM)] of 1-month-old animals. Serum calcitriol assays represent 1- to 3-month-old mice.

From: Beck, L. *et al.*, 1998. *Proc. Natl. Acad. Sci.USA* 95:5372-5377.

in BBM Npt2 protein and renal mRNA abundance that leads to levels comparable to those of normal mice (42). The discrepancies in the adaptive response mechanisms between the normal and the *Hyp* mice to Pi restriction may be attributable to differences in vitamin D metabolism.

The disturbed vitamin D metabolic response to hypophosphatemia is one of the distinguishing features of XLH and *Hyp* mice (97,98). Recall that the normal vitamin D metabolic response to hypophosphatemia is to stimulate the production of $1,25(OH)_2D_3$. While the Npt2 KO mouse exhibits elevated levels of circulating $1,25(OH)_2D_3$, *Hyp* mice, which are also chronically hypophosphatemic, have normal levels of serum $1,25(OH)_2D_3$ (97), due to low levels of 1α-hydroxylase activity (99) and increased catabolism of $1,25(OH)_2D_3$ by 24-hydroxylase (100,101). Additionally, when *Hyp* mice are further Pi-deprived by altering their dietary Pi intake, $1,25(OH)_2D_3$ production is inhibited (102,103). Neither the vitamin D response, nor the renal BBM response of the Npt2 KO mouse to dietary Pi deprivation is known.

The biochemical features of the Npt2 KO mouse are similar to those of patients with hereditary hypophosphatemic rickets with hypercalciuria (HHRH). Tieder *et al.* first described HHRH in a Bedouin kindred in 1985 (104). The shared features of both the Npt2 KO mouse and HHRH include hypophosphaturia, hypophosphatemia, hypercalciuria and elevated levels of serum $1,25(OH)_2D_3$. However, HHRH is further characterized by rickets, short stature, and increased GI absorption of both calcium and phosphorous (104). The bone phenotype of the Npt2 KO mouse differs, and altered Pi and Ca absorption in the GI has not been investigated.

8.10 AIM OF THE PRESENT STUDY

Recognizing that Npt2 represents the major renal Na^+-Pi cotransporter in the kidney, and that the impact of hypophosphatemia on skeletal development can be substantial, it was of utmost interest to determine the consequences of Npt2 gene ablation to Pi homeostasis and bone development. Renal Pi transport and its regulation is a well described study area. This allowed for an effective evaluation of Npt2 gene ablation on the characteristics of renal Pi transport. The goals of the study were to:

(1) determine how age and *Npt2* gene ablation affect renal Na^+-Pi cotransporter gene expression, and renal BBM Na^+-Pi cotransport;

(2) evaluate the response of the Npt2 KO mouse to dietary Pi restriction as compared to the WT mouse;

(3) analyze the effect of age and *Npt2* gene ablation on certain features and effects of vitamin D metabolism as they pertain to Pi homeostasis;

(4) examine the effects of age and *Npt2* gene ablation on a variety of bone histological and histomorphometrical parameters in an effort to improve our understanding of the novel bone phenotype observed in the Npt2 KO mouse.

9 MATERIALS AND METHODS

9.1 Npt2 MOUSE COLONY

WT and Npt2 KO mice were generated and raised in our laboratory. Mice homozygous for *Npt2* gene ablation lack exons VI to X in both *Npt2* alleles, as a result of homologous recombination of an *Npt2* targeting vector with the wildtype allele (see Figure 5a). The construction of the *Npt2* gene targeting vector is described in detail in Hewson (105) and the generation of the Npt2 KO mice is described in depth in Beck *et al.* (93). We generated WT, heterozygous, and Npt2 KO mice by breeding male and female Npt2 heterozygote mice.

9.2 COMPOSITION OF MOUSE DIETS

The mice were maintained on a Rodent Laboratory Chow (5001, Purina Lab Chow) unless otherwise indicated. This diet contained 0.6% Pi, 1.0% calcium, 4.5 UI vitamin D_3/g.

Pregnant mice were isolated until the pups had been weaned (21 days). Throughout the pregnancy and until weaning, the mothers were maintained on a Mouse Breeder Diet (Harlan Teklad, 8626), composed of 1.23% Pi, 1.36% Ca, and 6.0 UI/g vitamin D_3.

Low phosphate diet experiments were performed using a control Pi diet and a low Pi diet. The control diet was composed of 1.0% Pi (Harlan Teklad 86129), while the low Pi diet consisted of 0.02% Pi (Harlan Teklad 86128). Apart from the Pi content, both diets were identical and contained approximately 1.0% Ca.

9.3 DIET MANIPULATION

9.3.1 Fast and Oral Calcium Load Test

Urine Ca-, Pi-, and Mg/Cr ratios were determined in both WT and Npt2 KO mice fed our control diet, and were referred to as *baseline*. Mice were then fasted overnight (~18 hours), at which point an additional urine sample was obtained (*fasting*). Following the fast, the normal diet was returned, while simultaneously, the drinking water was supplemented with a 1% calcium gluconate solution for 24 hours. At this point a 3rd urine sample was obtained (*Ca supplement*). This modified test provides an indirect measure of intestinal Ca absorption (104,106).

9.3.2 Dietary Phosphate Restriction

45-day-old mice (± 7 days) were fed either control or low phosphate diets for 5 days. Following phosphate restriction, the mice were sacrificed and tissue samples were collected as described subsequently (section 7.7).

9.4 EXTRACTION OF DNA FROM MOUSE TAIL TISSUE

Mice were genotyped by PCR amplification of genomic DNA obtained from tail tissue. Genomic DNA was extracted from a 0.5 cm piece of tail cut from each mouse at approximately 21 days of age. Each sample of tail tissue was incubated in 1.5 ml microfuge tubes with 300 µl of digestion buffer (100 mM NaCl; 50 mM Tris-HCl, pH 8.0; 1% SDS; 50 mM EDTA, pH 8.0). Proteinase K (10 mg/ml) was added to a final concentration of 100 µg/ml, and the samples incubated for 2 hours at 50°C, followed by an overnight incubation at 37°C. Following digestion, LiCl was added to a final concentration of 2.5M, and the digestion mixture shaken thoroughly for 1 minute by

hand. One volume of chloroform was added, and the samples were shaken rapidly on a clinical rotator (Fisher Scientific) for 30 minutes. The samples were centrifuged 15 minutes, at 15,000 rpm in a bench-top microfuge. 500 µl of the upper phase was removed and placed in a new microfuge tube. 2 volumes of ice-cold 100% EtOH were added and the tube inverted several times to precipitate the DNA. The DNA was pelleted by centrifuging at 15,000 rpm for 2-5 minutes, the supernatant discarded and the DNA pellet washed briefly in 70% EtOH. The ethanol was removed and the pellet allowed to air dry. The pellets were resuspended in 25-100 µl of water (depending on pellet size), and allowed to dissolve.

9.5 POLYMERASE CHAIN REACTION (PCR) OF THE MURINE Npt2 GENE

The mice were genotyped by PCR amplification of genomic DNA obtained from tail tissue, using *Taq* polymerase (GIBCO-BRL, Life Technologies) and 3 primers [sense primer 3F (5'-TGC CCA GGT TGG CAC GAA GC-3') in exon 4 of *Npt2*, antisense primer 4R (5'-AGT CCT GTC CCC TGC CTG CA-3') in exon 6 of *Npt2*, and antisense primer PGKR (5'-TGC TAC TTC CAT TTG TCA CGT CC-3') in the *neo*^{r} gene cassette] as described previously (93). The expected sizes of the amplified products are 1.8 kb for the normal allele (primers 3F and 4R) and 1.4 kb for the disrupted allele (primers 3F and PGKR). The reagents for the PCR reaction were obtained from GIBCO/BRL. The conditions for the PCR reaction were: 1x PCR buffer, 1.3 mM $MgCl_2$, 0.1 mM dNTPs, 0.2 µM each sense and antisense primers, 0.3 µl Taq polymerase. 0.5-2 µl of the resuspended genomic DNA solution was added to each PCR reaction, followed by a mineral oil overlay. The reaction was performed in a DNA Thermal Cycler (Perkin Elmer Cetus) with the following program: initial denaturation (3 mins., 94°C), 30 cycles

of denaturation, annealing and extension (1 min, 94°C; 1 min, 62°C; 2 min, 72°C), and a final, long extension step (7 min, 72°C).

9.6 AGAROSE GEL ELECTROPHORESIS

PCR fragments were visualized on a 1% TAE (Tris-Acid EDTA) agarose gel with 0.12 µg/ml ethidium bromide (EtBr) by the method of Sambrook *et al.* (107). DNA loading buffer (10x) was added to all DNA samples to a final concentration of 1x. Samples were loaded into the gel and electrophoresed in 1x TAE running buffer at 75-120 volts, until the bromophenol blue dye front had migrated 50-75% of the gel length. The gels were examined using a Spectroline transilluminator, and photographed with a Polaroid Camera using Polaroid type 52 instant sheet film.

9.7 URINE, BLOOD, AND TISSUE COLLECTION

Urine, blood, kidney, and bone were routinely collected from each mouse. Urine was collected on a clean surface using a sterile pipette or syringe, placed in a 1.5-ml microfuge tube and stored at –20°C until further use. Serum, kidney and bone samples were collected following anaesthesia of the mouse with halothane, supplied via a Fluotec 3 machine (Benson Medical Industries, Inc.). The mice were decapitated, and blood collected into a capillary blood microvette CB 1000 S, containing gel/clot activator (Sarstedt). The tubes were shaken briefly by hand and placed on ice. The microvettes were centrifuged at 9,000 rpm using a bench-top microfuge for 1-2 minutes within 1 hour of collection. The serum was removed from the tube and placed in a 1.5-ml microfuge tube and stored at –20°C for future use. To remove the kidneys, the abdominal cavity of the mice was opened and the kidneys extracted, decapsulated, and placed on dry ice to

quick-freeze them. Similarly, both long bones (femur and tibia) of the mouse were removed and scraped clean of tissue, and quick-frozen. Both kidneys and bones were stored at –80°C until future use.

9.8 DETERMINATION OF SERUM AND URINE PHOSPHORUS [CALCIUM, MAGNESIUM AND CREATININE (Cr)]

Serum Pi, Ca and Mg and urine Pi, Ca, Mg, and Cr were determined using kits obtained from Stanbio (procedure numbers: 0830, 0150, 0130 and 0400, respectively) according to the package insert. Each procedure requires that the sample be diluted with the provided solution. The concentration of Pi, Ca, Mg, or Cr in the solution was determined using a spectrophotometer (CARY 210, Varian). Urine Pi, Ca, and Mg concentrations are expressed in relation to the urine Cr concentration. The fractional excretion indexes (FEI) of Pi, and of Ca were calculated as follows:

urine Pi or Ca (mM)/[urine Cr (mM) x serum Pi or Ca (mM)].

9.9 PREPARATION OF TOTAL RIBONUCLEIC ACID (RNA) FROM TISSUE

Total RNA was isolated from kidney or bone using TRIzol reagent according to the manufacturer's specifications (GIBCO BRL, Life Technologies, Inc.). Frozen tissues were weighed and ground in liquid N_2. Then, the tissues were homogenized in 15-ml polypropylene tubes (Falcon) in 1 ml of TRIzol per 50-100 mg tissue using a Polytron homogenizer (Brinkman). The homogenized solution was incubated at room temperature for 5 minutes, transferred to 1.5-ml microfuge tubes, and centrifuged at 12,000g for 10 minutes to remove insoluble materials. The supernatant was then removed and placed in clean microfuge tubes and 0.2-ml of chloroform added. The samples were shaken

vigorously for 15 seconds and incubated at room temperature for 2-3 minutes, then centrifuged at 10,000g for 15 minutes. 0.5-ml of the aqueous phase was removed and transferred to another microfuge. The RNA was precipitated by adding 0.5-ml of isopropanol to each tube and incubating at room temperature (or lower) for 10 minutes. The RNA was pelleted by centrifugation at 10,000g for 10 minutes, and the supernatant discarded. The pellet was washed three times with 75% EtOH, and the pellets were air dried. All reagents and materials used were RNase free, and centrifugation was performed at 4°C (Centrifuge 5403, eppendorf). The RNA was dissolved in 50-100 µl of DEPC water to a final concentration of 3-7 µg/µl. RNA concentration was measured on a spectrophotometer (Spectronic 1001 plus, Milton Roy) at 260 nm. The purity of the RNA sample was estimated by determining the 260 nm/280 nm ratio.

9.10 PREPARATION OF RIBOPROBES

Riboprobes for mouse Npt1, Npt2, Glvr-1, Ram-1, ß-actin, Phex, Osteocalcin, 1α-hydroxylase, and 24-hydroxylase were prepared by transcription of subcloned cDNA fragments for the respective genes, using either T3 or T7 RNA polymerases and [α-^{32}P]UTP (ICN, Mississauga, ON) as described previously (19) (Table 1).

Table 1.
Specifics of riboprobes used in this study.

Gene of interest	[α-^{32}P]UTP (cpm)	Polymerase	Probe size (bp)	Size of protected fragment	Amount of RNA (μg)	Amount of RNase T1 (units)	Approximate Exposure time
Npt1 (kidney)	500,000	T7	500	430	5	200	3 hours
Npt2 (kidney)	500,000	T7	471	351	5	200	3 hours
Glvr-1 (kidney)	500,000	T3	593	492	20	40	3 days
Glvr-1 (bone)	100,000	T3	593	492	10	200	1 day
Ram-1 (kidney)	500,000	T7	587	507	20	40	3 days
Osteocalcin (bone)	100,000	T3	520	420	10	200	1 day
h'Phex (bone)	100,000	T7	397	317	20	200	1 day
1α-hydroxylase (kidney)	100,000	T7	N/A	494	20	62	3 days
24-hydroxylase (kidney)	100,000	T3	450	376	20	62	3 days

9.11 RIBONUCLEASE PROTECTION ANALYSIS

The ribonuclease protection assay was performed as previously described (19,93). Total RNA was hybridized with the appropriately labeled riboprobes at 50°C for 18 hours and treated with RNaseT1 for 1 hour at 30°C. The protected fragments were precipitated, heat denatured, and electrophoresed on 6% denaturing polyacrylamide gels. The gels were dried and exposed to a PhosphorImager screen for quantification of radioactive signals using PhosphorImaging software (Fuji) under conditions where linearity is achieved, and to Kodak Biomax MR1 film for photography. Refer to Table 1 for the specific parameters of each riboprobe.

9.12 PREPARATION OF RENAL BRUSH BORDER MEMBRANE VESICLES

Renal BBM vesicles were prepared from kidney cortex by the $MgCl_2$ precipitation method as described previously (94) and used for both transport studies and Western blot analysis. One kidney from each of 3-5 mice was used for each BBM vesicle preparation. Frozen kidneys were thawed in 0.9% ice cold NaCl, hemisectioned, and the medulla removed. Kidneys were weighed and homogenized with 10x volume of Buffer A (10 mM mannitol, 2 mM HEPES/Tris, pH 7.4) with a Teflon homogenizer (Jumbo Stirrer, Fisher Scientific) while on ice. 100 µl of the crude kidney homogenate was reserved for an alkaline phosphatase assay and to determine protein concentration by Lowry assay. The remaining kidney homogenate was transferred to glass erlenmyers. 1 M $MgCl_2$ was added to a final concentration of 0.01 M (1/83.3 of the volume) and the solution stirred for 15 minutes, on ice. The homogenate was then centrifuged at 3,500 rpm for 10 minutes at 4°C. The supernatant was retained and centrifuged at 12,000 rpm for 10 minutes at 4°C. The pellet was resuspended in Buffer B (300 mM mannitol, 2 mM HEPES/Tris, pH 7.4) and centrifuged at 12,500 rpm for 10 minutes at 4°C. This wash was repeated, and the suspension centrifuged at 13,000 rpm for 20 minutes at 4°C. The final pellet was resuspended in 0.5 ml of Buffer C (300 mM mannitol, 10 mM HEPES/Tris, pH 7.4) per gram of kidney. 20 µl of this suspension was diluted ¼ for alkaline phosphatase and Lowry assays. BBM protein concentration was assayed using the method by Lowry *et al.* (108), and the enrichment of BBM was determined by relating the alkaline phosphatase specific activity of the BBM to that of crude kidney homogenate. BBMs were typically enriched 7-10 fold. BBMs were used in Pi and

glucose uptake experiments within 24 hours and stored at –80°C prior to Western protein analysis.

9.13 BRUSH BORDER MEMBRANE TRANSPORT

The uptakes of Pi (100 μM) and glucose (10 μM), each performed in quadruplicate, were measured at 6 sec (initial rate) and 90 min (steady state) in incubation medium containing either 100 mM NaCl or 100 mM KCl (plus, 100 mM mannitol, 10 mM HEPES/Tris, pH 7.4, 0.1 mM ^{32}P K_2HPO_4 (Dupont NEN) (6 μCi/ml), 0.01 mM ^{3}H-glucose (Dupont NEN)(8 μCi/ml)) by rapid filtration technique (94). Uptake was terminated by adding 9 ml stop solution (100 mM KCl, 100 mM mannitol, 10 mM HEPES/Tris, pH 7.4, 10 mM $NaAsO_4$, 1 mM Na-azide. Filters were rinsed quickly with stop solution and inserted in vials with Ecolume to measure radioactive counts.

9.14 SDS POLYACRYLAMIDE GEL ELECTROPHORESIS AND WESTERN ANALYSIS

BBM proteins (10-40 μg) were fractionated on 10% SDS-PAGE gels according to the method of Laemmli (109), transferred to supported nitrocellulose membranes (Hybond-C extra, Amersham), and probed either sequentially, or simultaneously with a rabbit polyclonal anti-rat Npt2 antibody (gift of H. Murer, University of Zurich) and a monoclonal antibody raised against the α-subunit of rat renal endopeptidase-24.18 (meprin) (kindly provided by Dr. P. Crine, Université du Montréal) as described previously (42). Immunoblotting was also performed with a rabbit polyclonal antibody raised against a C-terminal peptide of rabbit Npt1 (15) (gift of H. Murer) and a rabbit

polyclonal antibody raised against a Glvr-1 peptide (64) (gift of Dr. R. Beliveau, Université de Québec à Montréal). Primary antibodies were visualized using an enhanced chemiluminescence kit (ECL) (Amersham Pharmacia Biotech) and exposed to Kodak Biomax MRI film. Protein abundance, relative to that of meprin, was estimated using PhosphorImager analysis of scanned images.

9.15 HISTOCHEMICAL AND HISTOMORPHOMETRIC ANALYSIS OF MURINE BONE SAMPLES

Animal breeding, injections, tissue samples, and some sample processing was performed in our laboratory, while embedding and sectioning of the samples, bone histology and histomorphometry measurements were performed by Drs. Keith Hruska and Anandarup Gupta of the University of Washington, St. Louis, MO.

To estimate the mineral apposition rate (MAR) and the bone formation rate (BFR), 25- and 113-day-old WT and Npt2 KO mice were injected intraperitoneally with 20 mg/kg of calcein, 7 and 2 days before sacrifice. The calcein solution was made up to a concentration of 4 mg/ml by dissolving 20 mg of calcein (Sigma #C-0875) in a 2% sodium bicarbonate (Sigma #S-5761) solution. The tibia and femur were dehydrated in 70% ethanol for 24 hours, followed by 100% ethanol, and subsequently embedded in plastic. Bone histomorphometry was performed in the metaphyseal region, distal to the growth plate, in 5 μm thick, longitudinal sections cut from these bones. To estimate BFR, double-labeled and single labeled areas were traced, and BFR was calculated as described previously (110,111).

In addition, femur and tibia were collected from WT and Npt2 KO mice, cleaned of tissue, and immediately fixed in 4% phosphate buffered paraformaldehyde, then

decalcified in 14% EDTA for 10-14 days. The bones were washed in 50, 70, and 90% ethanol and embedded in paraffin. Longitudinal sections 5 μm in thickness were cut, and stained with toluidine blue, or for tartrate-resistant acid phosphatase (TRAPase) to identify osteoclasts.

Trabecular number (Tb.N), trabecular perimeter (Tb.Pm), trabecular area (Tb.Ar), osteoclast index (nOC/TA), % labeled surface (%L), eroded perimeter (E.Pm), MAR, mineralizing surface (MS), and BFR were determined in both WT and Npt2 KO mice at 25- and 115 days of age. These abbreviations are derived from the recommendations of the American Society for Bone and Mineral Research Histomorphometry Nomenclature Committee (112).

Both static and dynamic histomorphometric measurements were made using a computer and digitizer tablet (Osteomeasure; Osteometrics Inc., Atlanta, GA) interfaced to a Leitz microscope (Leitz Wetzlar, Germany) with a drawing tablet. 3 mice and 5 sections were analyzed per group for each measurement, with each measurement performed 6 times per section.

9.16 STATISTICS

For all data, statistical comparisons were performed on Means ± SEM, using one-factor analysis of variance and Student's t test. Differences between the means were considered statistically significant at $p<0.05$.

10 RESULTS

10.1 ONTOGENY OF RENAL Na^+-Pi COTRANSPORT AND Na^+-Pi COTRANSPORTER GENE EXPRESSION IN WILDTYPE AND Npt2 KO MICE.

The initial rates of BBM Na^+-Pi cotransport in WT and Npt2 KO mice were determined at 21-, 45-, and 115-days of age. Figure 6 indicates that at each of the ages examined, Npt2 KO mice have severely compromised Na^+-Pi cotransport in comparison to WT mice. In addition, by measuring the initial BBM Na^+-Pi cotransport in mice of increasing age, it became apparent that BBM Na^+-Pi cotransport is age-dependent in WT mice, but not in Npt2 KO mice. By 115 days of age, Na^+-Pi cotransport activity in WT mice falls to 77 ± 8% of that at 21 days of age ($p<0.05$).

BBM Na^+-glucose transport in Npt2 KO mice was not reduced relative to age-matched WT mice (Table 2), demonstrating that the decrease in Na^+-Pi cotransport observed in Npt2 KO mice is specific to the ablation of *Npt2*.

Table 2
Initial rates of renal BBM glucose uptake in WT and Npt2 KO mice.

Glucose uptake (Na^+-K) (pmoles/mg protein/6 sec)
Values represent Mean ± SEM

	Wildtype (n)	Npt2 KO (n)
21 days	68 ± 8 (15)	53 ± 4 (4)
45 days	59 ± 6 (20)	63 ± 11 (8)
115 days	55 ± 9 (7)	53 ± 5 (4)

Western blot analysis (Figure 7) and band densitometry were used to determine whether changes in Npt2 protein abundance contributed to the age-dependent decrease in BBM Na^+-Pi cotransport in WT mice. The 83 kDa Npt2 protein band was quantified relative to that of meprin (65 kDa), and revealed a 13% decrease in Npt2 protein by 115-

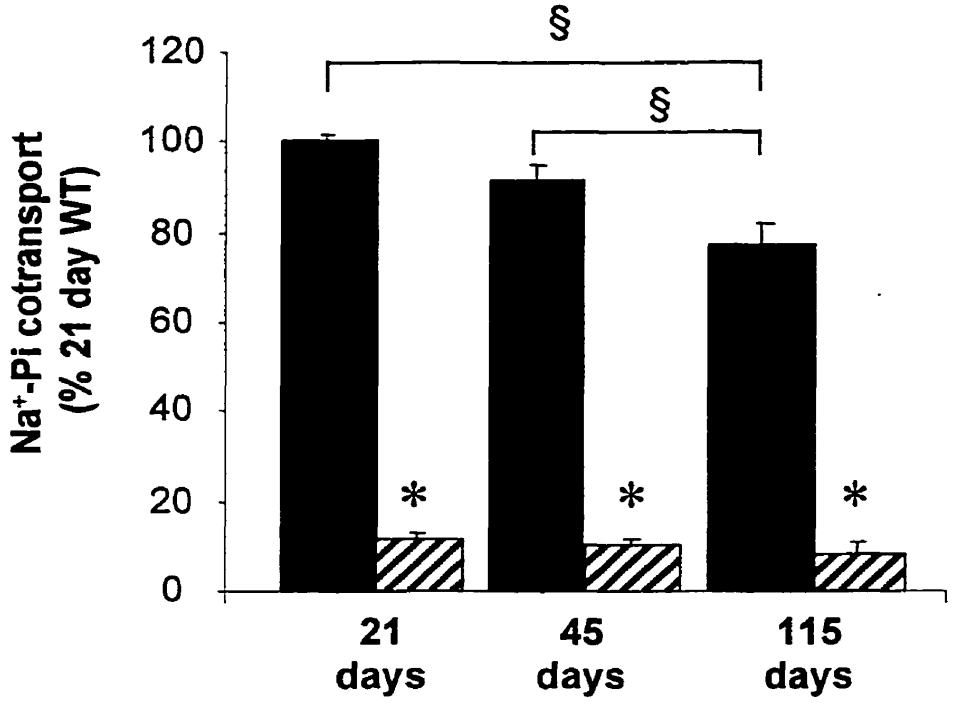

Figure 6: Effect of age and *Npt2* gene ablation on renal BBM Na^+-Pi cotransport.

Renal BBM vesicles were prepared from WT (filled bars) and Npt2 KO mice (hatched bars) at 21, 45, and 115 days of age, as described in Methods. The vesicles were used for both transport studies and Western analysis (Figure7). One hundred percent activity represents the Na^+ dependent component of Pi transport in BBMs from 21-day-old WT mice (590 ± 30 pmol/mg protein per 6 seconds). Values represent means ± SEM. * Effect of genotype, $p<0.05$. § Effect of age, $p<0.05$.

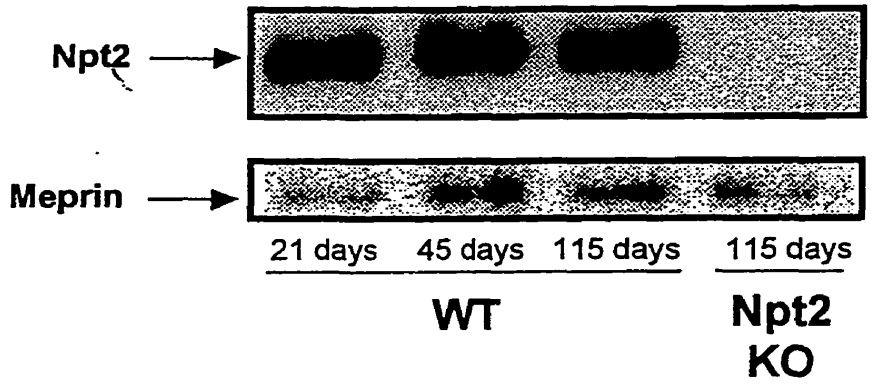

Figure 7: Effect of age and *Npt2* gene ablation on renal BBM Npt2 protein abundance.

BBM proteins, prepared from WT mice at 21, 45, and 115 days of age and from 115-day-old Npt2 KO mice were fractionated on 10% SDS-PAGE gels, transferred to nitrocellulose membranes, and probed with a rabbit polyclonal anti-rat Npt2 antibody and a monoclonal antibody raised against the α subunit of rat meprin. Bands depicting Npt2 (83 kDa) and meprin (65 kDa) immunoreactive proteins are indicated by the arrows.

days of age (n=4) that was not significantly different from that at 21 days. In addition, there was no significant age-dependent decrease in renal Npt2 mRNA abundance, relative to that of β-actin, in WT mice (Figure 8a). As previously reported, Npt2 KO mice produce neither immunoreactive Npt2 protein (Figure 7) nor Npt2 mRNA (Figure 8b).

In order to understand the age-dependent contribution of renal *Npt1*, *Glvr-1*, and *Ram-1* to renal BBM Na^+-Pi cotransport in aging WT and Npt2 KO mice, we measured the renal mRNA abundance, relative to that of β-actin, of each of these Na^+-Pi cotransporters at 21-, 45-, and 115-days of age.

Renal Npt1 mRNA abundance increased with age in both genotypes (21 vs. 115 days of age, $p<0.05$ for both genotypes). However, in Npt2 KO mice Npt1 mRNA abundance was significantly reduced at both 21 and 45 days of age, relative to that of WT mice (Npt2 KO vs. WT at 21, and at 45 days, $p<0.05$) (Figure 9a). While age had no effect on the renal mRNA abundance of Glvr-1 or Ram-1 in WT mice, Npt2 KO mice demonstrated a significant age-related increase in the mRNA abundance of both of these Na^+-Pi cotransporters (21 vs. 115 days of age, $p<0.05$ for both Glvr-1 and Ram-1) (Figure 9b and c).

The renal mRNA abundance of Glvr-1 and of Ram-1 is significantly reduced in Npt2 KO mice at 21 days of age compared to that of WT mice (Npt2 KO vs. WT mice, $p<0.05$, for both Glvr-1 and Ram-1). However, this difference was eliminated by 115 days of age as a result of the age-dependent increase in both Glvr-1 and Ram-1 that was observed in the Npt2 KO mouse. By 115 days of age, the mRNA abundance of Ram-1 is similar in both WT and Npt2 KO mice, while Glvr-1 mRNA abundance is significantly greater in Npt2 KO mice at 115 days of age ($p<0.05$).

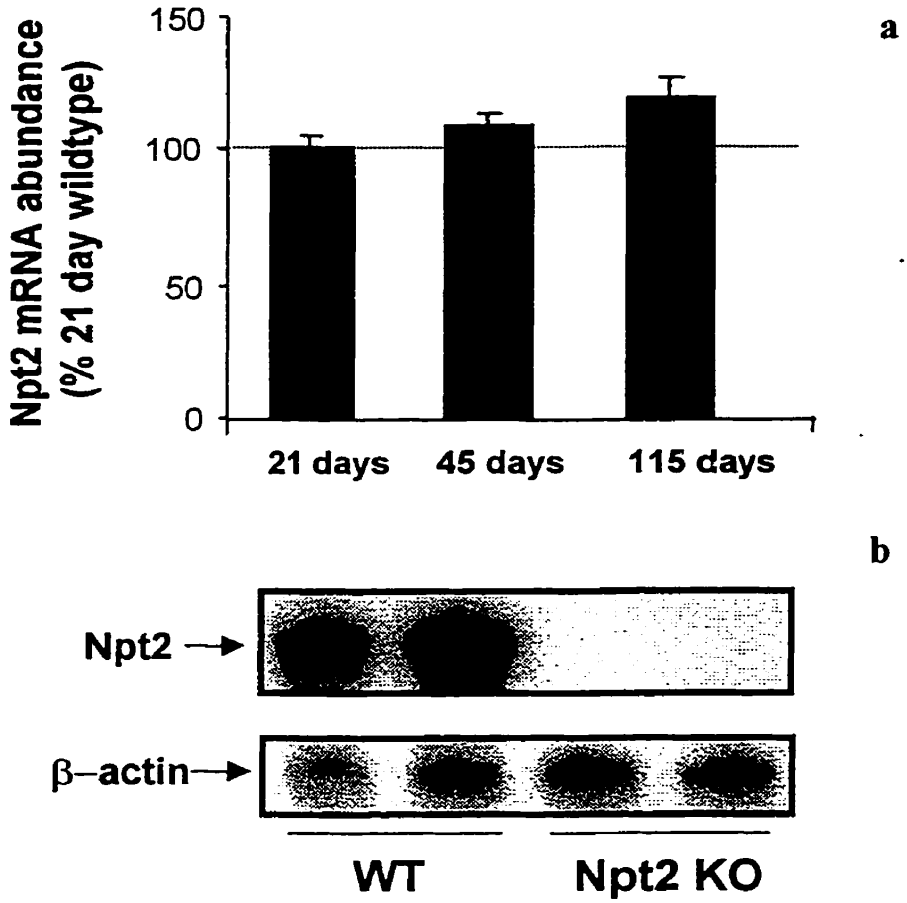

Figure 8: Effect of age on renal mRNA abundance of Npt2 in WT mice (a) and ribonuclease protection assay of renal RNA from WT and Npt2 KO mice.

Renal mRNA was prepared from WT mice at 21, 45, and 115 days of age, and the abundance of Npt2 mRNA, relative to β-actin mRNA, was determined by ribonuclease protection assay as described in Methods. The values are mean ± SEM derived from 5-8 mice per group (a). Ribonuclease protection assay of renal mRNA from WT and Npt2 KO mice. Protected Npt2 and β-actin mRNA fragments are evident with renal mRNA from 45-day-old WT mice, whereas only a protected β-actin mRNA fragment is detected with RNA from age-matched Npt2 KO mice (b).

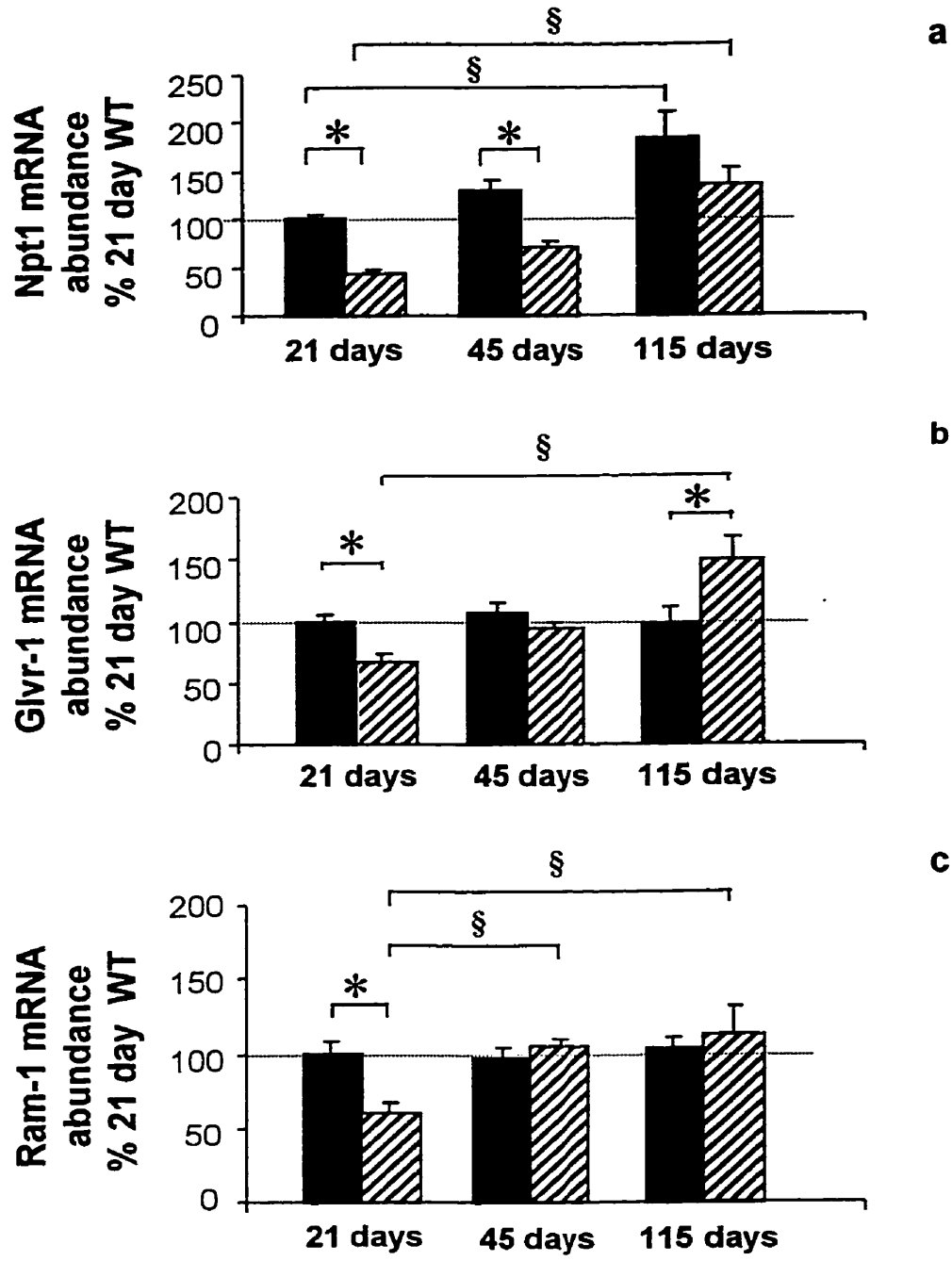

Figure 9: Effect of age and *Npt2* gene ablation on renal mRNA abundance of Npt1 (a), Glvr-1 (b), Ram-1 (c).

The abundance of each transcript, relative to β-actin mRNA, was determined in renal mRNA samples derived from 21-, 45-, and 115-day-old WT (filled bars) and Npt2 KO (hatched bars) mice by ribonuclease protection assay as described in Methods. The values depict the mean ± SEM derived from 5-8 mice per group. * Effect of genotype, $p<0.05$. §Effect of age, $p<0.05$.

10.2 EFFECT OF Npt2 KO ON THE PHYSIOLOGICAL RESPONSE TO CHRONIC PHOSPHATE RESTRICTION--Npt2 KO MICE CANNOT ADAPT TO LOW Pi DIET

As previously reported (93), Npt2 KO mice are hypophosphatemic and have elevated FEI_{Pi} on a normal Pi diet (1.0% Pi), in comparison to age matched WT mice (Table 3). Low Pi diet (0.02% Pi) caused a significant decline in serum Pi in both WT and Npt2 KO mice in comparison to mice fed the control Pi diet (1.0% Pi) ($p<0.005$) (Table 3).

Table 3
Effect of low Pi diet on blood and urine profiles of WT and Npt2 KO mice
Values represent Mean ± SEM

	Control		Low Pi	
	WT (n)	**Npt2 KO (n)**	**WT (n)**	**Npt2 KO (n)**
Serum Pi (mM)	3.46 ± 0.41 (6)	2.24 ± 0.09* (4)	1.14 ± 0.07‡ (6)	1.14 ± 0.09‡ (7)
Urine Pi/Cr	32.77 ± 4.1 (6)	61.97 ± 11.7* (6)	0.14 ± 0.05‡ (5)	1.36 ± 0.22*‡ (7)
FEI_{Pi}	11.82 ± 1.95 (6)	20.78 ± 1.95* (4)	0.13 ± 0.05‡ (5)	1.21 ± 0.24*‡ (7)
Serum Ca (mM)	1.88 ± 0.12 (6)	2.17 ± 0.06* (7)	2.82 ± 0.08‡ (6)	2.87 ± 0.08‡ (7)
Urine Ca/Cr	0.31 ± 0.06 (5)	1.1 ± 0.39* (6)	12.45 ± 4.21‡ (5)	13.63 ± 3.33‡ (7)
FEI_{Ca}	0.28 ± 0.10 (6)	0.34 ± 0.04 (6)	4.33 ± 1.38‡ (5)	4.67 ± 1.0‡ (7)

* Effect of genotype, $p<0.05$. ‡ Effect of diet, $p<0.05$.

Both WT and Npt2 KO mice experienced a significant decrease in the FEI_{Pi} in response to dietary Pi restriction (WT, control vs. low Pi diet, $p<0.005$; Npt2 KO, control vs. low Pi diet, $p<0.05$) (Table 3).

Serum Pi values for Npt2 KO mice on a low Pi diet were equivalent to those obtained for the WT mice on the same diet. However, the FEI_{Pi} remained elevated in Npt2 KO mice in comparison to WT mice (WT vs. Npt2 KO, $p<0.005$), demonstrating the preservation of the renal Pi leak (Table 3).

Table 3 also shows the calcemic response of WT and Npt2 KO mice to dietary Pi restriction. On a normal Pi diet, Npt2 KO mice are hypercalcemic in comparison to WT

mice ($p<0.05$). When Pi-deprived, both genotypes experienced a significant increase in serum Ca (control vs. low Pi diet, $p<0.001$) and in FEI_{Ca} (control vs. low Pi diet, $p<0.05$), such that both serum Ca and FEI_{Ca} in WT and Npt2 KO mice were comparable.

BBM Na^+-Pi cotransport increased 3.4 fold in WT mice following Pi restriction (Figure 10a) and correlated with an increase in immunoreactive BBM Npt2 protein, relative to meprin (Figure 10b). Low Pi diet caused a 1.3-fold increase in renal Npt2 mRNA abundance in WT mice (Figure 10c). It is of interest that Npt2 KO mice failed to exhibit any adaptive increase in BBM Na^+-Pi cotransport in response to Pi deprivation; impaired BBM Na^+-Pi cotransport did not change (Figure 10a). As expected, no Npt2 protein or mRNA was detected in Npt2 KO mice under either dietary condition (Figure 10b and c).

Npt1 protein abundance was examined in both WT and Npt2 KO mice under control and low Pi dietary conditions (Figure 11a). The Npt1 antibody recognized a single band of 64 kDa in BBM from WT and Npt2 KO mice. Quantitation of this band relative to that of meprin revealed no increase in Npt1 protein abundance as a result of *Npt2* gene ablation or dietary Pi restriction. The size of the detected Npt1 protein and the lack of dietary Pi regulation correspond with other reports (16,17,19,24). Quantitation of the BBM abundance of Npt1 protein was of interest as the renal mRNA abundance of Npt1 was consistently, although not significantly, decreased in Npt2 KO mice in comparison to age-matched WT mice (Figure 9a). In contrast to other reports, both genotypes experienced an increase in renal Npt1 mRNA abundance as a result of dietary Pi restriction (Figure 11b). Npt1 mRNA abundance increased 1.3 and 1.4 fold, respectively, ($p<0.05$) in WT and Npt2 KO mice fed the low Pi diet in comparison to

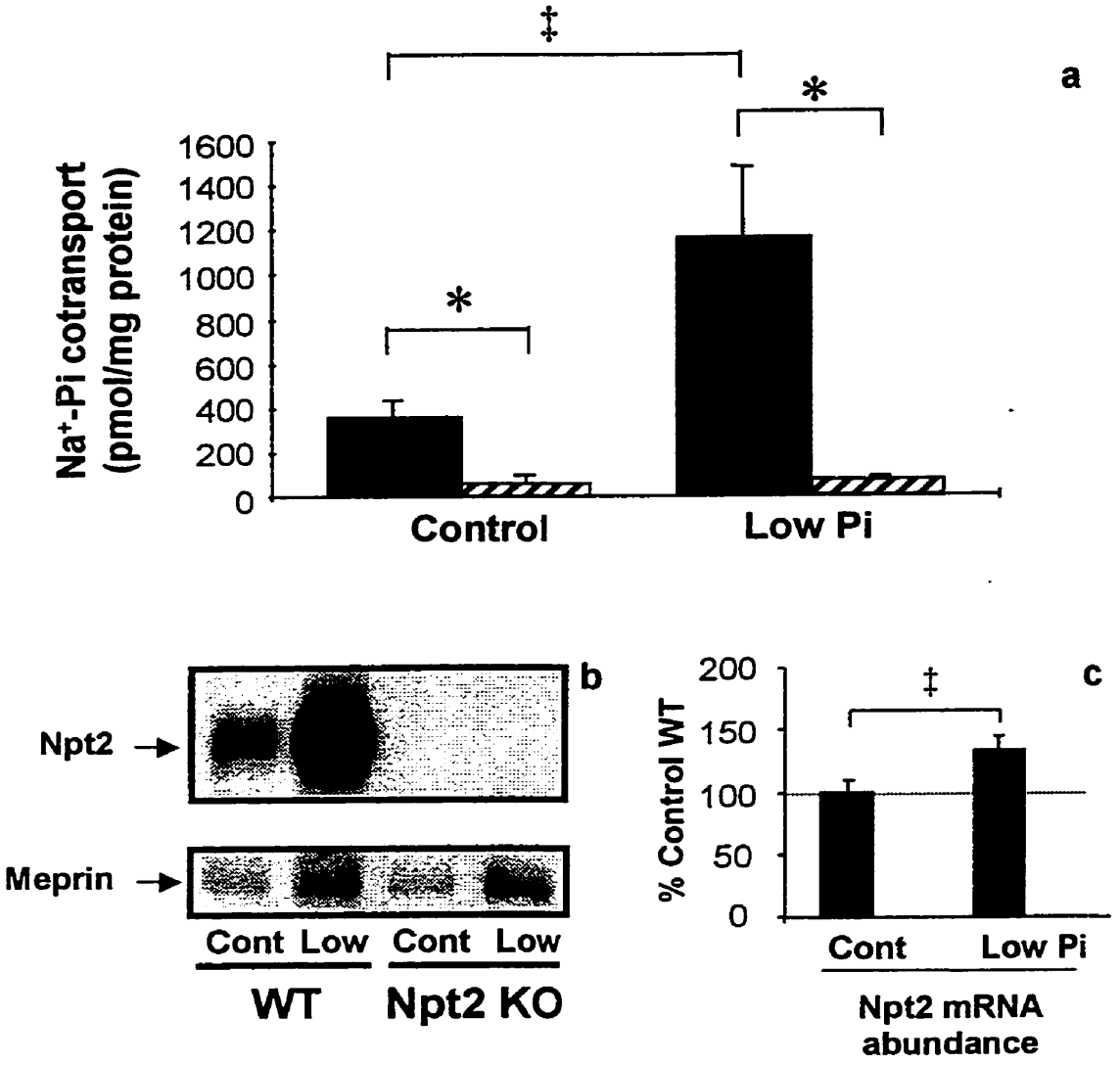

Figure 10: Effect of low Pi diet on renal BBM Na^+-Pi cotransport (a), Npt2 protein abundance (b), and Npt2 mRNA abundance (c), in WT and Npt2 KO mice.

45-day-old WT (filled bars) and Npt2 KO (hatched bars) mice were fed control (1%) and low Pi (0.02%) diets for 5 days. One kidney from each mouse was used for the BBM vesicle preparations. These BBMs were used for both transport studies (a), and Western analysis (b), as described in Methods. Each bar represents the Na^+-dependent component of Pi transport (mean ± SEM of 2 typical experiments) (a). Renal mRNA was prepared from the remaining kidney. The abundance of Npt2 mRNA, relative to β-actin mRNA, was determined by ribonuclease protection assay as described in Methods (c). The values depict means ± SEM derived from 5-8 mice per group. * Effect of genotype, $p<0.05$. ‡ Effect of diet, $p<0.05$.

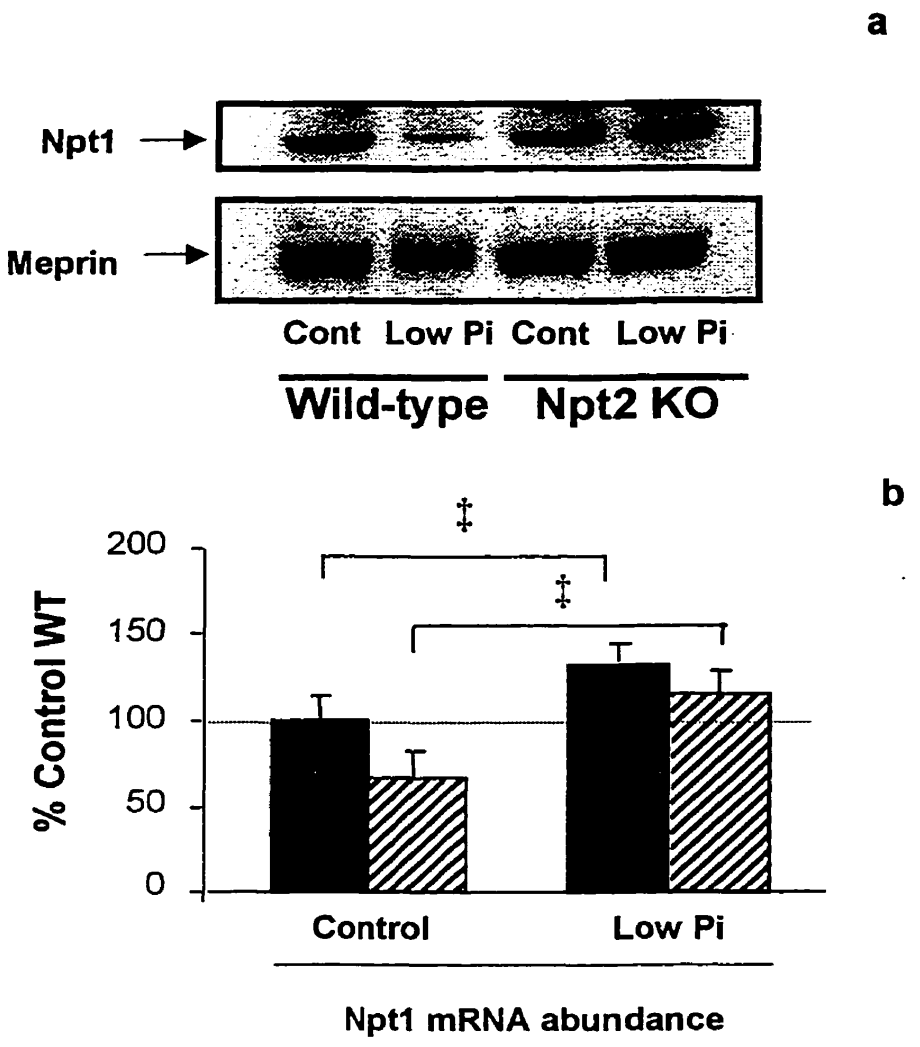

Figure 11: Effect of low Pi diet on renal BBM Npt1 protein abundance (a), and on the renal abundance of Npt1 mRNA (b).

Renal BBM vesicles were prepared from 55-day-old WT and Npt2 KO mice fed the control (1%) and low Pi (0.02%) diets for 5 days, and used for Western analysis as described in Methods. Bands depicting Npt1 (64 kDa) and meprin (65 kDa) are indicated by arrows (a). Renal mRNA was prepared from 45-day-old WT (filled bars) and Npt2 KO (hatched bars) mice fed the control (1%) and low Pi (0.02%) diets for 5 days (b). The abundance of Npt1 mRNA, relative to β-actin mRNA, was determined by ribonuclease protection assay as described in Methods. The values depict the mean ± SEM derived from 5-8 mice per group. ‡Effect of diet, $p<0.05$.

those fed the control diet (Figure 11b). This alteration in mRNA abundance was not functionally relevant since it did not correlate with Npt1 protein abundance, nor did it alter BBM Na^+-Pi cotransport in Npt2 KO mice (Figure 10a).

Dietary Pi restriction had no effect on the renal mRNA abundance of either Glvr-1 or Ram-1 in WT or Npt2 KO mice (Figure 12a and b). In addition, using a rabbit antibody, immunoreactive Glvr-1 protein was not detected in the BBMs of either WT or Npt2 KO mice (data not shown).

10.3 EVIDENCE FOR INTESTINAL CALCIUM HYPERABSORPTION IN Npt2 KO MICE.

10.3.1 Effect of Fasting and Oral Ca Load on Urine Calcium, (Phosphorous, and Magnesium) Excretion

Three to five, 21- or 45-day-old, WT and Npt2 KO mice, were used to determine whether intestinal hyperabsorption of Ca contributed to the hypercalcemia and hypercalciuria observed in Npt2 KO mice. This was accomplished by examining the effects of fasting and of calcium supplementation on urine Ca/Cr. In addition, the urine Pi- and Mg/Cr were evaluated. Prior to fasting, baseline urine Ca-, Pi-, and Mg/Cr were determined in each group. Serum electrolyte concentrations could not be examined as we wished to use the same mice throughout the experiment.

Figures 13a, b, and c show that Npt2 KO mice had substantially elevated baseline urine Ca/Cr and urine Pi/Cr, and equivalent urine Mg/Cr in comparison to the baseline values obtained for WT mice (effect of genotype, $p<0.01$; $p<0.05$; $p=0.09$, respectively for each mineral).

Fasting caused a significant decrease in urine Ca/Cr in Npt2 KO mice, but had no significant effects on urine Ca/Cr in WT mice (Figure 13a). Urine Pi/Cr increased

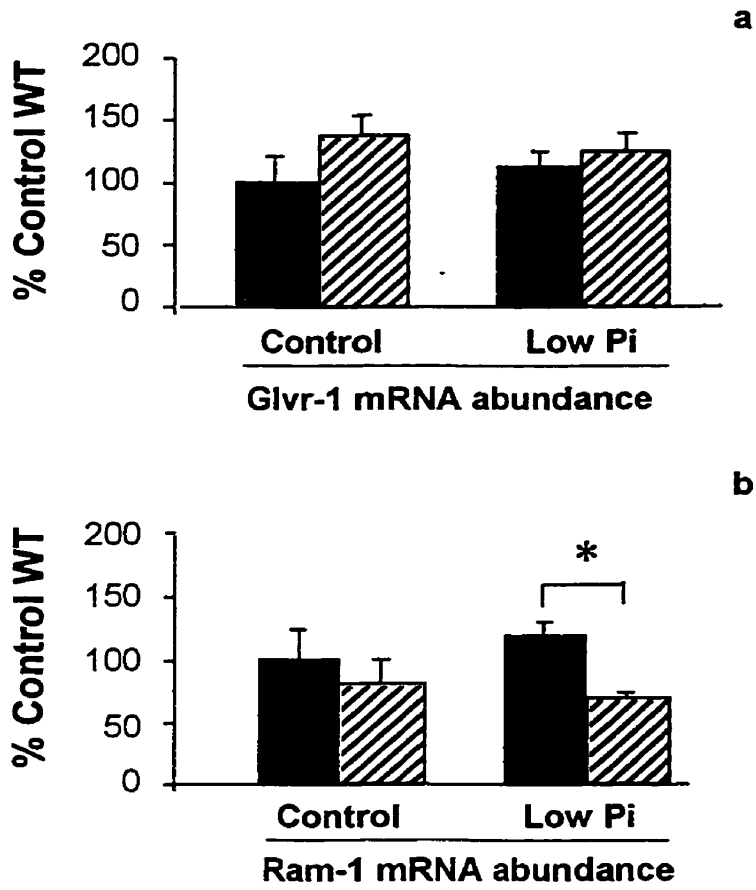

Figure 12: Effect of Low Pi diet on renal mRNA abundance of Glvr-1 (a) and Ram-1 (b) in WT and Npt2 KO mice.

Renal mRNA was prepared from 45-day-old WT (solid bars) and Npt2 KO (hatched bars) mice fed the control (1%) and low Pi (0.02%) diets for 5 days. The abundance of Glvr-1 and Ram-1 mRNAs, relative to β-actin, was determined by ribonuclease protection assay as described in Methods. The values depict the mean ± SEM derived from 5-8 mice per group.

* Effect of genotype, $p<0.05$.

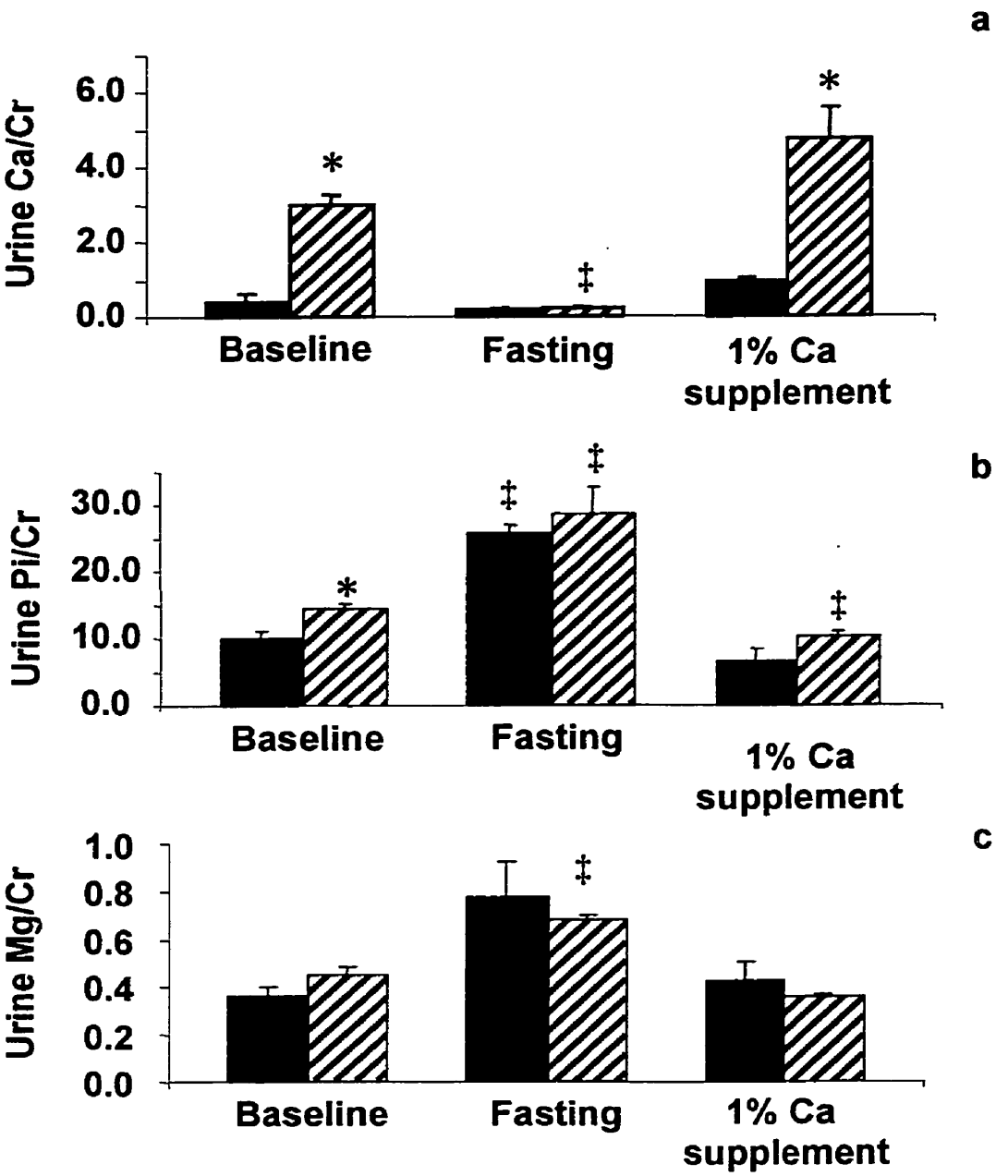

Figure 13: Effect of fasting and oral calcium load on urine Ca/Cr (a), Pi/Cr (b), and Mg/Cr (c) ratios in WT and Npt2 KO mice.

Urine Ca-, Pi-, Mg/Cr ratios were measured in WT (solid bars) and Npt2 KO (hatched bars) mice fed our control diet (baseline), following an overnight fast (fasting), and following an oral Ca supplement (Ca supplement) as described in Methods. Values represent means ± SEM derived from 3-5 mice per group.

* Effect of genotype, $p<0.05$. ‡ Effect of diet, $p<0.05$.

significantly in both WT and Npt2 KO mice with fasting ($p<0.001$ and $p<0.05$, respectively), such that urine Pi/Cr were similar in WT and Npt2 KO mice (Figure 13b). Mg/Cr values were increased in fasted WT and Npt2 KO mice, however, the increase was significant in only the Npt2 KO mice (Figure 13c).

Calcium supplementation elicited a significant increase in the urine Ca/Cr of Npt2 KO mice, to levels slightly greater than that of Npt2 KO baseline values (Fasting vs. Ca supplement, $p<0.05$). Wildtype mice had no significant change in urine Ca/Cr between overnight fasting and calcium supplementation (Figure 13a). The 1% calcium supplement returned both urine Pi/Cr (Figure 13b) and urine Mg/Cr (Figure 13c) to levels comparable to baseline values. Urine Mg/Cr ratios were similar in both genotypes regardless of the dietary challenge faced by the mice (Figure 13c).

10.3.2 Effect of Npt2 Gene Ablation on the Renal mRNA Abundance of 1α- and 24-hydroxylase

It was previously shown that serum 1,25-dihydroxyvitamin D_3 was substantially elevated in the Npt2 KO mouse in comparison to the WT mouse (93). To elucidate the mechanism for the elevated serum $1,25(OH)_2D_3$ in Npt2 KO mice, the renal mRNA abundance of 1α- and 24-hydroxylase was determined in WT and Npt2 KO mice (Table 4).

Table 4
Renal mRNA abundance of 1α-hydroxylase and 24-hydroxylase in WT and Npt2 KO mice at 21-, 45-, and 115-days-of-age

(expressed as %WT, control diet).
Values represent Mean ± SEM

	Wildtype			Npt2 KO		
	25 days (n)	**45 days (n)**	**115 days (n)**	**25 days (n)**	**45 days (n)**	**115 days (n)**
1-OHase mRNA abundance	100.0 ± 27.6 % (6)	109.9 ± 31.9 % (5)	76.9 ± 7.7 % (6)	160.4 ± 59.4 % (5)	254.3 ± 92.5 % (4)	63.0 ± 19.4 % (4)
24 OHase mRNA abundance	100.00 ± 29.2 % (6)	81.6 ± 23.0 % (6)	208.3 ± 31.9 % [§](6)	50.5 ± 16.0 % (5)	47.9 ± 12.8 % (4)	61.5 ± 16.2 % [*] (6)

[*] Effect of genotype, $p<0.05$. [§] Effect of age, $p<0.05$

RPA and PhosphorImager analysis demonstrated that the renal abundance of 24-hydroxylase mRNA in Npt2 KO mice was consistently lower than that of WT mice at all of the ages examined. However, this difference was significant only at 115 days of age, when the WT mice exhibited a substantial elevation in the renal mRNA abundance of 24-hydroxylase. Conversely, Npt2 KO mice tended to display levels of 1α-hydroxylase mRNA that were greater than that of WT mice. These studies are ongoing in our laboratory.

10.3.3 The Effect of Low Pi Diet on the Renal mRNA Abundance of 1α- And 24-hydroxylase

The effect of dietary Pi restriction on the renal mRNA abundance of 1α- and 24-hydroxylase was determined in WT and Npt2 KO mice. We determined that low Pi diet caused a 3.5-fold increase in renal mRNA abundance of 1α-hydroxylase in WT mice, and that the renal abundance of 1α-hydroxylase mRNA is the same in Pi-deprived WT and Npt2 KO mice (Figure 14a). Similarly, low Pi diet caused a 50% decrease in the renal

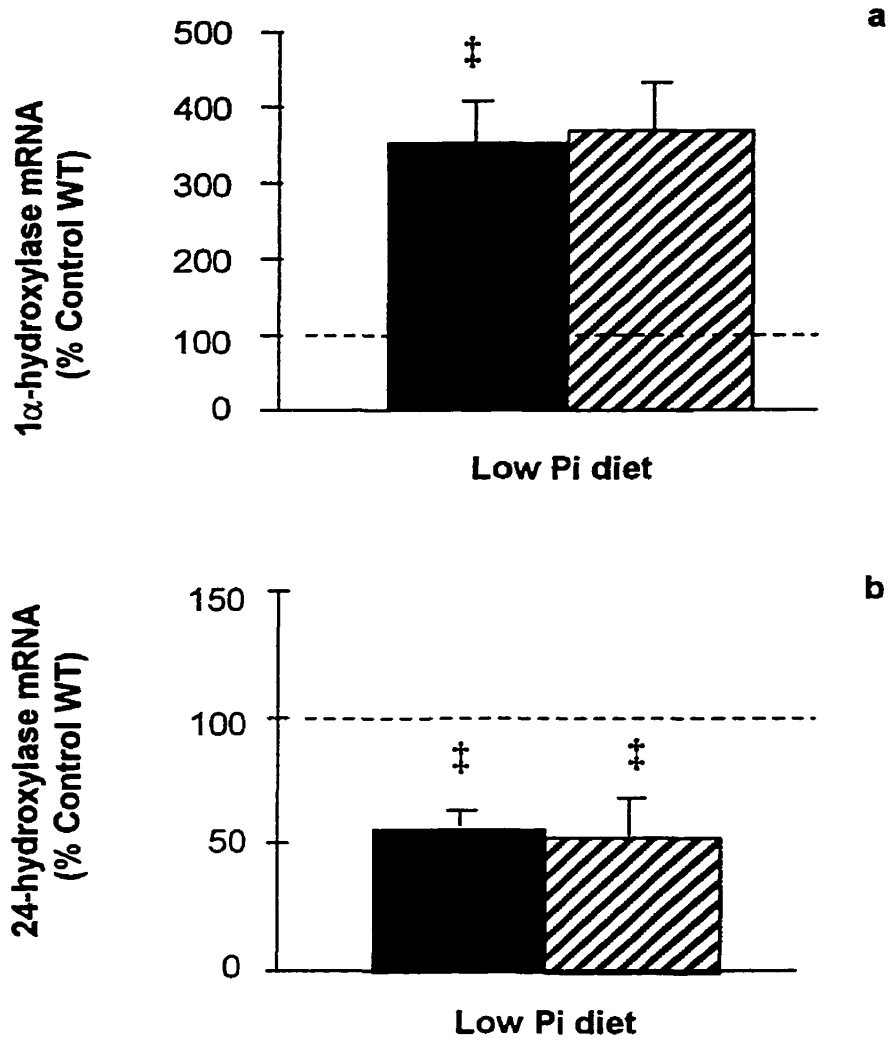

Figure 14: Effect of low Pi diet on renal mRNA abundance of 1α-hydroxylase (a), and 24-hydroxylase (b) in WT and Npt2 KO mice.

Renal mRNA was prepared from 45-day-old WT (solid bars) and Npt2 KO (hatched bars) fed the low Pi diet (0.02%) for 5 days. The abundance of 1α-hydroxylase, and 24-hydroxylase mRNAs, relative to β-actin mRNA, was determined by ribonuclease protection assay as described in Methods. The values depict the mean ± SEM derived from 5-8 mice per group. ‡ Effect of diet, $p<0.05$.

mRNA abundance of 24-hydroxylase in WT mice, and we could determine that 24-hydroxylase renal mRNA abundance was similar in Pi-deprived WT and Npt2 KO mice (Figure 14b).

10.4 EFFECT OF AGE AND Npt2 GENE ABLATION ON THE GENE EXPRESSION OF OSTEOBLAST AND OF CHONDROBLAST MARKERS, AND ON BONE HISTOMORPHOMETRY

10.4.1 Ontogenic Expression of Skeletal Glvr-1, Osteocalcin, and Phex in WT and Npt2 KO Mice

The expression of Glvr-1, osteocalcin, and Phex were measured as a means of determining the effect of Npt2 KO and age on gene expression in bone. The results are displayed in Figures 15a, b, and c.

Although the expression of Glvr-1 was similar in the WT and Npt2 KO mice at 21-days of age, Npt2 KO mice exhibited substantially reduced levels of Glvr-1 expression at 45-days of age (Figure 15a). While the expression of Glvr-1 declined slightly in the WT mice with age, the reduction was not significant. Conversely, Glvr-1 mRNA abundance in Npt2 KO mice diminished significantly as they aged ($p<0.05$).

The genotypic pattern of osteocalcin expression in the osteoblast resembled that of Glvr-1 (Figure 15b). At 21 days of age, there were no differences between WT or Npt2 KO osteocalcin mRNA abundance. However, at 45-days of age, the Npt2 KO mice experienced a dramatic fall in osteocalcin mRNA abundance, to approximately 20% of that of the age-matched WT mouse ($p<0.005$). By 115-days of age, both WT and Npt2 KO mice exhibited similar levels of osteocalcin mRNA abundance. Aging had an effect on the expression of osteocalcin in both genotypes. Although WT mice did not display the same age effect at 45-days of age as the Npt2 KO mice did, by 115-days of age, both

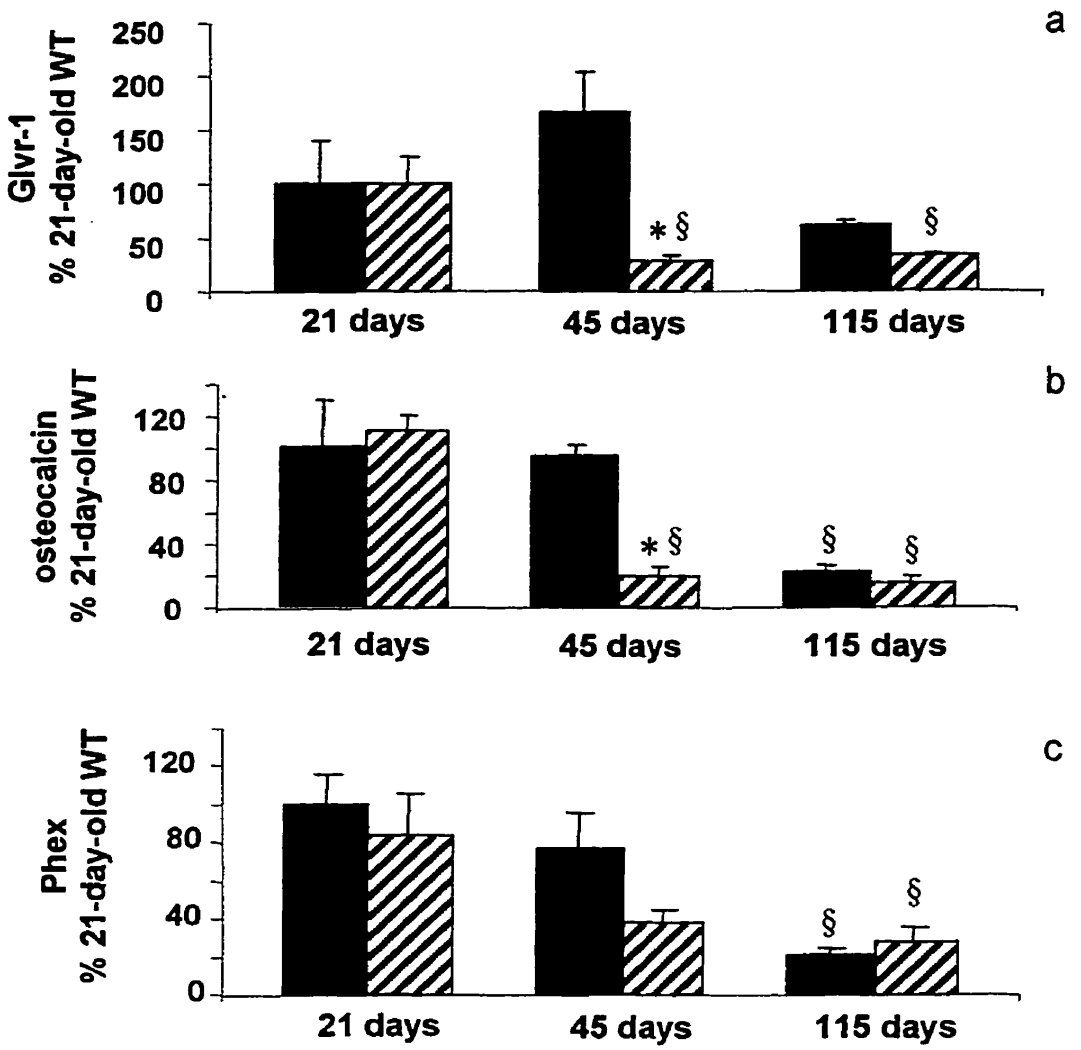

Figure 15: Effect of age and *Npt2* gene ablation on the skeletal mRNA abundance of Glvr-1 (a), osteocalcin (b), and Phex (c).
Bone mRNA was prepared from WT (solid bars) and Npt2 KO (hatched bars) mice at 21, 45, and 115 days of age, and the abundance of Glvr-1, osteocalcin, and Phex, relative to β-actin mRNA, was determined by ribonuclease protection assay as described in Methods. The values are means ± SEM derived from 5-8 mice per group.
* Effect of genotype, $p<0.05$. § Effect of age, $p<0.05$.

WT and Npt2 KO mice had experienced an ~80% reduction in the mRNA abundance of osteocalcin (Figure 15b).

Npt2 gene ablation had no effect on the renal mRNA abundance of Phex; WT and Npt2 KO mice consistently displayed similar levels of expression (Figure 15c). However, the effects of aging were significant. Phex mRNA abundance was 5-fold greater in 21-day-old mice than in 115-day-old mice (Figure 15c). This pattern of Phex gene expression was observed in both WT and Npt2 KO mice.

10.4.2 Analysis of Histomorphometric and Histological Parameters in Wildtype and Npt2 KO Mice

As reported previously, the trabecular bone of Npt2 KO mice is poorly developed at 25 days of age. Trabecular number (Tb.N), area (Tb.A), and perimeter (Tb.Pm) were all significantly decreased in 25-day-old Npt2 KO mice in comparison to age-matched WT mice (Table 5). However, at 115-days of age, Tb.N was greater in Npt2 KO mice in comparison to age-matched WT mice (Table 5). This was due to an increase in Tb.N in Npt2 KO mice (n.s), and a severe decrease in Tb.N in WT mice.

Table 5
Trabecular number, area, and perimeter in WT and Npt2 KO mice

	Wildtype		Npt2 KO	
	25 days	**115 days**	**25 days**	**115 days**
Trabecular number (Tb.N) (BV/TV)*Tb.Th	41.0 ± 3.0	16.0 ± 3.0[§]	21.0 ± 3.0*	25.0 ± 3.0*
Trabecular area (Tb.Ar)(mm^2)	0.03 ± 0.02	0.07 ± 0.06	0.008 ± 0.003*	0.012 ± 0.001
Trabecular perimeter (Tb.Pm) (mm)	2.60 ± 0.46	2.06 ± 012	1.50 ± 0.35*	2.0 ± 0.05

* Effect of genotype, $p<0.05$. [§] Effect of age, $p<0.05$.

Differences in osteoclast characteristics were ascertained by histochemical analysis of tibial bone sections. Osteoclast number (nOC/TA) refers to the number of osteoclasts within a defined tissue area. nOC/TA was significantly reduced in the Npt2 KO mice at both 21- and 115-days of age (Figure 16a). However, osteoclast perimeter (OC.Pm) was reduced in Npt2 KO mice of 25 days of age (WT: 0.45 ± 0.05 μm vs. Npt2 KO: 0.26 ± 0.03 μm, $p<0.01$), but not 115 days (WT: 0.39 ± 0.19 μm vs. Npt2 KO: 0.32 ± 0.04 μm), when compared to age-matched WT mice. The decrease in nOC/TA can be observed in Figure 16b, where osteoclasts are identified by dark pink staining.

The eroded perimeter (E.Pm) is a static measurement that reflects *in vivo* osteoclast activity. The E.Pm measurement includes the surface of the osteoclast that is in contact with the bone surface and the reversal surface where bone is being resorbed (71). This parameter was significantly reduced in the 25-day-old Npt2 KO mice compared to age matched WT mice (WT: 0.52 ± 0.03 mm vs. Npt2 KO: 0.31 ± 0.05 mm, $p<0.01$), however, these differences were not conserved at 115 days of age (WT: 0.39 ± 0.02 mm vs. Npt2 KO: 0.34 ± 0.02 mm). The age-dependent effects on E.Pm were

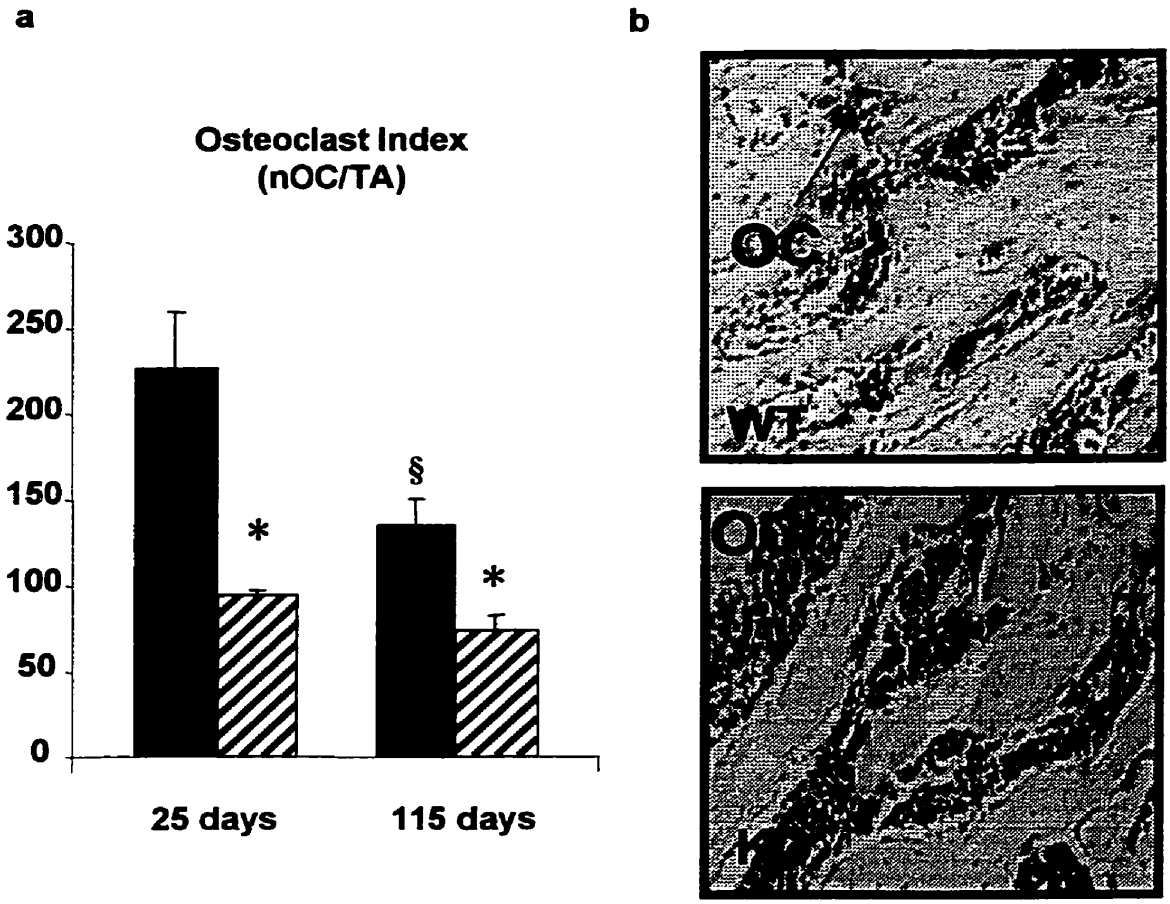

Figure 16: Effect of age and *Npt2* gene ablation on osteoclast index.
Tibial sections of WT (solid bars) and Npt2 KO (hatched bars) mice were stained with TRAPase to identify osteoclasts as described in Methods and represented as nOC/TA (a). Values represent the mean ± SEM. * Effect of genotype, $p<0.05$. § Effect of age, $p<0.05$.
Sample photograph of TRAPase positive staining for osteoclasts in 21-day-old WT (top) and Npt2 KO (bottom) mice (b).

distinctly different in WT and Npt2 KO mice. WT mice experienced a decrease in E.Pm between 25- and 115-days of age (25d: 0.52 ± 0.03 mm vs. 115d: 0.39 ± 0.02 mm, $p<0.01$), whereas Npt2 KO mice did not.

Histomorphometric evaluation of calcein double labeling permits the estimation of dynamic parameters that are indicative of bone remodeling (Figure 17). The calcein label is incorporated into mineralized bone as it is formed. At 115-days of age, there was a 2-fold increase in the percentage of calcein labeled surface (%L) in the Npt2 KO mice as compared to the WT mice (WT: 31.2 ± 6.44% vs. Npt2 KO: 63.4 ± 8.6%, $p<0.05$). This difference was not apparent at 25-days of age. MAR is calculated by measuring the distance between the calcein labels divided by the time period over which calcein was administered (Ir.L.Th/Ir.L. time)[1]. Calculating the MAR provides some indication as to the activity of the osteoblasts. MAR was similar in WT and Npt2 KO mice at both 25 and 115 days of age, suggesting that Npt2 gene ablation does not compromise osteoblast activity (Table 6). Mineralizing surface (MS) estimates the extent of bone surface that is active in mineralization at the time of measurement [MS=(dLS + sLS/2)/BS][2](112) did not differ between WT and Npt2 KO mice at 25 days of age. However, at 115 days of age the MS of Npt2 KO mice was approximately 2-times that of WT mice (Table 6). Thus, age had opposite effects on the MS of WT and Npt2 KO mice. While the MS of WT mice decreased significantly with age, the MS of Npt2 KO mice actually increased with age (Table 6).

[1] Ir.L.Th – Interlabel thickness.
[2] dLS – double label surface; sLS – single label surface.

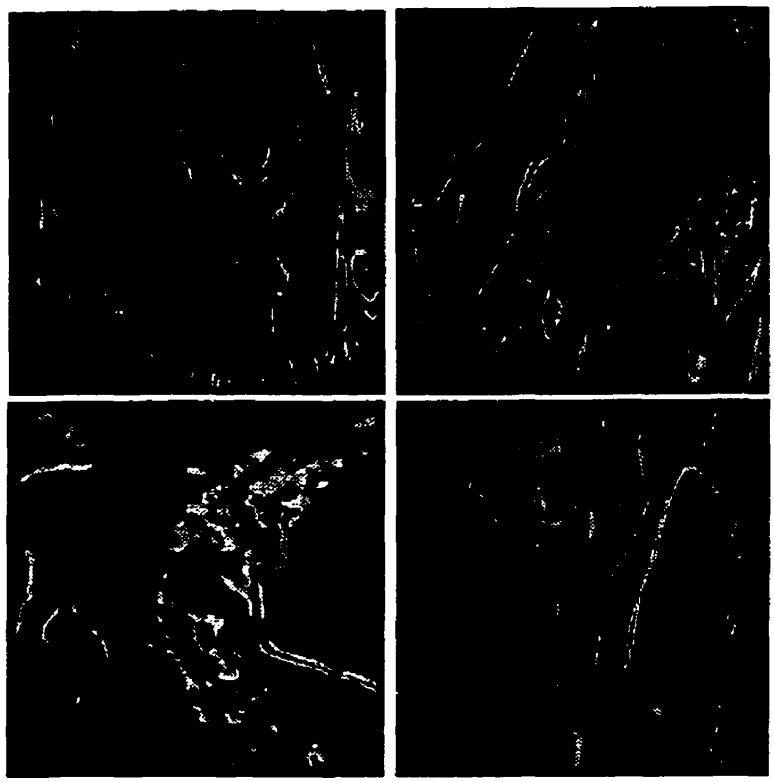

WT **Npt2 KO**

Figure 17: Calcein double label in tibial sections of WT (left) and Npt2 KO (right) mice.
To estimate MAR and BFR WT and Npt2 KO mice were injected intraperitoneally with 20 mg/kg of calcein 7 and 2 days before sacrifice as described in Methods.
The use of calcein double labeling permits the estimation of MAR and BFR. In 115 day old Npt2 KO mice the % labeled surface was 2-fold that of age-matched WT mice.

Table 6
Effect of age and *Npt2* gene ablation on the dynamic parameters of bone remodeling.

Values represent means ± SEM

	Wildtype		Npt2 KO	
	25 days	115 days	25 days	115 days
Mineral Apposition Rate (MAR, μm/day)	3.15 ± 1.05	3.15 ± 0.99	2.94 ± 0.98	2.98 ± 0.99
***Mineralizing Surface* (MS)**	0.49 ± 0.14	0.31 ± 0.06[§]	0.47 ± 0.09	0.63 ± 0.08*

* Effect of genotype, $p<0.05$. [§] Effect of age, $p<0.05$.

BFR is the volume of mineralized bone formed for unit time. Calculating the product of MAR and MS and expressing it relative to the bone surface (BS) can acceptably estimate BFR [(MAR*MS)/BS] (112). This calculation uses all double calcein labels and 50% of the single calcein labels in the sample. BFR was similar in both WT and Npt2 KO mice at 25-days of age (Figure 18). However, at 115-days of age, the BFR was significantly increased in Npt2 KO mice ($p<0.01$). Thus, age had a similar effect on BFR as it did on MS in both WT and Npt2 KO mice. While BFR decreased with age in the WT mice, it increased in Npt2 KO mice. The similarities between BFR and MS are due mainly to the fact that BFR is a histomorphometric parameter that is partially derived from MS.

Further evaluation of the histological and histomorphometrical features of the bones of Npt2 KO mice are underway. There is preliminary data that suggests that Npt2 KO mice have an increase in osteoblast surface at 115-days of age in comparison to that of 25-days of age, and that WT mice experience an age-dependent decrease in osteoblast surface (data not shown). There does not appear to be any increase in the amount of osteoid present in Npt2 KO mice (data not shown).

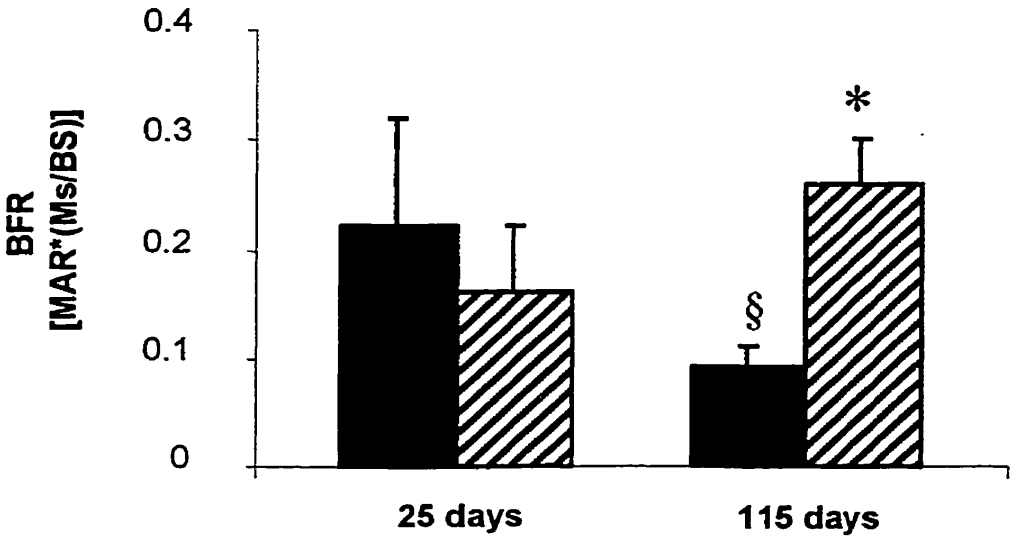

Figure 18: Effect of age and *Npt2* gene ablation on the rate of bone formation. BFR was estimated in WT (solid bars) and Npt2 KO (hatched bars) by calculating the product of mineral apposition rate (MAR) and mineralizing surface (MS) and expressing it relative to the bone surface (BS): [(MAR*MS)/BS]. The calculation incorporates all of the double calcein labels and 50% of the single labels of the section. * Effect of genotype, $p<0.05$. § Effect of age, $p<0.05$.

11 DISCUSSION

11.1 SUMMARY OF RESULTS

Firstly, this report examines the effects of *Npt2* gene ablation and age on renal BBM Na^+-Pi transport, Na^+-Pi gene expression, and the renal adaptive response to dietary Pi restriction. We show that BBM Na^+-Pi cotransport is significantly compromised in mice lacking *Npt2*, and it is not age-dependent, as it is in WT mice. Furthermore, we show that Npt2 KO mice exhibit age-dependent increases in the renal abundance of Npt1, Glvr-1, and Ram-1 mRNAs that are unable to correct BBM Pi transport following *Npt2* gene ablation, or alter age-dependent functional activity. In addition, we have determined that Npt2 KO mice are unable to mount a renal adaptive response to Pi restriction, attesting to the importance of *Npt2* in effecting this response. Secondly, we have pursued the mechanism of elevated serum $1,25(OH)_2D_3$ and attendant hypercalcemia and hypercalciuria observed in the Npt2 KO mouse. We determined that the hypercalcemia and hypercalciuria observed in Npt2 KO mice is due, in part, to increased intestinal Ca absorption. We provide evidence that suggests that elevations in serum $1,25(OH)_2D_3$ of Npt2 KO mice may be mediated through altered expression of the synthetic and catabolic enzymes, 1α- and 24-hydroxylase, as indicated by the increased abundance of 1α-hydroxylase mRNA, and decreased abundance of 24-hydroxylase mRNA. Finally, we have gained additional insight into the age-dependent bone phenotype observed in the Npt2 KO mouse. The most notable features are that osteoclast number and activity are persistently compromised in Npt2 KO mice. Concomitant to the osteoclast defect, WT and Npt2 KO mice display opposing age-related changes in mineralizing surface and, subsequently, bone formation rate.

11.2 EFFECT OF AGE AND Npt2 GENE ABLATION ON RENAL BBM Na^+-Pi COTRANSPORT, RENAL BBM Npt2 PROTEIN ABUNDANCE, AND RENAL Na^+-Pi COTRANSPORTER mRNAS

We have characterized renal BBM Na^+-Pi cotransport and Na^+-Pi cotransporter gene expression in WT and Npt2 KO mice between weaning (21 days) and 115 days of age. Our results show that renal BBM Na^+-Pi cotransport undergoes an age-dependent decrease between weaning and 115 days of age in WT mice (Figure 6). This is in agreement with the theory that the phosphate requirement of the younger, more quickly growing mammal is greater than that of the slow growing adult. Previous studies in the rat (55,59,60,113) and in guinea pigs (114) have also identified age-related decreases in BBM Na^+-Pi cotransport activity. Moreover, the age-dependence is specific to Pi transport, and does not involve the sodium-coupled transports of sulfate, D-glucose, or L-proline (59), indicating that the driving force for Pi transport (i.e. the sodium gradient) is *not affected by age.*

One study recently reported a 2-fold decrease in BBM Na^+-Pi cotransport in aged (12-16 months) rats, relative to young (3-4 months) rats (59). The decline in V_{max} was attributed to a similar decrease in both Npt2 protein and mRNA abundance (59). We, however, did not observe a significant decrease in either Npt2 protein or mRNA with increasing age. The discrepancy might be attributed to differences in the age, or the species investigated, with the age of the older mice in this study comparable to that of the younger rats in the previous report (59). Alternatively, the magnitude of the decrease in BBM Na^+-Pi cotransport in this study (23%) may have been insufficient to detect changes in Npt2 protein abundance and mRNA; recall that the previous study observed a 50% decrease in BBM Na^+-Pi cotransport (59).

There has been some suggestion that the greater Na^+-Pi cotransport activity in the BBM of weanling rats as compared to 3 month old rats is mediated by a growth-related Na^+-Pi cotransporter that is distinct, yet highly homologous to Npt2 (46). However, this putative growth-related Na^+-Pi cotransporter remains to be identified at the molecular level. In this study, we establish that the compromised BBM Na^+-Pi cotransport activity observed in Npt2 KO mice is not age-dependent as it is in WT mice (Figure 1). The absence of an age-dependent decrease in renal BBM Na^+-Pi cotransport in Npt2 KO mice suggests that the effects of a novel growth-related Pi transporter on Pi transport are either undetectable at weaning or require the presence of Npt2. We did not evaluate BBM Na^+-Pi cotransport activity in Npt2 KO mice prior to weaning. Previous accounts of age-dependent decreases in Npt2 protein abundance and our observation of uniform BBM Na^+-Pi cotransport in Npt2 KO mice at all ages examined provide unequivocal evidence that the age-related changes in Na^+-Pi cotransport in WT mice can be attributed to changes in Npt2 gene expression.

Previous studies indicate that Npt2 is the dominantly expressed renal Na^+-Pi cotransporter, accounting for approximately 84% of total cotransporter transcript in the murine kidney (19). RNaseH hybrid depletion studies suggest that Npt2 mediates most renal Na^+-Pi cotransport in the mouse (115). The current findings, along with a previous report from our laboratory (19) also suggest that Npt2 is a substantial contributor to renal BBM Na^+-Pi cotransport. Ablation of the Npt2 gene causes an 80-90% reduction in renal BBM Na^+-Pi cotransport depending on the age studied (Figure 6 and (93)).

Given that the magnitude of Pi resorption proposed to be mediated by *Npt2* is large, and that the Npt2 KO mouse appears to have a relatively normal growth rate, it was

of significant interest to evaluate the expression of Npt1, Glvr-1, and Ram-1 in the Npt2 KO mouse. We wished to determine whether the expression of another renal Na^+-Pi cotransporter was upregulated upon the loss of *Npt2*. However, aside from a moderate increase in the mRNA abundance of Glvr-1 in 115-day-old Npt2 KO mice relative to age-matched WT mice, there was no evidence of compensatory regulation from the other Na^+-Pi cotransporters. In fact, at 21 days of age, the renal mRNA abundance of Npt1, Glvr-1, and Ram-1 were all less in the Npt2 KO mouse than that of the age-matched WT mouse. However, we observed significant age-dependent increases in the renal abundance of Npt1, Glvr-1, and Ram-1 mRNAs in the Npt2 KO mouse that were not uniformly observed in the WT mouse. In spite of increases in the renal mRNA abundance of these transporters, renal BBM Na^+-Pi cotransport was unchanged with age, and remained compromised in the Npt2 KO mouse.

Understandably, changes in mRNA abundance need not reflect the abundance, or activity of BBM Na^+-Pi cotransporter protein. Thus, we quantified immunoreactive Npt1 protein in the BBM of WT and Npt2 KO mice (Figure 11a). We did not observe any change in the expression of Npt1 in Npt2 KO mice. While we attempted to quantify Glvr-1 protein abundance on these same samples, we could not detect any immunoreactive protein in the BBM of either WT or Npt2 KO mice (data not shown). Although, Boyer *et al.* detected Glvr-1 protein in crude kidney membrane preparations (64), the failure to detect Glvr-1 in PT BBMs is readily explained by the emerging hypothesis that Glvr-1 is not located on the apical membrane. There are several lines of evidence to support this, including the data we present here. While the distribution of Glvr-1 is tissue ubiquitous (19,63), its expression relative to other Na^+-Pi cotransporters

in the kidney is fairly insignificant (<1%). The affinity of Glvr-1 for Pi is ~10-fold greater than that of Npt2 (Glvr-1: 10 μM vs. Npt2: 100 μM), and it is regulated by extracellular Pi (65). Furthermore, the primarily identified function of Glvr-1 was that of a blood-borne viral receptor (116). Taken together, these properties suggest that Glvr-1 may in fact be located on the basolateral membrane. As such, Glvr-1 would not be involved in renal Pi resorption, but function in the capacity of a housekeeping transporter to meet the cellular metabolic requirement of Pi in the event of insufficient filtered Pi. The increase in the renal mRNA abundance of Glvr-1 that is observed in 115-day-old Npt2 KO mice might reflect an increased cellular need for Pi in the hypophosphatemic state.

At this point, it is worth emphasizing that the measurement of BBM Pi transport activity isolates and demarcates renal Pi transport in the PT cells only, whereas, the quantification of mRNA abundance is more global, describing the kidney as a whole. Thus, while we were able to measure Pi resorption at the PT, our methodology does not take into account the activity and the regulation of more distally located Na^+-Pi cotransporters.

Npt1, *Glvr-1*, and *Ram-1*, but not *Npt2*, are also expressed in the distal tubule (117). Na^+-Pi cotransport in immortalized murine distal convoluted tubule (MDCT) cells is regulated differentially from that in the PT: Pi transport is stimulated with low pH, and is not altered by PTH. Pi uptake, however, is also stimulated by extracellular Pi concentration (118-120). The relative mRNA abundance of Npt1 compared to Glvr-1 and Ram-1 as assessed by RPA is 0.17, 0.41, and 0.43, respectively (117), and preincubation of MDCT cells with Npt1 antisense oligonucleotides indicated that in these

cells ~20% of Pi uptake appears to be mediated by Npt1 (117). We did not observe an increase in BBM Npt1 protein in the Npt2 KO mouse. Thus, the observed increase in Npt1 mRNA abundance might reflect changes in the expression and activity of more distally located Npt1 protein, which could lead to an increase in Pi transport in the distal nephron of Npt2 KO mice that we would not have detected. However, this, and another study have shown that the abundance of Npt1 protein was not increased in response to Pi deprivation (refer to Figure 11a)(16). Whether *Npt2* gene ablation itself is sufficient to cause an increase in Npt1 protein in the distal tubule is not known. If Glvr-1 and Ram-1 are indeed located on the basolateral membrane of the cell, then increases in distal tubule mRNA abundance of these type III transporters are extraneous to Pi reabsorption. It is of interest to determine what other Na^+-Pi cotransporter(s) mediate the distal tubule Pi transport that is not attributable to Npt1 (i.e. the remaining 80%), particularly since Npt1 appears to have multiple activities that may outweigh its action as a Pi transporter.

In addition to PT BBM localization, *Npt1* has been identified at the basolateral (sinusoidal) membrane of murine hepatocytes (21). Npt1 has capacity to transport β-lactam antibiotics (21) and Cl^- (23) in addition to Pi. Npt1 is not regulated by extracellular or dietary Pi (16), while its expression is regulated by glucose, insulin, and glucagon (20). The regulation of Npt1 by PTH has not been documented. It is quite possible that Npt1 does not contribute significantly to Pi homeostasis. To further characterize the role of Npt1 in Pi homeostasis, the murine *Npt1* gene has recently been cloned with the intention to disrupt the *Npt1* gene in mice through homologous recombination (121).

We conclude that *Npt2* is primarily responsible for the age-related decline in BBM Na^+-Pi cotransport observed in the WT mouse, and confirm the significant contribution of Npt2 to renal Pi handling. In addition, we find that age-dependent increases in the renal abundance of Npt1, Glvr-1, and Ram-1 do not compensate for the loss of *Npt2*.

11.3 ROLE OF Npt2 IN THE RENAL ADAPTIVE RESPONSE TO DIETARY Pi DEPRIVATION

The role of Npt2 in the renal BBM response to low Pi diet is well-established (6,18,39,42,122). In agreement with previous studies, this study found that Pi deprivation of WT mice elicited a 3.4 fold increase in BBM Na^+-Pi cotransport, a similar increase in Npt2 protein, and an increase in Npt2 mRNA abundance. In contrast, Npt2 KO mice were unable to mount an adaptive response to low Pi diet, reinforcing the notion that Npt2 is essential to the BBM adaptive response to low Pi diet.

The effects of low Pi diet on the abundance of Npt1, Glvr-1, and Ram-1 mRNAs were examined in WT and Npt2 KO mice. Pi restriction caused an increase in the abundance of renal Npt1 mRNA in both genotypes. Previous studies in our lab have not documented a similar increase in normal mice (19). However, in the current study, we did not observe a parallel increase in Npt1 protein abundance in response to low Pi diet (Figure 11a). As mentioned in the preceding section, we did not measure the effects of Npt2 KO or dietary Pi deprivation on distal tubule Pi transport. We do not know whether the increase in Npt1 mRNA also reflects an increase in Npt1 protein abundance or activity in the distal portion of the nephron.

Pi deprivation has been shown to stimulate an increase in Glvr-1 and Ram-1 mRNA abundance and consequently Pi transport in rat 208F fibroblasts (62), and to increase Ram-1 mRNA abundance in a variety of human cell lines (65). Chien *et al.* demonstrated that under conditions of Pi deprivation, the observed increase in Ram-1 mRNA abundance was post-transcriptionally mediated and could be attributed to an increase in mRNA stability (65). However, incubating OK cells in Pi free media has no effect on the protein abundance of type III Na^+-Pi cotransporters (64), nor are Glvr-1 or Ram-1 renal mRNA abundance upregulated in Pi-deprived normal or *Hyp* mice (19). In the current study, we did not observe an increase in either Glvr-1 or Ram-1 mRNA abundance in either Pi-deprived WT or Npt2 KO mice.

It is interesting to consider the expression and activity of Npt2 in *Hyp* mice under both normal and Pi-deprived conditions, and to compare these data with those of the current study to document the importance of Npt2 to the adaptive response to Pi deprivation. *Hyp* mice are the murine homologue of the dominantly inherited human disorder, X-linked hypophosphatemia. Like Npt2 KO mice, *Hyp* mice are hypophosphatemic, but the defect in Pi transport is secondary to a mutation in the *Phex* gene and a lack of Phex protein. Although the function of Phex is unknown, it affects the expression and activity of Npt2, such that Na^+-Pi cotransport, Npt2 protein abundance, and the renal abundance of Npt2 mRNA are all significantly decreased in the *Hyp* mouse (94). The limited renal Pi reabsorption in *Hyp* mice leads to serum Pi values about 65% of that of normal mice (19).

Hyp mice are able to respond to low Pi diet with an increase in BBM Na^+-Pi cotransport that is mediated through an increase in BBM Npt2 protein (42). Although the

increase in BBM Na^+-Pi cotransport in response to low Pi diet is not as great as that in normal mice, the protein abundance of Npt2, relative to that of meprin, increases to identical levels in normal and *Hyp* mice. However, serum Pi in Pi-deprived *Hyp* mice is significantly lower than that in normal mice on the same low Pi diet (19). This suggests that in spite of having the ability to mount an adaptive response to dietary Pi restriction, albeit blunted, *Hyp* mice retain the functional defect in Na^+-Pi cotransport for unknown reasons (42).

Conversely, Npt2 KO mice are devoid of the Npt2 protein and do not exhibit the adaptive increase in Na^+-Pi cotransport in response to low Pi diet. However, serum Pi levels are similar in Pi-deprived WT and Npt2 KO mice. The discrepancy in serum Pi between normal/WT, *Hyp*, and Npt2 KO mice may lie in the regulation of vitamin D metabolism.

Thus, by comparing normal/WT, *Hyp*, and Npt2 KO mice, we can conclude that the adaptive response to a low Pi diet requires the expression of Npt2 in the PT BBM. WT mice do not show increases in Npt1 protein in response to low Pi diet, nor does Npt1 protein abundance in Npt2 KO mice differ from WT mice under control or low Pi dietary conditions.

11.4 MECHANISM AND EFFECTS OF ELEVATED $1,25(OH)_2D_3$ ON INTESTINAL ABSORPTION IN Npt2 KO MICE

Npt2 KO mice are both hypophosphatemic and hypercalcemic. Both are normal systemic responses to dietary Pi deprivation. The primary cause of hypercalcemia in normal Pi-deprived rats has long been attributed to an increase in bone resorption (123,124) as opposed to a vitamin D-dependent increase in intestinal Ca absorption (125).

We previously showed that Npt2 KO mice are still hypophosphatemic and hypercalcemic when compared to WT mice at 5 months of age, yet their bone phenotype has improved by this time (93). The improvements in the bone phenotype of the Npt2 KO mouse do not support the suggestion that the observed hypercalcemia is mediated by excessive bone resorption. With the knowledge that Npt2 KO mice have elevated serum $1,25(OH)_2D_3$, we investigated the possibility of vitamin-D dependent intestinal Ca hyperabsorption as the cause of the hypercalcemia in these mice.

Under conditions of Pi deprivation serum Pi values in *Hyp* mice are lower than those of normal mice, whereas serum Pi in Npt2 KO mice is equivalent to the WT mice. The differences in serum Pi values in Pi-deprived normal/WT, *Hyp*, and Npt2 KO mice could reflect the appropriate or inappropriate regulation of $1,25(OH)_2D_3$. The Ca load test provided evidence that Npt2 KO mice experience vitamin D-mediated intestinal Ca hyperabsorption. In the absence of food, Npt2 KO mice are not hypercalciuric (Figure 13a), demonstrating that available dietary Ca and its intestinal absorption are necessary for hypercalciuria in the Npt2 KO mice.

In normal mice, Pi restriction causes a decrease in serum Pi, which in turn leads to an adaptive increase in the synthesis of $1,25(OH)_2D_3$ by renal 1α-hydroxylase (126,127). This in turn, causes an increase in serum $1,25(OH)_2D_3$ levels (128) which stimulates intestinal Ca (129) and Pi (129,130) absorption. In spite of the physiological adaptations that ensue to maintain Pi homeostasis (i.e. an Npt2-mediated adaptive increase in BBM Na^+-Pi cotransport), serum Pi remains depressed in Pi-deprived normal mice (Table 3) (19,42). At the same time there is virtually no Pi excreted in the urine (Table 3)(129).

In contrast to the normal response, *Hyp* mice fail to elicit an appropriate increase in $1,25(OH)_2D_3$. Under normal dietary Pi conditions *Hyp* mice have elevated levels of 24-hydroxylase activity (101) which leads to decreased levels of circulating $1,25(OH)_2D_3$ by increased catabolism. Pi-deprived *Hyp* mice demonstrate a further increase renal 24-hyroxylase activity (128), 24-hydroxylase immunoreactive protein, and mRNA abundance (131), resulting in a further decrease in serum $1,25(OH)_2D_3$ (128).

We previously reported that $1,25(OH)_2D_3$ is elevated in Npt2 KO mice under normal dietary conditions (93). This study and ongoing studies in our lab indicate that the abundance of 1α-hydroxylase mRNA is increased, and 24-hydroxylase mRNA is decreased in Npt2 KO mice (Table 4). These directional changes in mRNA abundance are opposite to those observed in the *Hyp* mouse, and promote the increase in serum $1,25(OH)_2D_3$ observed in Npt2 KO mice.

In summary, Pi-deprived *Hyp* mice demonstrate the adaptive increase in BBM Na^+-Pi cotransport but lack the appropriate regulation of $1,25(OH)_2D_3$, whereas, Npt2 KO mice cannot mount the adaptive BBM response, but demonstrate the correct regulation of $1,25(OH)_2D_3$ (Table 7).

Table 7
Renal BBM and vitamin D adaptive response to Pi-deprivation in Normal/WT, *Hyp*, and Npt2 KO mice.

	BBM adaptive response to Pi-restriction	Vitamin D response to hypophosphatemia		
		Serum $1,25(OH)_2D_3$	1α-hydroxylase	24-hydroxylase
Normal or WT mice	↑	↑	↑	↓
Hyp mice	↑	--	--	↑
Npt2 KO mice	--	↑	↑	↓

The effects of fasting and oral Ca loading on urine Pi/Cr and Mg/Cr were also measured in WT and Npt2 KO mice. Both genotypes experienced an increase in urinary Pi excretion when fasted, a phenomenon that has been previously documented (20,132). Although an increase in urinary Pi excretion seems counterintuitive to the conservation of Pi, there are additional metabolic changes associated with fasting that alter the renal handling of Pi reabsorption. Metabolic acidosis has been shown to contribute to the increase in Pi excretion that is associated with fasting (132). Fasting has been found to decrease renal Pi resorption via the down-regulation of renal tubular Na^+-Pi cotransport activity and renal Npt1 mRNA in the rat (20). In contrast to a low Pi diet, fasting neither upregulates renal Na^+-Pi cotransport (133) nor affects *Npt2* gene expression in the rat (20). Thus, it is not entirely surprising that both WT and Npt2 KO mice experienced a similar response to fasting.

Approximately 97% of filtered Mg is reabsorbed in the renal tubules; 25-30% in the proximal tubule, 60- 65% in the thick ascending limb of the loop of Henle (TALH), and 5% in the distal tubule. Mg absorption from the small intestine does not appear to be influenced by PTH, calcitonin, or $1,25(OH)_2D_3$ (134). Both hypercalcemia and Pi depletion inhibit the reabsorption of Mg in the TALH (135). Perhaps this explains the slight elevation in urine Mg/Cr at baseline in Npt2 KO mice in comparison to WT mice. Although urine Mg/Cr is elevated with fasting in both genotypes, urine Mg/Cr does not vary significantly between the genotypes under the examined dietary conditions. This supports the notion that the regulation of Ca and Mg homeostasis occurs by different mechanisms.

11.5 EFFECT OF AGE AND Npt2 GENE ABLATION ON THE SKELETAL EXPRESSION OF Glvr-1, OSTEOCALCIN, AND Phex mRNAS

Glvr-1, osteocalcin, and Phex are expressed in the bone. Although the function of these genes in bone is not fully identified, their expression has been associated with different stages of bone development and/or mineralization. In this study we determined the effects of Npt2 KO and age on Glvr-1, osteocalcin, and Phex mRNA abundance.

11.5.1 Glvr-1

There is evidence for Glvr-1 expression in bone (19), and it has been identified in human osteoblast-like cells, SaOS-2 (136). The pH dependence of osteoblast Pi transport and that of Glvr-1 are similar (75), and osteoblastic Pi transport is thought to be important for the initiation of bone matrix calcification. However, more recently, an *in vivo* model of endochondral bone formation failed to detect Glvr-1 in osteoblasts (76). Therefore, it is likely that there are other, as yet unidentified, Pi transporters that are expressed in osteoblasts and mediate Pi transport in these cells.

As indicated above, *in vivo* expression of Glvr-1 during embryonic endochondral bone formation was detected in mouse metatarsal sections by *in situ* hybridization (76). Expression of Glvr-1 was confined to populations of hypertrophic chondrocytes involved in the active mineralization of bone matrix, but was not observed in either fully differentiated chondrocytes or in osteoblasts (76). Glvr-1 expression in the chondrocytes was isolated to a subpopulation that localized to the mineralization zone, suggesting that Glvr-1 may be involved in matrix calcification (76). While there is no data on the patterns of Glvr-1 expression in bone after birth, we found that in both WT and Npt2 KO mice, there is a significant decrease in Glvr-1 mRNA abundance between 21- and 115-days of age (Figure 15a). Glvr-1 expression was the same in both WT and Npt2 KO mice

at 21- and at 115-days of age, however at 45-days of age Glvr-1 expression was significantly reduced in Npt2 KO mice (Figure 15a). The reason for altered Glvr-1 expression at 45-days of age in Npt2 KO mice is not clear. However, it is between 21- and 115-days of age that the age-dependent changes in the bone phenotype of the Npt2 KO mouse occur (93). Altered Glvr-1 expression in Npt2 KO mice at 45-days of age may reflect the number of hypertrophic chondrocytes present in the zone of mineralization and/or those that are active in the mineralization process.

11.5.2 Osteocalcin

Osteocalcin is an extracellular matrix protein that is synthesized by fully differentiated osteoblasts and chondrocytes (137). The protein binds calcium, has a strong affinity for hydroxyapatite, and its secretion by osteoblast cells coincides with mineralization in osteoblast cultures and developing bone (84,86,137-139). Thus, the measurement of serum osteocalcin has traditionally been used as an indicator of bone formation. Changes in the abundance of murine osteocalcin mRNA abundance appear to reflect changes in osteocalcin protein, as demonstrated by comparable effects of $1,25(OH)_2D_3$ on both osteocalcin mRNA abundance and serum osteocalcin (84).

We show that the mRNA abundance of osteocalcin decreased with age in WT mice (Figure 15b), thus correlating with the rate of bone formation (Figure 18). However, osteocalcin mRNA abundance also decreased with age in Npt2 KO mice, but it did not correlate to BFR. The increase in BFR observed in Npt2 KO mice has been partially attributed to an intrinsic defect of the osteoclast and decreased bone resorption, which may uncouple the relationship of osteocalcin gene expression and BFR.

As with the expression of Glvr-1, Npt2 KO mice experienced a significant decrease in the mRNA abundance of osteocalcin in comparison to WT mice at 45 days of age. At this time, we are unable to determine whether the decrease is mRNA abundance accurately reflects osteocalcin protein abundance, and if so, the specific cause or the effect of limited osteocalcin production at 45-days of age on the bone phenotype of Npt2 KO mice.

11.5.3 Phex

Recently, Phex expression has been localized to human osteosarcoma-derived MG-63 osteoblasts (90), differentiated MC3T3-E1 osteoblasts (90,92), and in murine osteoblasts and odontoblasts from embryonic day 15 forward (78). The timing and localization of Phex expression correlates strongly with the stage of osteoblast development and possibly matrix mineralization (78,90,92). In agreement with Ruchon *et al.*(78), we found that Phex mRNA abundance was decreased in older mice as compared to younger mice. The age-related decline in Phex expression was observed in both WT and Npt2 KO mice.

As with the osteoblast-specific expression of osteocalcin (84-86), Phex is negatively regulated by $1,25(OH)_2D_3$ (92). Thus, we can propose that the differences in abundance of osteocalcin and Phex mRNAs in Npt2 KO mice at 45 days of age may be due to differences in the level of circulating $1,25(OH)_2D_3$, perhaps in combination with other developmental changes that occur at or around 45 days of age. Whether Glvr-1 is controlled by vitamin D in a similar manner is not known.

11.6 EFFECT OF AGE AND NPT2 KO ON BONE HISTOMORPHOMETRY AND HISTOLOGY

Clearly, there are significant differences in the renal handling of Pi and of Ca in Npt2 KO mice in comparison to WT mice. Alterations in renal Pi and Ca reabsorption can have significant effects on Ca and Pi homeostasis and, in turn, on the bone phenotype. As mentioned earlier, Pi-deprivation induces osteoclast-mediated bone resorption in a vitamin D dependent manner, and an increase in the number and size of actively resorbing osteoclasts (140). Beck *et al.* showed that the Npt2 KO mouse is chronically hypophosphatemic and exposed to high levels of $1,25(OH)_2D_3$ (93). However, we found that osteoclast number is not increased in the Npt2 KO mouse, and the improvement of the bone phenotype is inconsistent with increased osteoclast bone resorption.

We examined the age-dependence of the bone phenotype of the Npt2 KO mouse. Histological and histomorphometric analysis revealed striking differences between WT and Npt2 KO mice. The primary finding was a significant reduction in osteoclast index at both 21 and 115-days of age (Figure 16a). While the mechanism for this finding is not fully understood, the identification of Npt2 in the osteoclast (manuscript in preparation) strongly suggests that Npt2 is necessary for normal osteoclast performance. Despite the surplus of circulating $1,25(OH)_2D_3$ in Npt2 KO mice, osteoclasts do not appear able to proliferate appropriately without Npt2. It has been suggested that an osteoclast Pi transporter, such as Npt2, might be necessary to ensure that the ATP/energy requirement of the osteoclast is met during the processes of migration, attachment, and resorption (35).

The ruffled border of the osteoclast is a highly acidic environment due to the protonation required to dissolve bone mineral. The resulting acidic environment is not optimal for Npt2-mediated Pi transport since the affinity of Npt2 for Pi is significantly reduced at acidic pH (31). Thus, the basolateral localization of osteoclast Npt2 might be predictable. Gupta *et al.* (35)recently characterized Pi transport in the osteoclast, and identified an Npt2 immunoreactive protein that translocated to the basolateral membrane of the polarized resorbing osteoclast.

The decrease in osteoclast index of Npt2 KO mice suggests that the lack of Npt2 in the osteoclast may prevent proper osteoclast proliferation or cause early apoptosis. Decreased Pi uptake may prevent the osteoclast from meeting normal cellular metabolic requirements, and lead to a decrease in osteoclast number. The effects of Npt2 gene ablation and decreased osteoclast number are evident in the measurement of osteoclast eroded perimeter. Osteoclast-mediated bone resorption was significantly decreased at 25-days of age in comparison to WT mice. However, while bone resorption remained constant with age in Npt2 KO mice, it decreased with age in the WT mice, making the rate of bone resorption in WT and Npt2 KO mice equal by 115 days of age. During this time MAR remained constant in both WT and Npt2 KO mice (Table 6). Disrupting the relationship of bone resorption and bone formation in the Npt2 KO mouse increased the BFR as compared to WT mice by 115 days of age (Figure 18).

The situation in the *Hyp* mouse model differs from that in the Npt2 KO mice. In the *Hyp* mice there is a defect in osteoblast-mediated mineralization (for review, see (87)). These mice have an enlarged osteoid thickness of both the caudal vertebrae (141), and the calvaria (91). In contrast, Npt2 KO mice show no evidence of an osteoblast

mineralization defect. Neither MAR or BFR are decreased in Npt2 KO mice in comparison to age-matched WT mice. In fact, osteoblast surface is increased in Npt2 KO mice at 115 days of age, and there is no evidence for increased osteoid thickness in Npt2 KO mice (data not shown). These findings lend support to the previously stated hypothesis that the *Hyp* defect in bone mineralization is due to an intrinsic osteoblast defect in addition to a hypophosphatemic environment. However the results do not fully explain the failure of Npt2 KO mice to have normal bone histology at weaning. In an effort to explain this, we suggest that in the balance of reciprocal osteoclast-mediated bone resorption and osteoblast-mediated mineral apposition, the primary ARF cycle is more dependent on osteoclast resorption than subsequent ARF cycles. The initial ARF cycle requires the resorption of the cartilage scaffold prior to the initial deposition of mineral matrix by osteoblasts, while subsequent ARF cycles involve the resorption of mineralized bone matrix in order to remodel existing trabeculae.

11.7 A MOUSE MODEL FOR A HUMAN DISEASE?

When the biochemical phenotype of the Npt2 KO mouse was first described, we noted that it closely resembled that of the human disorder hereditary hypophosphatemic rickets with hypercalciuria (HHRH) (104). NPT2 had been a candidate gene for HHRH due to the renal phosphate wasting phenotype characteristic of HHRH (104) and the demonstration that all pathological abnormalities (except the defect in Pi reabsorption) are corrected by Pi supplementation (104). The biochemical features of the Npt2 KO mouse seemed to support this (93). However, there appeared to be distinct discrepancies in the human and murine bone phenotypes, namely that the bone phenotype of Npt2 KO mice improved with age, where no improvements had been reported in untreated HHRH

patients. Moreover, histologically, the bone phenotype of HHRH is characterized by wide osteoid seams, irregular mineralization fronts, and single wide tetracycline bands upon labelling (104), a description typical of osteomalacia. In contrast, this study provides concrete evidence that the Npt2 KO mouse does not display osteomalacic bone disease. Npt2 KO mice show normal to increased mineralizing surface, distinct double labels, and no increase in osteoid (preliminary data, data not shown). Furthermore, single stranded conformation polymorphism (SSCP) and direct sequence analysis of DNA samples from the Bedouin HHRH pedigree originally reported by Tieder *et al.* (104) show no mutations in the exons of the NPT2 gene (142). At this time, there does not appear to be a human disease that is homologous to the Npt2 KO mouse.

11.8 FUTURE STUDIES

There remain many aspects of the Npt2 KO mouse to be investigated at the renal, intestinal, and skeletal levels. As PTH is another important regulator of renal Pi resorption that mediates its effects through Npt2, it would be of considerable interest to determine the effects of PTH on renal Pi resorption in the Npt2 KO mouse. For similar reasons, the effect of a diet high in Pi on the biochemical and renal features of the Npt2 KO mouse would also be of interest. We have yet to thoroughly examine the gross effects of Npt2 KO on renal histology, either. In addition, this study focused on renal PT Pi transport, and did not take into account Pi transport in more distal segments of the nephron. It would be informative to determine whether the Npt2 KO mouse exhibits adaptive properties in the distal tubule in response to chronic hypophosphatemia.

The intestinal phenotype of the Npt2 KO mouse requires more clarification. Functional studies on intestinal Ca and Pi resorption in WT and Npt2 KO mice would

corroborate the evidence that we provide in this study for intestinal Ca hyperabsorption in the Npt2 KO mouse. A multitude of molecular studies could examine the expression of genes implicated in intestinal Ca and/or Pi reabsorption in the GI tract, such as ECaC (71) or the type IIb Na^+-Pi cotransporter (34).

Finally, our understanding of the bone phenotype of the Npt2 KO mouse is still in its infancy. Although we have evidence that the osteoclast defect observed in the Npt2 KO mouse is the direct consequence of osteoclast *Npt2* gene ablation, we do not understand the mechanism by which this affects osteoclast number. Osteoclast formation assays would help us determine whether osteoclast formation from precursor cells is compromised, or whether the osteoclasts of Npt2 KO mice undergo enhanced rates of apoptosis. In this study we examined a tightly defined range of ages. We are thus unaware of the long-term effects of Npt2 gene ablation on bone remodelling, and the differences in the bone phenotypes of the aged WT and Npt2 KO mouse.

12 SUMMARY AND CONCLUSIONS

This study succeeded in characterizing some of the salient features of Pi homeostasis in the young, and aging mouse, and the consequences of ablating the predominant renal Na^+-Pi cotransporter, Npt2. Although the kidney is the major determinant of Pi homeostasis, dietary Pi intake, intestinal Pi absorption, and bone Pi flux are also important mediators of Pi homeostasis. In addition, physiological changes that attempt to normalize Pi levels have an impact the homeostasis of other minerals, such as Ca, and have the potential of affecting normal skeletal growth.

The Npt2 KO mouse served as an excellent model in which to demonstrate that the age-dependent decline in renal Na^+-Pi cotransport in the WT mouse is dependent

primarily on a decrease in Npt2 gene expression; Npt2 KO mice showed no age-related decline in renal Na^+-Pi cotransport. This mouse model also allowed us to conclude that Npt2 is essential to the normal adaptive increase in renal BBM Na^+-Pi cotransport in response to dietary Pi restriction. We have also established that the other known renal Na^+-Pi cotransporters are unable to compensate for the loss of Npt2 during growth, or during Pi deprivation.

With respect to the distinctive bone phenotype of the Npt2 KO mouse, we have made the observation that contrary to the normal osteoclast response to hypophosphatemia, the Npt2 KO mouse exhibits a decrease in osteoclast number and resorptive capacity. We also provide considerable histological and histomorphometric evidence that allow us to conclude that the Npt2 KO mouse does not display the characteristics of osteomalacia and/or rickets. This, in turn, builds upon the growing evidence that NPT2 is not a candidate gene for HHRH. Although Npt2 KO mice are hypophosphatemic, neither mineral apposition rate, nor mineralizing surface are impaired. We are currently unable to specify the exact mechanism of reduced osteoclast number, however, we explain the age-dependent bone phenotype in the Npt2 KO mouse as a consequence of limited bone resorption coupled with normal or increased bone formation. In addition, at the skeletal level, Npt2 KO mice appear to be resistant to many of the consequences associated with aging and bone remodeling that are observed in the WT mouse.

We provide evidence that there is significant Ca hyperabsorption occurring in the in the intestine of the Npt2 KO mouse. Given the paucity of osteoclasts, and the respective increase and decrease in the mRNA abundance of the vitamin D synthetic and

catabolic enzymes, 1α-hydroxylase and 24-hydroxylase, we conclude that the hypercalciuria and hypercalcemia associated with Npt2 gene ablation are primarily dependent on vitamin D-mediated intestinal Ca absorption.

The sum of these results supports the concept that Npt2 is crucial to normal Pi homeostasis. Furthermore, these data demonstrate that Npt2 gene ablation has an impact on the integrated functions of the intestine, kidney, and bone in both Pi and Ca homeostasis.

13 Reference List

1. Berndt, T. and F. Knox. 1992. Renal regulation of phosphate excretion. In: The kidney, physiology and pathophysiology. D. Sledin and G. Giebisch, editors. Raven Press, New York. 2511-2532.

2. Murer, H. 1992. Cellular mechanisms in proximal tubular Pi reabsorption: Some answers and more questions. *Journal of the American Society of Nephrology* 2:1649-1665.

3. Murer, H. and J. Biber. 1992. Renal tubular phosphate transport cellular mechanisms. In: The Kidney: Physiology and Pathophysiology. D. Seldin and G. Giebisch, editors. Raven Press, New York. 2481-2509.

4. Murer, H., A. Werner, S. Reshkin, R. Wuarin, and J. Biber. 1991. Cellular mechanisms in proximal tubular reabsorption of inorganic phosphate. *American Journal of Physiology* 260:C885-C899

5. Biber, J., J. Forgo, and H. Murer. 1988. Modulation of Na^+-Pi cotransport in opossum kidney cells by extracellular phosphate. *American Journal of Physiology* 255:C155-C161

6. Lötscher, M., P. Wilson, S. Nguyen, B. Kaissling, J. Biber, H. Murer, and M. Levi. 1996. New aspects of adaptation of rat renal Na-Pi cotransporter to alterations in dietary phosphate. *Kidney International* 49:1012-1018.

7. Werner, A., M. Moore, N. Mantei, J. Biber, G. Semenza, and H. Murer. 1991. Cloning and expression of cDNA for a Na/Pi cotransport system of kidney cortex. *Proceedings of the National Academy of Science USA* 88:9608-9612.

8. Biber, J., G. Caderas, G. Stange, A. Werner, and H. Murer. 1993. Effect of low-phosphate diet on sodium/phosphate cotransport, mRNA and protein content and on oocyte expression of phosphate transport. *Pediatric Nephrology* 7:823-826.

9. Chong, S., K. Kristjansson, H. Zoghbi, and M. Hughes. 1993. Molecular cloning of the cDNA encoding a human renal sodium phosphate transport protein and its assignment to chromosome 6p21.3-p23. *Genomics* 18:355-359.

10. Ni, B., Y. Du, X. Wu, B. DeHoff, B. Rosteck, and S. Paul. 1996. Molecular cloning, expression and chromosomal localization of a human brain specific Na^+-dependent inorganic phosphate cotransporter. *Journal of Neurochemistry* 66:2227-2238.

11. Miyamoto, K., S. Tatsumi, T. Sonoda, H. Yamamoto, H. Minami, Y. Taketani, and E. Takeda. 1995. Cloning and functional expression of a Na^+-dependent phosphate co-transporter from human kidney: cDNA cloning and functional expression. *Biochemical Journal* 305:81-85.

12. Li, H. and Z. Xie. 1995. Molecular cloning of two rat Na^+/Pi cotransporters: evidence for differential tissue expression of transcripts. *Cellular and Molecular Biology Research* 41:451-460.

13. Ni, B., P. Rosteck, N. Nadi, and S. Paul. 1994. Cloning and expression of a cDNA encoding a brain-specific Na^+-dependent inorganic phosphate cotransporter. *Proceedings of the National Academy of Science USA* 91:5607-5611.

14. Chong, S., C. Kozak, L. Liu, K. Kristjansson, S. Dunn, J. Bourdeau, and M. Hughes. 1995. Cloning, genetic mapping, and expression analysis of a mouse renal sodium-dependent phosphate cotransporter. *American Journal of Physiology* 268:F1038-F1045

15. Biber, J., M. Custer, A. Werner, B. Kaissling, and H. Murer. 1993. Localization of NaPi-1, a Na/Pi cotransporter, in rabbit kidney proximal tubules. II. Localization by immunohistochemistry. *Pflügers Archiv European Journal of Physiology* 424:210-215.

16. Delisle, M.-C., C. Boyer, V. Vachon, S. Giroux, and R. Béliveau. 1994. Immunodetection and characterization of proteins implicated in renal sodium/phosphate cotransport. *Biochimica et Biophysica Acta* 1190:289-296.

17. Custer, M., F. Meier, E. Schlatter, R. Greger, A. Garcia-Perez, J. Biber, and H. Murer. 1993. Localization of NaPi-1, a Na-P_i cotransporter, in rabbit kidney proximal tubules. I. mRNA localization by reverse transcription/polymerase chain reaction. *Pflügers Archiv European Journal of Physiology* 424:203-209.

18. Werner, A., S. Kempson, J. Biber, and H. Murer. 1994. Increase of Na/Pi-cotransport encoding mRNA in response to low Pi diet in rat kidney cortex. *Journal of Biological Chemistry* 269:F900-F908

19. Tenenhouse, H., S. Roy, J. Martel, and C. Gauthier. 1998. Differential expression, abundance, and regulation of Na^+-phosphate cotransporter genes in the murine kidney. *American Journal of Physiology* 275:F527-F534

20. Li, H., M. Onwochei, R. Ruch, and Z. Xie. 1996. Regulation of rat Na/Pi cotransporter-1 gene expression: the roles of glucose and insulin. *American Journal of Physiology* 271:E1021-E1028

21. Yabuuchi, H., I. Tamai, K. Morita, T. Kouda, K. Miyamoto, E. Takeda, and A. Tsuji. 1998. Hepatic sinusoidal membrane transport of anionic drugs mediated by anion transporter *Npt*1. *The Journal of Pharmacology and Experimental Therapeutics* 286:1391-1396.

22. Busch, A., A. Schuster, S. Waldegger, C. Wagner, G. Zempel, S. Broer, J. Biber, H. Murer, and F. Lang. 1996. Expression of a renal type I sodium/phosphate-transporter (NaPi-1) induces a conductance in *Xenopus* oocytes permeable for organic and inorganic anions. *Proceedings of the National Academy of Science USA* 93:5347-5351.

23. Broer, S., A. Schuster, C. Wagner, A. Broer, I. Forster, J. Biber, H. Murer, A. Werner, F. Lang, and A. Busch. 1998. Chloride conductance and Pi transport are separate functions induced by the expression of NaPi-1 in *Xenopus* Oocytes. *Journal of Membrane Biology* 164:71-77.

24. Verri, T., D. Markovich, C. Perego, F. Norbis, G. Stange, V. Sorribas, J. Biber, and H. Murer. 1995. Cloning of a rabbit renal Na-Pi cotransporter, which is regulated by dietary phosphate. *American Journal of Physiology* 268:F626-F633

25. Magagnin, S., A. Werner, D. Markovich, V. Sorribas, G. Stange, J. Biber, and H. Murer. 1993. Expression cloning of human and rat renal cortex Na/Pi cotransport. *Proceedings of the National Academy of Science USA* 90:5979-5983.

26. Murer, H. and J. Biber. 1997. A molecular view of proximal tubular inorganic phosphate (Pi) reabsorption and of its regulation. *Pflügers Archiv European Journal of Physiology* 433:379-389.

27. Forster, I., N. Hernando, J. Biber, and H. Murer. 1998. The voltage-dependence of a cloned mammalian renal type II Na^+/Pi cotransporter (NaP_i-2). *Journal of General Physiology* 112:1-18.

28. Collins, J. and F. Ghishan. 1994. Molecular cloning, functional expression, tissue distribution, and in situ hybridization of the renal sodium phosphate (Na^+/Pi) transporter in the control and hypophosphatemic mouse. *FASEB* 8:862-868.

29. Helps, C., H. Murer, and J. Mcgivan. 1995. Cloning, sequence analysis and expression of the cDNA encoding a sodium-dependent phosphate transporter from the bovine renal epithelial cell line NBL-1. *European Journal of Biochemistry* 228:927-930.

30. Sorribas, V., D. Markovich, G. Hayes, G. Stange, J. Forgo, J. Biber, and H. Murer. 1994. Cloning of a Na/Pi cotransporter from opossum kidney cells. *Journal of Biological Chemistry* 269:6615-6621.

31. Werner, A., H. Murer, and R. Kinne. 1994. Cloning and expression of a renal Na-Pi cotransport system from flounder. *American Journal of Physiology* 267:F311-F317

32. Custer, M., M. Lötscher, J. Biber, H. Murer, and B. Kaissling. 1994. Expression of Na-Pi cotransport in rat kidney: localization by RT-PCR and immunohistochemistry. *American Journal of Physiology* 266:F767-F774

33. Kohl, B., P. Herter, R. Kinne, M. Elger, H. Hentschel, and A. Werner. 1996. Na-P_i cotransport in flounder: same transport system in kidney and intestine. *American Journal of Physiology* 270:F937-F944

34. Hilfiker, H., O. Hattenhauer, M. Traebert, I. Forster, H. Murer, and J. Biber. 1998. Characterization of a murine type II sodium-phosphate cotransporter expressed in mammalian small intestine. *Proceedings of the National Academy of Science USA* 95:14564-14569.

35. Gupta, A., X. Guo, U. Alvarez, and K. Hruska. 1997. Regulation of sodium-dependent phosphate transport in osteoclasts. *Journal of Clinical Investigation* 100:538-549.

36. Tatsumi, S., K. Miyamoto, T. Kouda, K. Motonaga, K. Katai, I. Ohkido, K. Morita, H. Segawa, Y. Tani, H. Yamamoto, Y. Taketani, and E. Takeda. 1998. Identification of three isoforms for the Na^+-dependent phosphate cotransporter (NaPi-1) in rat kidney. *The Journal of Biological Chemistry* 273:28568-28575.

37. Huelseweh, B., B. Kohl, H. Hentschel, R. Kinne, and A. Werner. 1998. Translated anti-sense product of the Na/phosphate co-transporter (NaPi-II). *Biochemical Journal* 332:483-489.

38. Boyer, C., Y. Xiao, A. Dugre, E. Vincent, M. Delisle, and R. Beliveau. 1996. Phosphate deprivation induces overexpression of two proteins related to the rat renal phosphate cotransporter NaPi-2. *Biochimica et Biophysica Acta* 1281:117-123.

39. Levi, M., M. Lötscher, V. Sorribas, M. Custer, M. Arar, B. Kaissling, H. Murer, and J. Biber. 1994. Cellular mechanisms of acute and chronic adaptation of rat renal Pi transporter to alterations in dietary Pi. *American Journal of Physiology* 267:F900-F908

40. Lötscher, M., B. Kaissling, J. Biber, H. Murer, and M. Levi. 1997. Role of microtubules in the rapid regulation of renal phosphate transport in response to acute alterations in dietary phosphate content. *The Journal of Clinical Investigation* 99:1302-1312.

41. Hilfiker, H., C. Hartmann, G. Stange, and H. Murer. 1998. Characterization of the 5'-flanking region of OK cell type II Na-P_i cotransporter gene. *American Journal of Physiology* 274:F197-F204

42. Tenenhouse, H., J. Martel, J. Biber, and H. Murer. 1995. Effect of Pi restriction on renal Na^+-Pi cotransporter mRNA and immunoreactive protein in X-linked *Hyp* mice. *American Journal of Physiology* 268:F1062-F1069

43. Lötscher, M., Y. Scarpetta, M. Levi, H. Wang, H. Zajicek, J. Biber, H. Murer, and B. Kaissling. 1999. Rapid downregulation of rat renal Na/Pi-cotransporter in response to parathyroid hormone: role of microtubule rearrangement. *Journal of Clinical Investigation* submitted:

44. Hansch, E., J. Forgo, H. Murer, and J. Biber. 1993. Role of microtubules in the adaptive response to low phosphate of Na/Pi-cotransport in opossum kidney cells. *Pflügers Archiv European Journal of Physiology* 422:516-522.

45. Pfister, M., I. Ruf, G. Stange, U. Ziegler, E. Lederer, J. Biber, and H. Murer. 1998. Parathyroid hormone leads to the lysosomal degradation of the renal type II Na/Pi cotransporter. *Proceedings of the National Academy of Science USA* 95:1909-1914.

46. Silverstein, D., M. Barac-Neito, H. Murer, and A. Spitzer. 1997. A putative growth-related renal Na^+-Pi cotransporter. *American Journal of Physiology* 273:R928-R933

47. Kempson, S., M. Lötscher, B. Kaissling, J. Biber, H. Murer, and M. Levi. 1995. Parathyroid hormone action on phosphate transporter mRNA and protein in rat renal proximal tubules. *American Journal of Physiology* 268:F784-F791

48. Pfister, M., E. Lederer, J. Forgo, U. Ziegler, M. Lötscher, E. Quabius, J. Biber, and H. Murer. 1997. Parathyroid hormone-dependent degradation of type II Na^+/P_i cotransporters. *The Journal of Biological Chemistry* 272:20125-20130.

49. Keusch, I., M. Traebert, M. Lötscher, B. Kaissling, H. Murer, and J. Biber. 1998. Parathyroid hormone and dietary phosphate provoke a lysosomal routing of the proximal tubular Na/Pi-cotransporter type II. *Kidney International* 54:1224-1232.

50. Malstrom, K. and H. Murer. 1987. Parathyroid hormone regulates phosphate transport in OK cells via an irreversible inactivation of a membrane protein. *FEBS Letters* 216:257-260.

51. Sorribas, V., D. Markovich, T. Verri, J. Biber, and H. Murer. 1995. Thyroid hormone stimulation of Na/Pi cotransport in opossum kidney cells. *Pflügers Archiv European Journal of Physiology* 431:266-271.

52. Caverzasio, J. and J.-P. Bonjour. 1989. Insulin-like growth factor simulates Na-dependent Pi transport in cultured kidney cells. *American Journal of Physiology* 257:F712-F717

53. Levi, M., J. Shayman, A. Abe, S. Gross, R. McCluer, J. Biber, H. Murer, M. Lötscher, and R. Cronin. 1995. Dexamethasone modulates rat renal brush border membrane phosphate transporter mRNA and protein abundance and glycosphingolipid composition. *Journal of Clinical Investigation* 96:207-216.

54. Arar, M., M. Baum, J. Biber, H. Murer, and M. Levi. 1995. Epidermal growth factor inhibits Na-Pi cotransport and mRNA in OK cells. *American Journal of Physiology* 268:F309-F314

55. Arar, M., H. Zajicek, I. Elshihabi, and M. Levi. 1999. Epidermal growth factor inhibits Na-Pi cotransport in weaned and suckling rats. *American Journal of Physiology* 276:F72-F78

56. Kurnik, B. and K. Hruska. 1984. Effects of 1-25 dihydroxycholecalciferol on phosphate transport in vitamin D-deprived rats. *American Journal of Physiology* 247:F177-F184

57. Kurnik, B. and K. Hruska. 1985. Mechanism of stimulation of renal phosphate transport by 1,25-dihyroxycholecalciferol. *Biochimica et Biophysica Acta* 817:42-50.

58. Taketani, Y., H. Segawa, M. Chikamori, K. Morita, H. Tanaka, S. Kido, H. Yamamoto, Y. Iemori, S. Tatsumi, N. Tsugawa, T. Okano, T. Kobayashi, K. Miyamoto, and E. Takeda. 1998. Regulation of type II renal Na^+-dependent inorganic phosphate transporters by 1,25-dihydroxyvitamin D_3. Identification of a vitamin D-responsive element in the human NaPi-3 gene. *Journal of Biological Chemistry* 273:14575-14581.

59. Sorribas, V., M. Lötscher, J. Loffing, J. Biber, B. Kaissling, H. Murer, and M. Levi. 1996. Cellular mechanisms of the age-related decrease in renal phosphate reabsorption. *Kid* 50:855-860.

60. Silverstein, D., M. Barac-Neito, and A. Spitzer. 1996. Mechanism of renal phosphate retention during growth. *Kidney International* 49:1023-1026.

61. Pegorier, L. and C. Merlet-Benichou. 1993. Effects of weaning on phosphate transport maturation in the rat kidney. Clearance and brush border membrane studies. *Pediatric Nephrology* 7:807-814.

62. Kavanaugh, M., D. Miller, W. Zhang, W. Law, C. Kozak, D. Kabat, and A. Miller. 1994. Cell-surface receptors for gibbon ape leukemia virus and amphotropic murine retrovirus are inducible sodium-phosphate symporters. *Proceedings of the National Academy of Science USA* 91:7071-7075.

63. Kavanaugh, M. and D. Kabat. 1996. Identification and characterization of a widely expressed phosphate transporter/retrovirus receptor family. *Kidney International* 49:959-963.

64. Boyer, C., A. Baines, E. Beaulieu, and R. Beliveau. 1996. Immunodetection of a type III sodium-dependent phosphate cotransporter in tissues and OK cells. *Biochimica et Biophysica Acta* 1281:117-123.

65. Chien, M., E. O'Neill, and J. Garceia. 1998. Phosphate depletion enhances the stability of the amphotropic murine leukemia virus receptor mRNA. *Virology* 240:109-117.

66. Armbrecht, H. and T. Hodam. 1994. Parathyroid hormone and 1,25-dihydroxyvitamin D synergistically induce the 1,25-dihydroxyvitamin D-24-hydroxylase in rat UMR-106 osteoblast-like cells. *Biochemical and Biophysical Research Communication* 205:674-679.

67. Armbrecht, H., V. Wongsurawat, T. Hodam, and N. Wongsurawat. 1996. Insulin markedly potentiates the capacity of parathyroid hormone to increase expression of 25-hydroxyvitamin D_3-24 hydroxylase in rat osteoblastic cells in the presence of 1,25-hydroxyvitamin D_3. *FEBS Letters* 393:77-80.

68. Friedman, P. and F. Gesek. 1995. Cellular calcium transport in renal epithelia: measurement, mechanisms, and regulation. *Physiological Reviews* 75:429-471.

69. Nemere, I. 1996. Apparent nonnuclear regulation of intestinal phosphate transport: effects of 1,25-dihydroxyviatmin D_3, and 25-dihyroxyvitamin D_3. *Endocrinology* 137:2254-2261.

70. Brandis, M., J. Harmeyer, R. Kaune, M. Mohrmann, H. Murer, and Z. Zimlo. 1988. Phosphate transport in brush border membranes from control and rachitic pig kidney and small intestine. *Journal of Physiology* 384:479-490.

71. Hoenderop, J., A. van der Kemp, A. Hartog, S. van de Graaf, C. van Os, P. Willems, and R. Bindels. 1999. Molecular identification of the apical Ca^{2+} channel in 1,25-dihydroxyvitamine D_3-responsive epithelia. *The Journal of Biological Chemistry* 274:8375-8378.

72. Takeda, S., T. Yoshizawa, Y. Nagai, H. Yamato, S. Fukumoto, K. Sekine, S. Kato, T. Matsumoto, and T. Fujita. 1999. Stimulation of osteoclast formation by 1,25-dihydroxyvitamin D requires its binding to vitamin D receptor (VDR) in osteoblastic cells: studies using VDR knockout mice. *Endocrinology* 140:1005-1008.

73. Malluch, H. and M. Faugere. 1986. Defective mineralization and osteomalacia. In Atlas of Mineralized Bone Histology. Anonymous Karger, New York. 60-63.

74. Marie, P., M. Hott, and M. Garba. 1985. Contrasting effects of 1,25-dihydroxyvitamin D_3 on bone matrix and mineral appositional rates in the mouse. *Metabolism* 34:777-783.

75. Caverzasio, J., T. Selz, and J.-P. Bonjour. 1988. Characteristics of phosphate transport in osteoblast-like cells. *Calcified Tissue International* 43:83-87.

76. Palmer, G., J. Zhao, J.-P. Bonjour, W. Hofstetter, and J. Caverzasio. 1999. In vivo expression of transcripts encoding the Glvr-1 phosphate transporter/retrovirus receptor during bone development. *Bone* 24:1-7.

77. Hauschka, P., J. Lian, D. Cole, and C. Gundberg. 1989. Osteocalcin and matrix Gla protein: Vitamin K-dependent proteins in bone. *Physiological Reviews* 69:990-1047.

78. Ruchon, A., M. Marcinkiewicz, G. Siegfried, H. Tenenhouse, L. DesGroseillers, P. Crine, and G. Boileau. 1998. Pex mRNA is localized in developing mouse osteoblasts and odontoblasts. *The Journal of Histochemistry and Cytochemistry* 46:459-468.

79. Desbois, C., D. Hogue, and G. Karsenty. 1994. The mouse osteocalcin gene cluster contains three genes with two separate spatial and temporal patterns of expression. *Journal of Biological Chemistry* 57:379-383.

80. Liu, F., A. Gupta, and J. Aubin. 1994. Simultaneous detection of multiple bone-related mRNAs and protein expression during osteoblast differentiation: polymerase chain reaction and immunocytochemical studies at the single cell level. *Developmental Biology* 166:220-234.

81. Price, P., M. Williamson, T. Haba, R. Dell, and W. Jee. 1982. Excessive mineralization with growth plate closure in rats on chronic warfarin treatment. *Proceedings of the National Academy of Science USA* 79:7734-7738.

82. Romberg, R., P. Werness, L. Riggs, and K. Mann. 1986. Inhibition of hydroxyapatite crystal growth by bone-specific and other calcium-binding proteins. *Biochemistry* 25:1176-1180.

83. Ducy, P., C. Desbois, B. Boyce, G. Pinero, B. Story, C. Dunstan, E. Smith, J. Bonadio, S. Goldstein, C. Gundberg, A. Bradley, and G. Karsenty. 1996. Increased bone formation in osteocalcin-deficient mice. *Nature* 382:1231-1235.

84. Clemens, T., H. Tang, M. Shigetao, R. Kesterson, F. Demayo, J. Pike, and C. Gundberg. 1997. Analysis of osteocalcin expression in transgenic mice reveals a species difference in vitamin D regulation of mouse and human osteocalcin genes. *Journal of Bone and Mineral Research* 12:1570-1576.

85. Staal, A., W. Geertsma-Kleinekoort, G. van Den Bemd, C. Buurman, J. Birkenhäger, H. Pols, and J. van Leeuwen. 1998. Regulation of osteocalcin production and bone resorption by 1,25-

dihydroxyvitamin D_3 in mouse long bones: interaction with the bone derived growth factors TGF-β and IGF-1. *Journal of Bone and Mineral Research* 13:36-43.

86. Lian, J., V. Shalhoub, F. Aslam, B. Frenkel, J. Green, M. Hamrah, G. Stein, and J. Stein. 1997. Species-specific glucocorticoid and 1,25-dihydroxyvitamin D responsiveness in mouse MC3T3-E1 osteoblasts: dexamethasone inhibits osteoblast differentiation and vitamin D down-regulates osteocalcin gene expression. *Endocrinology* 138:2117-2127.

87. Tenenhouse, H. 1999. X-linked hypophosphatemia: a homologous disorder in humans and mice. *Nephrology Dialysis Transplantation* 14:333-341.

88. Beck, L., Y. Soumounou, J. Martel, G. Krishnamurthy, C. Gauthier, C. Goodyer, and H. Tenenhouse. 1997. Pex/PEX tissue distribution and evidence for a deletion in the 3' region of the *Pex* gene in X-linked hypophosphatemic mice. *Journal of Clinical Investigation* 99:1200-1209.

89. Du, L., M. Desbarats, J. Viel, F. Glorieux, C. Cawthorn, and B. Ecarot. 1996. cDNA cloning of the murine Pex gene implicated in X-linked hypophosphatemia and evidence for expression in bone. *Genomics* 36:22-28.

90. Guo, R. and L. Quarles. 1997. Cloning and sequencing of Human PEX from a bone cDNA library: evidence for its developmental stage-specific regulation in osteoblasts. *Journal of Bone and Mineral Research* 12:1009-1017.

91. Ruchon, A., H. Tenenhouse, M. Marcinkiewicz, G. Siegfried, J. Aubin, L. DesGroseillers, P. Crine, and G. Boileau. 1999. Developmental expression and tissue distribution of Phex Protein: effect of the *Hyp* mutation and relationship to bone markers. *To be published*

92. Ecarot, B. and M. Desbarats. 1999. 1,25-$(OH)_2D_3$ down-regulates expression of *Phex*, a marker of the mature osteoblast. *Endocrinology* 140:1192-1199.

93. Beck, L., A. Karaplis, N. Amizuka, A. Hewson, H. Ozawa, and H. Tenenhouse. 1998. Targeted inactivation of Npt2 in mice leads to severe renal phosphate wasting, hypercalciuria, and skeletal abnormalities. *Proceedings of the National Academy of Science* 95:5372-5377.

94. Tenenhouse, H., A. Werner, J. Biber, S. Ma, J. Martel, S. Roy, and H. Murer. 1994. Renal Na^+-phosphate cotransport in murine X-linked hypophosphatemic rickets: Molecular characterization. *Journal of Clinical Investigation* 93:671-676.

95. Beck, L., R. Jr. Meyer, M. Meyer, J. Biber, H. Murer, and H. Tenenhouse. 1996. Renal expression of Na^+-phosphate cotransporter mRNA and protein: effect of the *Gy* mutation and low phosphate diet. *Pflügers Archiv European Journal of Physiology* 431:936-941.

96. Tenenhouse, H. and L. Beck. 1996. Renal Na^+-phosphate cotransporter gene expression in X-linked *Hyp* and *Gy* mice. *Kidney International* 49:1027-1032.

97. Meyer, R. Jr., R. Gray, and M. Meyer. 1980. Abnormal vitamin D metabolism in the X-linked hypophosphatemic mouse. *Endocrinology* 107:1577-1581.

98. Glorieux, F., P. Marie, J. Pettifor, and E. Delvin. 1980. Bone response to phosphate salts, ergocalciferol, and calcitriol in hypophosphatemic vitamin D-resistant rickets. *New England Journal of Medicine* 303:1023-1031.

99. Lobaugh, B. and M. Drezner. 1983. Abnormal regulation of renal 25-hydroxyvitamin D-1α-hydroxylase activity in the X-linked hypophosphatemic mouse. *Journal of Clinical Investigation* 71:400-403.

100. Cunningham, J., H. Gomes, Y. Seino, and L. Chase. 1983. Abnormal 24-hydroxylation of 25-hydroxyvitamin D in the X-linked hypophosphatemic mouse. *Endocrinology* 112:633-637.

101. Tenenhouse, H., A. Yip, and G. Jones. 1988. Increased renal catabolism of 1,25-dihydroxyvitamin D in murine X-linked hypophosphatemic rickets. *Journal of Clinical Investigation* 81:461-465.

102. Drezner, M. 1984. The role of abnormal vitamin D metabolism in X-linked hypophosphatemic rickets and osteomalacia. *Advances in Experimental Medical Biology* 178:399-404.

103. Yamaoka, K., Y. Seino, K. Satomura, Y. Tanaka, H. Yabuuchi, and M. Haussler. 1986. Abnormal relationship between serum phosphate concentration and renal 25-hydroxycholecalciferol-1-alpha-hydroxylase activity in X-linked hypophosphatemic mice. *Mineral and Electrolyte Metabolism* 12:194-198.

104. Tieder, M., D. Modai, R. Samuel, R. Arie, A. Halabe, I. Bab, D. Gabizon, and U. Liberman. 1985. Hereditary hypophosphatemic rickets with hypercalciuria. *New England Journal of Medicine* 312:611-617.

105. Hewson, A. 1996. Isolation and characterization of a mouse renal sodium phosphate cotransporter gene and construction of a gene targeting knock-out vector. M.Sc. Biology, McGill University.

106. Breslau, N. 1996. Calcium, Magnesium, and Phosphorus: Intestinal Absorption. In Primer on the Metabolic Bone Diseases and Disorders of Mineral Metabolism. M. Favus, editor. Lippincott-Raven, Philadelphia. 41-49.

107. Sambrook, J., E. Fritzch, and T. Maniatis. 1989. Gel electrophoresis. In Molecular Cloning: A Laboratory Manual. Anonymous Cold Spring Harbor Laboratory Press, Cold Spring Harbor, N.Y.

108. Lowry, O., N. Rosebrough, A. Farr, and R. Randall. 1951. Protein measurement with the Folin phenol reagent. *Journal of Biological Chemistry* 193:265-275.

109. Laemmli, U. 1970. Cleavage of structural proteins during the assembly of the head of bacteriophage T4. *Nature* 227:680-685.

110. Weinstein, R., R. Jilka, A. Parfitt, and S. Manolagas. 1997. The effects of androgen deficiency on murine bone remodeling and bone mineral density are mediated via cells of the osteoblastic lineage. *Endocrinology* 138:4013-4021.

111. Jilka, R., R. Weinstein, A. Takahashi, A. Parfitt, and S. Manolagas. 1996. Linkage of decreased bone mass with impaired osteoblastogenesis in a murine model of accelerated senescence. *Journal of Clinical Investigation* 97:1732-1740.

112. Parfitt, A., M. Drezner, F. Glorieux, J. Kanis, H. Malluche, P. Meunier, S. Ott, and R. Recker. 1987. Bone histomorphometry: standardization of nomenclature, symbols, and units. Report of the ASBMR Histomorphometry Nomenclature Committee. *Journal of Bone and Mineral Research* 2:595-610.

113. Caverzasio, J., H. Murer, H. Fleisch, and J.-P. Bonjour. 1982. Phosphate transport in brush border membrane vesicles isolated from renal cortex of young growing and adult rats. *Pflügers Archiv European Journal of Physiology* 394:217-221.

114. Neiberger, R., M. Barac-Neito, and A. Spitzer. 1989. Renal reabsorption of phosphate during development: transport kinetics in BBMV. *American Journal of Physiology* 257:F268-F274

115. Miyamoto, K., H. Segawa, K. Morita, T. Nii, S. Tatsumi, Y. Taketani, and E. Takeda. 1997. Relative contributions of Na^+-dependent phosphate co-transporters to phosphate transport in mouse kidney: RNase-H mediated hybrid depletion analysis. *Biochemical Journal* 327:735-739.

116. O'Hara, B., S. Johann, H. Kilinger, D. Blair, H. Rubinson, K. Dunn, P. Sass, S. Vitek, and T. Robins. 1990. Characterization of a human gene conferring sensitivity to infection by gibbon ape leukemia virus. *Cellular Growth and Differentiation* 1:119-127.

117. Tenenhouse, H., C. Gauthier, J. Martel, F. Gesek, B. Coutermarsh, and P. Friedman. 1998. Na^+-phosphate cotransport in mouse distal convoluted tubule cells: evidence for *Glvr-1* and *Ram-1* gene expression. *Journal of Bone and Mineral Research* 13:590-597.

118. Haas, J., T. Berndt, and A. Haramati. 1984. Nephron sites of action of nicotinamide on phosphate reabsorption. *American Journal of Physiology* 246:F27-F31

119. Pastoriza-Munoz, E., D. Mishler, and C. Lechene. 1983. Effect of phosphate deprivation on phosphate reabsorption in rat nephron: Role of PTH. *American Journal of Physiology* 244:F140-F149

120. Gesek, A. and P. Friedman. 1995. Sodium entry mechanisms in distal convoluted tubule cells. *American Journal of Physiology* 268:F287-F300

121. Tenenhouse, H. and Y. Soumounou. 1998. Cloning and characterization of the mouse Na^+-phosphate cotransporter gene, Npt1, and construction of an Npt1 targeting vector. *Journal of Bone and Mineral Research* 23:S465

122. Pfister, M., H. Hilfiker, J. Forgo, E. Lederer, J. Biber, and H. Murer. 1998. Cellular mechanisms involved in the acute adaptation of OK cell Na/Pi-cotransport to high- or low-Pi medium. *Pflügers Archiv European Journal of Physiology* 435:713-719.

123. Baylink, D., J. Wergedal, and M. Stauffer. 1971. Formation, mineralization and resorption of bone in hypophosphatemic rats. *Journal of Clinical Investigation* 50:2519-2530.

124. Bruin, W., D. Baylink, and J. Wergedal. 1975. Acute inhibition of mineralization and stimulation of bone resorption mediated by hypophosphatemia. *Endocrinology* 96:394-399.

125. Kimmel, P., D. Watkins, E. Slatopolsky, and C. Langman. 1990. 1,25(OH)2D response to combined zinc and phosphorus depletion in rats. *American Journal of Physiology* 22:E319-E326

126. Baxter, L. and H. DeLuca. 1976. Stimulation of 25-hydroxyvitamin D3-1alpha-hydroxylase by phosphate depletion. *Journal of Biological Chemistry* 251:3158-3161.

127. Gray, R. and J. Napoli. 1983. Dietary phosphate deprivation increases 1,25-dihydroxyvitamin D3 synthesis in rat kidney in vitro. *Journal of Biological Chemistry* 258:1152-1155.

128. Tenenhouse, H. and G. Jones. 1990. Abnormal regulation of renal vitamin D catabolism by dietary phosphate in murine X-linked hypophosphatemic rickets. *Journal of Clinical Investigation* 85:1450-1455.

129. Lee, D., N. Brautbar, M. Walling, V. Silis, J. Coburn, and C. Kleeman. 1979. Effect of phosphorus depletion on intestinal calcium and phosphorus absorption. *American Journal of Physiology* 236:E451-E457

130. Cross, H., H. Debiec, and M. Perlik. 1990. Mechanism and regulation of intestinal phosphate absorption. *Mineral and Electrolyte Metabolism* 16:115-124.

131. Roy, S., J. Martel, S. Ma, and H. Tenenhouse. 1994. Increased renal 25-hydroxyvitamin D_3-24-hydroxylase messenger ribonucleic acid and immunoreactive protein in phosphate-deprived *Hyp* mice: a mechanism for accelerated 1,25-dihydroxyvitamin D_3 catabolism in X-linked hypophosphatemic rickets. *Endocrinology* 134:1761-1767.

132. Beck, N., S. Webster, and H. Reineck. 1979. Effect of fasting on tubular phosphorus reabsorption. *American Journal of Physiology* 237:F241-F246

133. Kempson, SA. 1985. Effects of fasting compared to low phosphorus diet on the kinetics of phosphate transport by renal brush-border membranes. *Biochimica et Biophysica Acta* 815:85-90.

134. Broadus, A. 1996. Mineral Balance and Homeostasis. In Primer on Metabolic Bone Diseases and Disorders of Mineral Metabolism. M. Favus, editor. Lippincott-Raven, Philadelphia. 57-63.

135. Breslau, N. 1996. Calcium, Magnesium, and Phosphorus: Renal Handling and Urinary Excretion. In Pimer on the Metabolic Bone Diseases and Disorders of Mineral Metabolism. M. Favus, editor. Lippincott-Raven, Philadelphia. 49-57.

136. Palmer, G., J.-P. Bonjour, and J. Caverzasio. 1997. Expression of a newly identified phosphate transporter/retrovirus receptor in human SaOS-2 osteoblast-like cells and its regulation by insulin-like growth factor I. *Endocrinology* 138:5202-5209.

137. Desbois, C. and G. Karsenty. 1995. Osteocalcin cluster: implications for functional studies. *Journal of Cellular Biochemistry* 57:379-383.

138. Bronckers, A., S. Gay, R. Finkelman, and W. Butler. 1987. Developmental appearance of Gla proteins (osteocalcin) and alkaline phosphatase in tooth germs and bones of the rat. *Bone Mineral* 2:361-373.

139. Carpenter, R., K. Moltz, B. Ellis, M. Andreoli, T. McCarthy, M. Centrella, D. Bryan, and C. Gundberg. 1998. Osteocalcin production in primary osteoblast cultures derived from normal and *Hyp* mice. *Endocrinology* 139:35-44.

140. Jara, A., E. Lee, D. Stauber, F. Moatamed, A. Felsenfeld, and C. Kleeman. 1999. Phosphate depletion in the rat: Effect of bisphosphonates and the calcemic response to PTH. *Kidney International* 55:1434-1443.

141. Marie, P., R. Travers, and F. Glorieux. 1981. Healing of rickets with phosphate supplementation in the hypophosphatemic male mouse. *Journal of Clinical Investigation* 67:911

142. Jones, A., J. Tzenova, T. Fujiwara, D. Frappier, M. Tieder, K. Morgan, and H. Tenenhouse. 1999. NPT2 is not the gene responsible for Hereditary Hypophosphatemic Rickets with

Hypercalciuria (HHRH) in a Bedouin kindred. *American Society of Nephrology 32nd Annual Meeting and Scientific Exposition* submitted:(Abstr.)